Université de Sherbrooke

**“Acid-spike” effect in spurs/tracks of the low/high linear energy transfer radiolysis of water: Potential implications for radiobiology and nuclear industry**

Par

Vanaja KANIKE
Département de médecine nucléaire et radiobiologie

Mémoire présenté à la Faculté de médecine et des sciences de la santé
en vue de l’obtention du diplôme de maître ès sciences (M.Sc.)
en "sciences des radiations et imagerie biomédicale"

Sherbrooke, Québec, Canada

November 2016

**Jury**

| | |
|---|---|
| Pr Klaus Klarskov | *Examinateur*, Département de pharmacologie-physiologie, Faculté de médecine et des sciences de la santé |
| Pr Richard J. Wagner | *Examinateur*, Département de médecine nucléaire et radiobiologie, Faculté de médecine et des sciences de la santé |
| Pr Jean-Paul Jay-Gerin | *Directeur de recherche*, Département de médecine nucléaire et radiobiologie, Faculté de médecine et des sciences de la santé |

# Résumé

**Effet de "pic acide" dans les grappes / trajectoires de la radiolyse de l'eau à faible / haut transfert d'énergie linéaire : implications potentielles pour la radiobiologie et l'industrie nucléaire**

Par
**Vanaja KANIKE**
Département de médecine nucléaire et radiobiologie

Mémoire présenté à la Faculté de médecine et des sciences de la santé en vue de l'obtention du diplôme de maître ès sciences (M.Sc.) en "sciences des radiations et imagerie biomédicale", Faculté de médecine et des sciences de la santé, Université de Sherbrooke, Sherbrooke, Québec, Canada J1H 5N4

Les ions hydronium ($H_3O^+$) sont formés, à temps courts, dans les grappes ou le long des trajectoires de la radiolyse de l'eau par des rayonnements ionisants à faible transfert d'énergie linéaire (TEL) ou à TEL élevé. Cette formation *in situ* de $H_3O^+$ rend la région des grappes/trajectoires du rayonnement temporairement plus acide que le milieu environnant. Bien que des preuves expérimentales de l'acidité d'une grappe aient déjà été signalées, il n'y a que des informations fragmentaires quant à son ampleur et sa dépendance en temps. Dans ce travail, nous déterminons les concentrations en $H_3O^+$ et les valeurs de pH correspondantes en fonction du temps à partir des rendements de $H_3O^+$ calculés à l'aide de simulations Monte Carlo de la chimie intervenant dans les trajectoires. Quatre ions incidents de différents TEL ont été sélectionnés et deux modèles de grappe/trajectoire ont été utilisés : 1) un modèle de grappe isolée "sphérique" (faible TEL) et 2) un modèle de trajectoire "cylindrique" (TEL élevé). Dans tous les cas étudiés, un effet de pH acide brusque transitoire, que nous appelons un effet de "pic acide", est observé immédiatement après l'irradiation. Cet effet ne semble pas avoir été exploré dans l'eau ou un milieu cellulaire soumis à un rayonnement ionisant, en particulier à haut TEL. À cet égard, ce travail soulève des questions sur les implications possibles de cet effet en radiobiologie, dont certaines sont évoquées brièvement. Nos calculs ont ensuite été étendus à l'étude de l'influence de la température, de 25 à 350 °C, sur la formation *in situ* d'ions $H_3O^+$ et l'effet de pic acide qui intervient à temps courts lors de la radiolyse de l'eau à faible TEL. Les résultats montrent une augmentation marquée de la réponse de pic acide à hautes températures. Comme de nombreux processus intervenant dans le cœur d'un réacteur nucléaire refroidi à l'eau dépendent de façon critique du pH, la question ici est de savoir si ces fortes variations d'acidité, même si elles sont hautement localisées et transitoires, contribuent à la corrosion et l'endommagement des matériaux.

Mots clés : Eau liquide, radiolyse, transfert d'énergie linéaire (TEL), structure de trajectoire, grappe, simulations Monte Carlo de la chimie des trajectoires, ion hydronium ($H_3O^+$), rendement radiolytique (valeur *G*), pH, pic acide, température, radiobiologie, radiothérapie, nucléaire réacteur refroidi à l'eau.

# Summary


**"Acid-spike" effect in spurs/tracks of the low/high linear energy transfer radiolysis of water: Potential implications for radiobiology and nuclear industry**

By
**Vanaja KANIKE**
Département de médecine nucléaire et radiobiologie

Thesis presented at the Faculty of Medicine and Health Sciences in order to obtain the Master of Sciences (M.Sc.) degree in "Radiation Sciences and Biomedical Imaging", Faculty of Medicine and Health Sciences, Université de Sherbrooke, Sherbrooke, Québec, Canada J1H 5N4

Hydronium ions ($H_3O^+$) are formed within spurs or tracks of the low or high linear energy transfer (LET) radiolysis of pure, deaerated water at early times. The *in situ* radiolytic formation of $H_3O^+$ renders the spur and track regions temporarily more acid than the surrounding medium. Although experimental evidence for an acidic spur has already been reported, there is only fragmentary information on its magnitude and time dependence. In this work, spur or track $H_3O^+$ concentrations and the corresponding pH values are obtained from our calculated yields of $H_3O^+$ as a function of time, using Monte Carlo track chemistry simulations. We selected four impacting ions and we used two different spur and track models: 1) an isolated "spherical" spur model characteristic of low-LET radiation and 2) an axially homogeneous "cylindrical" track model for high-LET radiation. Very good agreement was found between our calculated time evolution of $G(H_3O^+)$ in the radiolysis of pure, deaerated water by 300-MeV incident protons (which mimic $^{60}$Co γ/fast electron irradiation) and the available experimental data at 25 °C. For all cases studied, an abrupt transient acid pH effect, which we call an "acid spike", is observed during and shortly after the initial energy release. This acid-spike effect is virtually unexplored in water or in a cellular environment subject to the action of ionizing radiation, especially high-LET radiation. In this regard, this work raises a number of questions about the potential implications of this effect for radiobiology, some of which are briefly evoked. Our calculations were then extended to examine the effect of temperature from 25 to 350 °C on the yield of $H_3O^+$ ions that are formed in spurs of the low-LET radiolysis of water. The results showed an increasingly acidic spike response at higher temperatures. As many in-core processes in a water-cooled nuclear reactor critically depend on pH, the question here is whether these variations in acidity, even highly localized and transitory, contribute to material corrosion and damage.


Keywords : Liquid water, radiolysis, linear energy transfer (LET), track structure, spur, Monte Carlo track chemistry simulations, hydrogen ion ($H_3O^+$), radiation chemical yield (*G*-value), pH, acid spike, temperature, radiobiology, radiotherapy, water-cooled nuclear reactor.

# Table of Contents

# List of Figures

## Chapter 1



## Chapter 2

irradiated solution decreases from the initial pre-irradiation value of 7 to a value approaching pH = 3.25 at the highest dose rates used in liquid cell electron microscopy experiments. From SCHNEIDER et al. (2014), with permission, and private communication.

# List of Tables

# List of Abbreviations

| | |
|---|---|
| CONV | Conventional |
| $D$ | Diffusion coefficient |
| DEA | Dissociative electron attachment |
| DNA | Deoxyribonucleic acid |
| $e^-_{aq}$ | Hydrated electron |
| eV | Electron-volt |
| fs | Femtosecond |
| $G_X$ or $g$(X) | Primary yield of the radiolytic species X |
| $G$(X) | Experimental yield of the final product X |
| Gy/s | Gray/second (dose rate) |
| iNOS | Inducible nitric oxide synthase |
| IR | Infrared |
| IRT | Independent reaction times |
| $k$ | Reaction rate constant |
| keV | Kilo-electron-volts |
| LET | Linear energy transfer |
| MC | Monte Carlo |
| MeV | Mega-electron-volts |
| μm | micrometer |
| μs | microsecond |
| pH | $-\log_{10}[H^+]$, where the square brackets denote concentration |
| p$K_a$ | $-\log_{10} K_a$, where $K_a$ is the acid dissociation constant |
| ps | Picosecond |
| SOD | Superoxide dismutase |
| $^{60}$Co | Cobalt-60 |
| $^{137}$Cs | Cesium-137 |

# 1 - INTRODUCTION

Radiation chemistry is a mature branch of radiation science which is continually evolving and finding wider applications. The radiation chemistry of water is of considerable importance, for the intrinsic scientific interest it generates. This is particularly apparent in the study of the role of free radicals in biology generally, and radiation biology specifically because living cells and tissue consist mainly of water (~70%-85% by weight). Therefore, it is important to know how ionizing radiation interacts with water and aqueous solutions, what the subsequent water decomposition products are and how they are spatially distributed (what is commonly referred to as the "track structure"), depending on the radiation type and energy (a measure of which is given by the "linear energy transfer" or LET) and the irradiation conditions. Aqueous radiation chemistry is also of great importance in various areas of nuclear science and technology such as water-cooled nuclear power reactors where water, used both as moderator and as a heat transport medium, is circulating around the reactor core at temperatures of ~250-350 °C, and where the radiolytic processes need to be carefully controlled to avoid the deleterious effects of water radiolysis and minimize corrosion. For a detailed account of the history and present status of aqueous radiation chemistry, see, for example: ALLEN (1961), DRAGANIĆ and DRAGANIĆ (1971), FERRADINI and PUCHEAULT (1983), BUXTON (1987), KROH (1989), SPINKS and WOODS (1990), JONAH (1995), FERRADINI and JAY-GERIN (1999), ZIMBRICK (2002), LAVERNE (2004), ELLIOT and BARTELS (2009), WARDMAN (2009), and MEESUNGNOEN and JAY-GERIN (2011).

In a biological system, the cell is damaged by ionizing radiation. In this regard, a thorough knowledge of the radiation chemistry of water is critical to our understanding of early stages in the complicated chain of radiobiological events that follow the absorption of radiation. Indeed, in a cellular environment, reactive species generated by water radiolysis are likely to cause chemical modifications and changes in cells, which subsequently may act as triggers of signalling or damaging effects (MUROYA et al., 2006; AZZAM et al., 2012; O'NEILL and WARDMAN, 2009). Ultimately, this can lead to observable biological responses. Although damage can be randomly induced in all

biomolecules (*e.g.*, nucleic acids, proteins, and lipids), DNA and its associated water molecules are considered to be the most important target in defining the radiobiological response. Damage is caused either directly or indirectly through chemical attack by radiolytic products as the radiation track passes through and deposits energy near to (mostly bulk water) or in the DNA. Interestingly, it is the spatial distribution of the DNA lesions rather than their number that is most biologically relevant. Such damage can be repaired or, if unrepaired or mis-repaired, may result in cytotoxic and mutagenic effects and chromosomal instability, all of which can contribute to tumorigenesis, cell death, or long-term stressful effects in surviving cells (BECKER and SEVILLA, 1993; BECKER et al., 2011; CADET et al., 1997; von SONNTAG, 2006; O'NEILL, 2001; AZZAM et al., 2012). A goal of radiobiology research is to understand how radiation exposure deregulates molecular pathways that are important in maintaining genomic integrity.

Monte Carlo simulation methods are well suited to take into account the stochastic nature of the complex sequence of events that are generated in aqueous systems following the absorption of ionizing radiation. Simulations allow the reconstruction of the intricate action of radiation. This is a powerful tool for studying the relationship between the initial radiation track structure, the ensuing chemical processes, and the stable end products formed in the radiolysis of both pure water and water-containing solutes. Stochastic simulation codes employing Monte Carlo procedures have been used with success by a number of investigators to model the entire water radiolysis process as a function of time, LET of the radiation, pH, presence or absence of oxygen, temperature, *etc*. (for reviews, see, for example: BALLARINI et al., 2000; UEHARA and NIKJOO, 2006; KREIPL et al., 2009; MEESUNGNOEN and JAY-GERIN, 2011). In particular, these model calculations provide the user with detailed information on the early physicochemical track structure (*i.e.*, the physical and chemical events that occur in the "native" radiation track) and the spatio-temporal development of the track (*i.e.*, how the initial, spatially nonhomogeneous distribution of reactive species relaxes in time toward a homogeneous distribution). This information can then be used to develop a realistic description of all reactive fragment species created at early times and involved as precursors to radiobiological damage. Such knowledge is critical to unravel the

fundamental biochemical mechanisms leading to the biological consequences of ionizing radiation.

In such a perspective, we used in this study Monte Carlo track chemistry simulations to calculate, at 25 °C, the pH values prevailing in the track regions of the radiolysis of pure, deaerated water during and shortly after irradiation. The concentrations of hydronium ions ($H_3O^+$) generated *in situ* in these regions and the corresponding pH values were obtained from our calculated yields (or *G*-values) of $H_3O^+$ as a function of time (in the interval of ~1 ps to 1 ms), assuming two different track structure models: (1) an isolated "spherical" spur model characteristic of low-LET radiation and (2) an axially homogeneous "cylindrical" track model for high-LET radiation. For all cases studied, an abrupt transient acid pH effect, which we called an "acid spike", was observed at times immediately after the initial energy release (KANIKE et al., 2015*a*,*b*). Following this work, calculations were then extended to examine the effect of temperature on the magnitude and duration of this acid spike response in the range from ambient up to 350 °C (KANIKE et al., 2016). To the best of our knowledge, this early-time, acid-spike effect has never been explored in water either at ambient or at elevated temperatures, or in living cells subject to ionizing radiation. In this respect, the present study prompts a number of important questions about the potential implications of these *in situ* variations in acidity, even if transitory, for radiobiology or for water-cooled nuclear reactors in terms of biological damage or material corrosion and damage.

### 1.1 Radiolysis of water

Water radiolysis is the chemical decomposition of water molecules due to the action of ionizing radiation. A thorough understanding of the radiolysis of water involves knowledge of the early physical energy deposition around the path of the incident radiation (mainly through ionization, electronic excitation, and dissociation of the water molecules), and the subsequent physicochemical and nonhomogeneous chemical evolution of the system (PLATZMAN, 1958; KUPPERMANN, 1959) to times, at room temperature, on the order of the microsecond. The products obtained after nonhomogeneous stage are usually regarded as homogeneously distributed in the bulk of the solution. Indeed, in a cellular environment, reactive species generated by water

radiolysis are likely to cause chemical modifications and changes in cells, which subsequently may act as triggers of signalling or damaging effects (MUROYA et al., 2006; O'NEILL AND WARDMAN, 2009; WARDMAN, 2009; AZZAM et al., 2012). Ultimately, this can lead to observable biological responses.

It is noteworthy that the extent and nature of cellular radiobiological damage depends not only on the absorbed dose but also on the quality of radiation. The "linear energy transfer" (LET) (also called "stopping power" by physicists, in units of keV/μm) represents, to a first approximation, the nonhomogeneity of energy deposition on a sub-microscopic scale. Briefly, for low-LET, sparsely ionizing radiation (*e.g.*, γ-rays from $^{60}Co$ and $^{137}Cs$, hard X-rays, or high-energy charged particles, such as fast electrons or protons generated by a particle accelerator: LET ~ 0.3 keV/μm), the radiolysis of pure deaerated liquid water principally leads to the formation of the radicals and molecular products $e^-_{aq}$ (hydrated electron), $H^\bullet$ (hydrogen atom), $H_2$ (molecular hydrogen), $^\bullet OH$ (hydroxyl radical), $H_2O_2$ (hydrogen peroxide), $HO_2^\bullet/O_2^{\bullet-}$ (hydroperoxyl/superoxide anion radicals, $pK_a = 4.8$ in water at 25 °C), $H^+$ – or equivalently, $H_3O^+$ or $H^+_{aq}$ (hydrogen ion), $OH^-$ (hydroxide ion), *etc*. (for a review, see: BUXTON, 1987; SPINKS and WOODS, 1990; FERRADINI and JAY-GERIN, 1999; MEESUNGNOEN and JAY-GERIN, 2011). Under ordinary irradiation conditions (*i.e.*, at modest dose rates), these species are generated nonhomogeneously on subpicosecond time scales in small, spatially isolated regions of dense ionization and excitation events, commonly referred to as "spurs" (MAGEE, 1953), along the track of the incident radiation. At ~1 ps, all the species begin to diffuse away from the site where they were originally produced. The result is that a fraction of them react together within the spurs as they develop in time while the remainder escape into the bulk solution. At ambient temperature and pressure, the so-called "spur expansion" is essentially complete by ~0.2 μs after the initial energy deposition (SANGUANMITH et al., 2012). At this time, the species that have escaped from spur reactions become homogeneously distributed throughout the bulk of the solution and the track of the radiation no longer exists. The yields per 100 eV of absorbed energy of the species that remain after spur expansion and become available to react with dissolved solutes (if any) present in low or moderate concentrations, are the so-called

"primary" (or "escape") yields. They are denoted by $g(e^-_{aq})$, $g(H^\bullet)$, $g(H_2)$, $g(^\bullet OH)$, $g(H_2O_2)$, *etc*.[1]

For low-LET radiation, the radiolysis of pure, deaerated (air-free) liquid water can be represented conceptually by the following global equation, written for an absorbed energy of 100 eV (FERRADINI and JAY-GERIN, 1999):

$$g(-H_2O)\ H_2O \rightsquigarrow g(e^-_{aq})\ e^-_{aq} + g(H^\bullet)\ H^\bullet + g(H_2)\ H_2 + g(H^+)\ H^+ + g(OH^-)\ OH^- + g(^\bullet OH)\ ^\bullet OH + g(H_2O_2)\ H_2O_2 + g(HO_2^\bullet/O_2^{\bullet-})\ HO_2^\bullet/O_2^{\bullet-} + \ldots \quad [1]$$

where the symbol $\rightsquigarrow$ is used to distinguish reactions brought about by the absorption of ionizing radiation, the coefficients $g(X)$ are the primary yields of the various radiolytic species X, and $g(-H_2O)$ denotes the corresponding yield for net water decomposition. For $^{60}$Co γ-irradiated neutral water at 25 °C, $g(e^-_{aq}) = 2.65$, $g(H^\bullet) = 0.6$, $g(H_2) = 0.45$, $g(^\bullet OH) = 2.8$, and $g(H_2O_2) = 0.68$ molecules per 100 eV (ELLIOT et al., 1993; FERRADINI and JAY-GERIN, 2000; ELLIOT and BARTELS, 2009).

These product yields are connected by the following equations:

$$g(e^-_{aq}) + g(OH^-) = g(H^+)$$

$$g(e^-_{aq}) + g(H^\bullet) + 2g(H_2) = g(^\bullet OH) + 2g(H_2O_2) + 3g(HO_2^\bullet/O_2^{\bullet-}) \quad [2]$$

expressing the charge conservation (electro-neutrality) and material balance (stoichiometry) of Eq. [1]. We should note that, for low-LET radiolysis, $HO_2^\bullet/O_2^{\bullet-}$ has an extremely small yield in comparison to the other radiolytic species (about less than 1%) and can be usually ignored, although in aerated solution the yields of $O_2^{\bullet-}$ is high due to solvated electrons react with oxygen.

---

[1] The number of species produced (or consumed) per unit of energy absorbed is termed the *G*-value and is used to express the radiation chemical yield. *G*-values are quoted as $g(X)$ (some authors prefer to use $G_X$) for the so-called primary yields of the species X (normally measured at the time after which spurs have dissipated) and *G*(product) for experimentally measured or final yields. Throughout this work, *G*-values are quoted in units of molecules per 100 eV. For conversion into SI units (mol J$^{-1}$), 1 molecule per 100 eV $\approx 1.0364 \times 10^{-7}$ mol J$^{-1}$ (or 0.10364 μmol J$^{-1}$).

With in the lifetime of a spur, the yields of free radical and molecular species formed by the irradiation vary with time, and also depend on the LET of the incident radiation and the concentration of added solutes or scavengers. One of the main goals in the study of the radiation chemistry of water is to determine those yields and their time dependences, under different irradiation conditions.

### *1.1.1 The track structure in radiation chemistry and radiobiology*

The quantities and proportions of the chemical products formed in the radiolysis of water are highly dependent on the distances separating the primary radiolytic species from each other along the track of the ionization radiation. The distribution of separations, *i.e.*, the "track structure", is determined to a large extent by the distribution of the physical energy deposition events and their geometrical dispositions, or, in other words, by the radiation type and energy. The radiation track structure is of crucial importance in specifying the precise spatial location and identity of all the radiolytic species and free-radical intermediates generated in the tracks, and their subsequent radiobiological action at the molecular and cellular levels. Tracks are dynamic and are constantly expanding in time due to diffusion of the reactive species (LAVERNE, 2000, 2004). Track structure, combined with a reaction scheme and yields of primary species, forms the basis of radiation-chemical theory (MOZUMDER, 1999). It is now well accepted that differences in the biochemical and biological effects (*e.g.*, damage to DNA, changes in cell signalling, *etc*.) of different qualities (LET) of radiation must be analyzed in terms of track structure (CHATTERJEE and HOLLEY, 1993; MUROYA et al., 2006). Two different radiation track structures are generally considered as a function of LET:

i. Low-LET radiation tracks
ii. High-LET radiation tracks.

*i) Low-LET radiation tracks*

Ionizing radiations such as fast electrons generated from X- or γ-ray beams have high energy and low LET. For example, the average LET of a 1-MeV Compton electron in water is ~0.3 keV/μm. The track-averaged mean energy loss per collision event by such an electron is in the region ~47-56.8 eV (COBUT, 1993; LAVERNE and

PIMBLOTT, 1995; COBUT et al., 1998; AUTSAVAPROMPORN, 2006; MIRSALEH KOHAN et al., 2013). This means that the energy-loss events are, on the average, separated by distances of ~200 nm. This nonhomogeneous distribution of energy deposition events in space gives rise to the "spur" theory for low-LET track structure (ALLEN, 1948; MAGEE, 1953; MOZUMDER and MAGEE, 1966*a*,*b*), according to which the entire track is to be viewed as a random succession of (more or less spherical) spurs, or spatially localized energy-loss events. The few tens of electron-volts deposited in a spur cause a secondary electron to be ejected from a molecule. As the ejected electron moves away, it undergoes collisions with surrounding water molecules, loses its excess energy, and becomes thermalized (~0.025 eV at 25 °C) within ~8-12 nm of its geminate positive ion (GOULET et al., 1990, 1996; PIMBLOTT and MOZUMDER, 2004; MEESUNGNOEN and JAY-GERIN, 2005*a*; UEHARA and NIKJOO, 2006). This average "electron thermalization distance" or "penetration range" ($r_{th}$) can be viewed as an estimate of the spur's initial radius, prior to spur expansion. Thus, the individual spurs produced by low-LET radiation are so far apart along the track that they are not initially overlapping (but they will overlap somewhat later as they develop in time).

In their pioneering work to model the radiation-chemical consequences of different energy-loss processes, MOZUMDER and MAGEE (1966*a*,*b*) considered, somewhat arbitrarily, a low-LET track as composed of a random sequence of three types of essentially non-overlapping entities: "spurs, blobs, and short tracks" (Figure 1.1). The spur category contains all track entities created by the energy losses between the lowest excitation energy of water and 100 eV; in most cases, there are one to three ion pairs in such isolated spatial areas and about the same number of excited molecules (PIMBLOTT and MOZUMDER, 1991). Blobs were defined as track entities with energy transfers between 100-500 eV, and short tracks as those with energy transfers between 500 eV and 5 keV. Secondary electrons produced in energy transfers above 5 keV were considered as "branch tracks". Short and branch tracks are, collectively, described as δ-rays. This old concept of track entities proved to be very helpful in greatly facilitating the visualization of track processes and in modeling radiation-chemical kinetics. It is still a useful approach for the classification of track structures, since it takes into account the spatial arrangements of initial species, which affect their subsequent reactions.

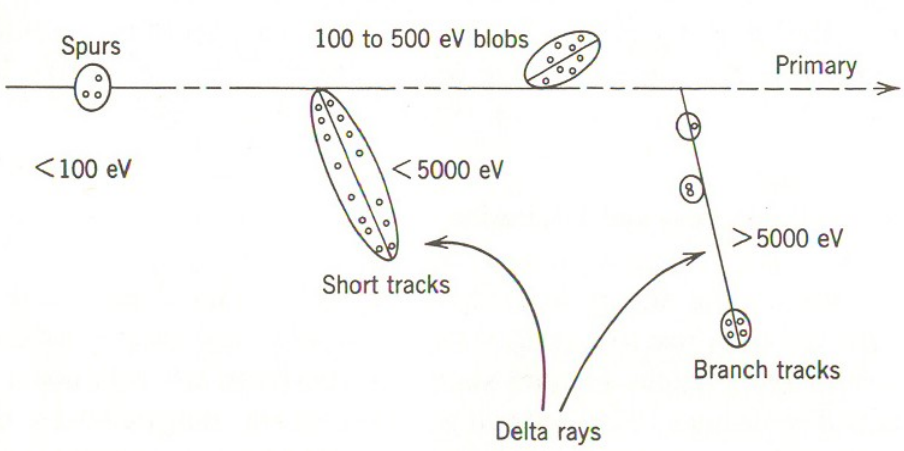


Figure 1.1 Classification of energy deposition events in water by track structure entities so-called spurs (spherical entities, up to 100 eV), blobs (spherical or ellipsoidal, 100-500 eV), and short tracks (cylindrical, 500 eV-5 keV) for a primary high-energy electron (not to scale). Short and branch tracks are, collectively, described as δ-rays. From BURTON (1969), with permission.

Figure 1.2 shows typical two-dimensional representations of the track segments of 300- and 0.15-MeV irradiating protons (LET ~ 0.3 and 70 keV/μm, respectively) on liquid water at 25 °C, calculated with our Monte Carlo simulation code (KANIKE et al., 2015*a*). It illustrates the non homogeneity of the energy deposition on a sub-microscopic scale. At the lowest LET (Figure 1.2*a*), tracks are formed initially by well-separated "spurs" (spherical in shape) that develop independently in time (without interference from the neighbouring spurs). As LET increases, the mean separation distance between the spurs decreases and the isolated spur structure changes to a situation in which the spurs overlap and form a dense continuous column (cylindrical shape) (Figure 1.2*b*).

*ii) High-LET radiation tracks*

The column of species defined initially by the overlapping spurs along the path of a high-LET particle makes up what is referred to as the "track core". It is surrounded by a coaxial region traversed by large numbers of emergent, comparatively low-LET secondary electrons (δ-rays), called the "penumbra" (for example, see: PUCHEAULT, 1961; MOZUMDER et al., 1968; CHATTERJEE and SCHAEFER, 1976; FERRADINI,

1979; MAGEE and CHATTERJEE, 1980, 1987; PARETZKE, 1987; MOZUMDER, 1999; LAVERNE, 2000, 2004). Such a "high-LET" radiation track structure can actually be seen in heavy-ion irradiations (PLANTE et al., 2005; MUROYA et al., 2006). It is illustrated schematically in Figure 1.3.

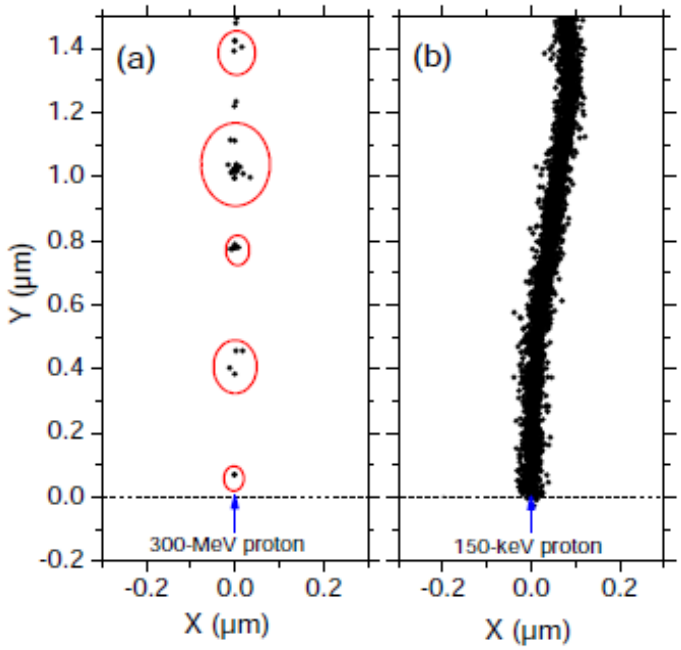


Figure 1.2 Projections into the *XY*-plane of figure of track segments of 300 (a) and 0.15 (b) MeV protons (LET ~ 0.3 and 70 keV/µm, respectively) incident on liquid water at 25 °C, calculated (at ~$10^{-13}$ s) with our Monte Carlo simulation code (KANIKE et al., 2015*a*). The two irradiating protons are generated at the origin and start moving along the *Y* axis. Dots represent the energy deposited at points where an interaction occurred.

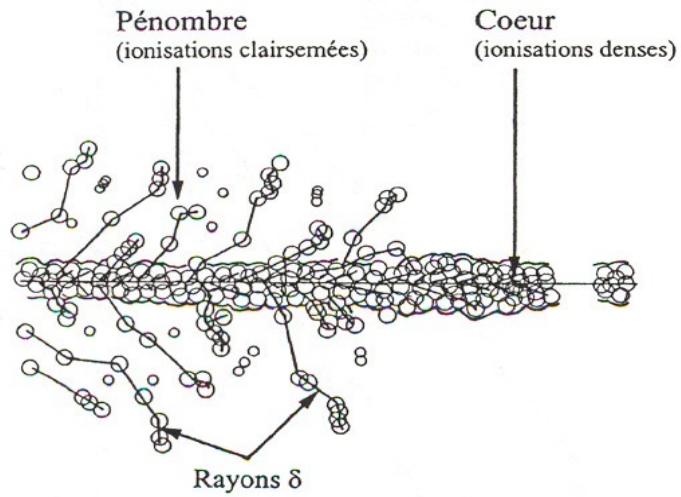


Figure 1.3 Primary energy-loss events in high-LET radiation tracks (FERRADINI, 1979).

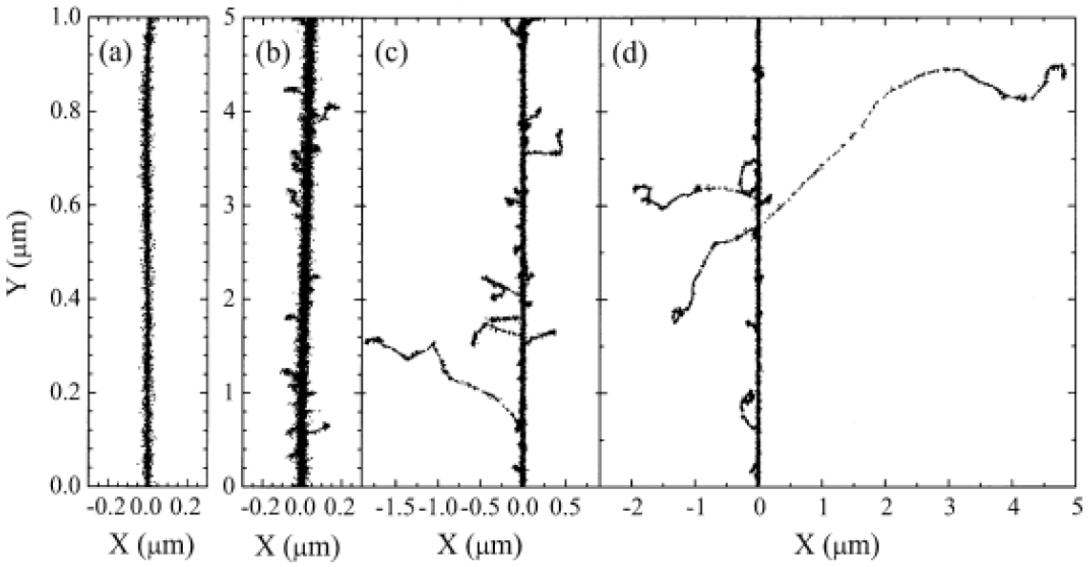


Figure 1.4 Projections over the *XY*-plane of track segments calculated (at ~$10^{-13}$ s) for (a) $H^+$ (0.15 MeV), (b) $^4He^{2+}$ (1.75 MeV/nucleon), (c) $^{12}C^{6+}$ (25.5 MeV/nucleon), and (d) $^{20}Ne^{10+}$ (97.5 MeV/nucleon) impacting ions. Ions are generated at the origin and along the *Y* axis in liquid water under *identical* LET conditions (~70 keV/μm). Dots represent the energy deposited at points where an interaction occurred. From MUROYA et al. (2006), with permission.

Figure 1.4 illustrates typical two-dimensional representations of short (1-5 μm) track segments of $H^+$, $^4He^{2+}$, $^{12}C^{6+}$, and $^{20}Ne^{10+}$ ions, calculated with our own Monte Carlo simulation code under the same LET conditions (~70 keV/μm). As one can see, these tracks can be considered as straight lines with the ejected high-energy secondary electrons travelling to a greater average distance away from the track core as the velocity of the incident ion increases, from protons to neon ions. In other words, even though all those particles are depositing the same amount of energy per unit path length, that energy is lost in a volume that increases in the order $H^+ < {}^4He^{2+} < {}^{12}C^{6+} < {}^{20}Ne^{10+}$, indicating that the higher-*Z* particle (where *Z* is the ion charge number) has the lower mean density of reactive species (MUROYA et al., 2006; MEESUNGNOEN and JAY-GERIN, 2011). The fact that tracks of different ions with the same LET have different radial distributions of energy deposited by δ-rays is in accord with Bethe's theory of stopping power (BETHE, 1930; BETHE and ASHKIN, 1953) and indicates that LET is not a unique descriptor of the radiation chemical effects within heavy-charged particle tracks

(SCHULER and ALLEN, 1957; SAUER et al., 1977; LAVERNE and SCHULER, 1987; KAPLAN and MITEREV, 1987; FERRADINI, 1990; FERRADINI and JAY-GERIN, 1999; LAVERNE, 2000, 2004). Attempts have been made to introduce other comparative characteristics of radiation track effects to replace LET like, for example, the $(Z^*/\beta)^2$ factor (where Z* is an energy-dependent effective charge of the ion and β is the ratio of its velocity to that of light) (KATZ, 1970; WALIGÓRSKI et al., 1986; YAMASHITA et al., 2008) or yet the parameter $MZ^2/E$ (where $M$ is the ion mass and $E = ½MV^2$ its kinetic energy) (LAVERNE, 2004). Several sets of radiation chemical data appear to be better unified using these phenomenological parameters instead of LET, others do not. Following PIMBLOTT and LAVERNE (2002), it should be recognized, however, that no deterministic parameterization can realistically represent a phenomenon that is stochastic in nature. Nevertheless, despite its limitations, LET still remains the most useful single parameter in the radiation chemistry of heavy ions.

### *1.1.2 Time scale of events and formation of primary free-radical and molecular products in neutral water radiolysis*

From the viewpoint of pure aqueous radiation chemistry, the successful prediction of the effects of radiation type and energy in radiolysis not only requires a realistic description of the early physical aspects of the radiation track structure, but also an accurate modelling of the temporal development of the track, in which the various radiolytic species are specified and allowed to diffuse from their initial positions and react with one another (or with the environment) (MUROYA et al., 2006). Therefore, it is critical to understand how the radiation quality (LET) and the irradiation conditions affect the subsequent water decomposition products, their space distribution and thereby the observed yields. Finally, it is also important to know how the initial, spatially nonhomogeneous distribution of reactive species relaxes in time toward a homogeneous distribution.

The complex events that accompany the absorption of high-energy photons or the passage of fast charged particles in liquid water can usually be divided into three, more or less clearly demarcated, consecutive, temporal stages: physical, physicochemical, and chemical (PLATZMAN, 1958; KUPPERMANN, 1959). These stages correspond with

the initial dissipation of energy in the system, the establishment of thermal equilibrium, and the establishment of chemical equilibrium, respectively (Figure 1.5). In a physiologic system, there follows a biological stage in which the cells respond to the damage resulting from the products formed in the preceding stages. These four different stages are briefly described below (for recent reviews on the subject, see: MEESUNGNOEN and JAY-GERIN, 2011; AZZAM et al., 2012).

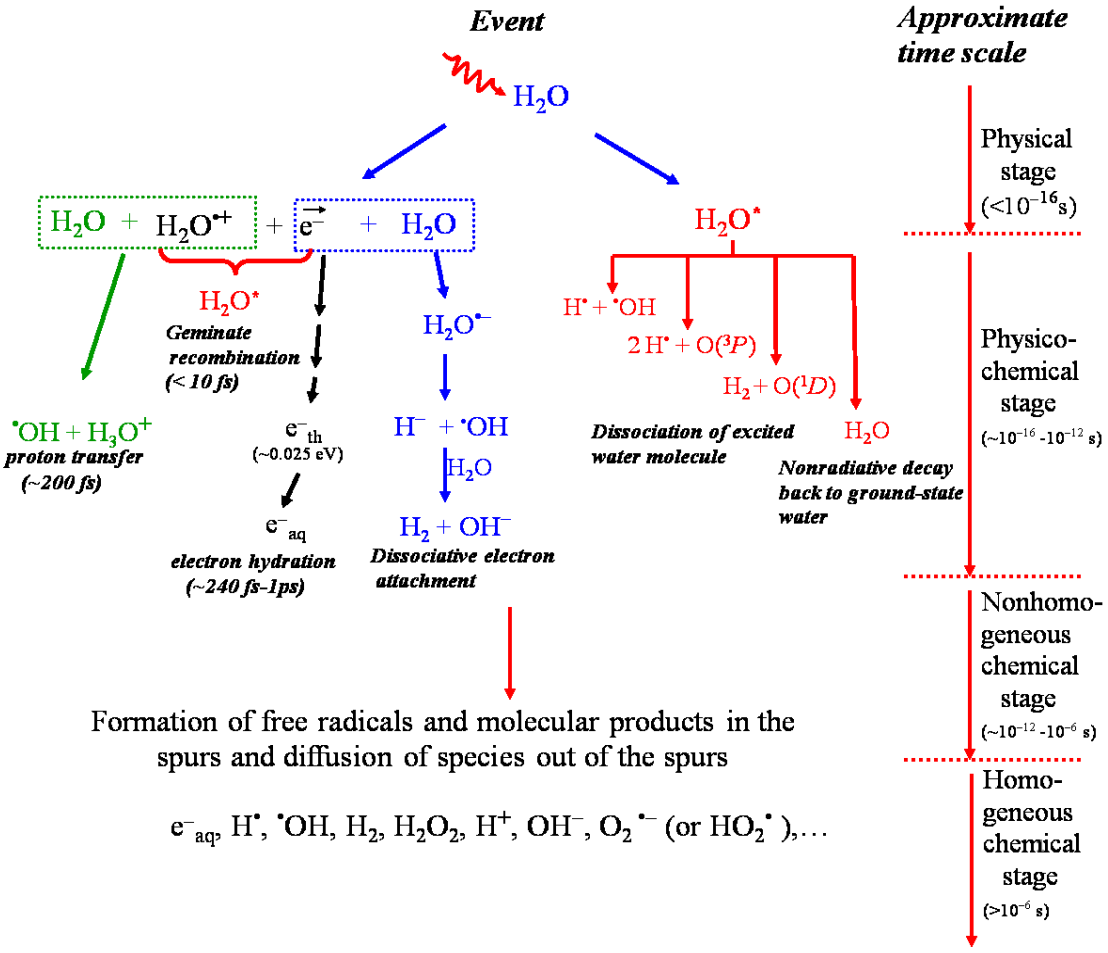


Figure 1.5 Time scale of events in the radiolysis of water by low-LET radiation. The time scale of chemical reactions leading to generation of specific radiolytic products is also shown.

### *(i) The "physical" stage*

The physical stage consists of the phenomena by which energy is transferred from the incident high-energy radiation to the water. Its duration is less than ~$10^{-16}$ s. The result of this energy absorption is the production, along the path of the radiation, of a large number of ionized and electronically excited water molecules, denoted $H_2O^{\bullet+}$ and $H_2O^*_{elec}$, respectively, and secondary electrons are generated:

$$H_2O \rightsquigarrow H_2O^{\bullet+} + e^- \text{ (ionization)} \qquad [3]$$

$$H_2O \rightsquigarrow H_2O^*_{elec} \text{ (excitation)} \qquad [4]$$

Note that $H_2O^*_{elec}$ represents here many excited states, including the so-called "superexcited" states (PLATZMAN, 1962*a*) and the excitations of collective electronic oscillations of the "plasmon" type (HELLER et al., 1974; KAPLAN and MITEREV, 1987; LAVERNE and MOZUMDER, 1993; WILSON et al., 2001).

Generally, the electron ejected in the ionization event has sufficient energy either to ionize or excite one or more other water molecules in the vicinity, and this leads, as mentioned above, to the formation of track entities, commonly known as "spurs", that contain the products of the events.

### *(ii) The "physicochemical" stage*

The ions and excited-state water molecules formed during the physical stage are extremely unstable and undergo fast reorganization in this second or physicochemical stage, which lasts not more than ~$10^{-12}$ s after the initial energy deposition. These processes produce radical and molecular products of the radiolysis that are distributed in a highly nonhomogeneous track structure.

In the time scale of ~200 fs (LI et al., 2013), the positive ion $H_2O^{\bullet+}$ decomposes to form an $^{\bullet}OH$ radical by transferring a proton to a neighbouring water molecule:

$$H_2O^{\bullet+} + H_2O \rightarrow H_3O^+ + {}^{\bullet}OH\,, \qquad [5]$$

where $H_3O^+$ (or equivalently, $H^+_{aq}$) represents the hydrated proton. However, before reaction [5] occurs, $H_2O^{\bullet+}$ may undergo a random walk via a sequence of resonant

electron transfers (about 21, on the average) from neighbouring water molecules to the $H_2O^{\bullet+}$ hole (or electron-loss center) (OGURA and HAMILL, 1973; MOZUMDER and MAGEE, 1975). The ranges of a migrating hole are a few molecular diameters (COBUT et al., 1998).

The secondary ("dry") electron ejected from an ionized water molecule undergoes scattering as it moves away from its parent cation. It can cause further ionization and excitation to occur if it has sufficient kinetic energy. Eventually, its energy falls below the first electronic excitation threshold of water (~7.3 eV; MICHAUD et al., 1991), forming the so-called "subexcitation electron" ($e^-_{sub}$) (PLATZMAN, 1955). The latter loses the rest of its energy relatively slowly by exciting vibrational and rotational modes of water molecules. Once it is thermalized ($e^-_{th}$) (after ~10-40 fs at 25 °C; see GOULET et al., 1990, 1996; MEESUNGNOEN et al., 2002*a*), it can get localized or "trapped" ($e^-_{tr}$) in a pre-existing potential energy well of appropriate depth in the liquid (then forming the so-called "wet" electron whose exact physicochemical nature is still the subject of investigation) before reaching a fully relaxed, hydrated state ($e^-_{aq}$) as the dipoles of the surrounding molecules orient in response to the negative charge of the electron. In liquid water at room temperature, thermalization, trapping, and hydration can then follow in quick succession (on the time scale of ~240 fs-1 ps, as revealed from time-resolved femtosecond laser spectroscopic studies) (MOZUMDER, 1999; JAY-GERIN et al., 2008; MEESUNGNOEN and JAY-GERIN, 2011):

$$e^- \rightarrow e^-_{sub} \rightarrow e^-_{th} \rightarrow e^-_{tr} \rightarrow e^-_{aq} \qquad [6]$$

In the course of its thermalization, the slowing-down electron can be recaptured by its parent cation (prior to the occurrence of reaction [5]) due to the Coulomb attraction of the latter which tends to draw them back together to undergo electron-cation "geminate" recombination:

$$e^- + H_2O^{\bullet+} \rightarrow H_2O^*_{vib} \, . \qquad [7]$$

As the electron is recaptured, the parent ion is transformed into a (vibrationally) excited neutral molecule.

In the course of its thermalization, the ejected electron can also be temporarily captured resonantly by a water molecule to form a transient molecular anion:

$$e^- + H_2O \rightarrow H_2O^- \, . \qquad [8]$$

This anion then undergoes dissociation mainly into $H^-$ and $^\bullet OH$ according to

$$H_2O^- \rightarrow H^- + {}^\bullet OH \, , \qquad [9]$$

followed by the reaction of the hydride anion ($H^-$) with another water molecule through a fast proton transfer reaction:

$$H^- + H_2O \rightarrow H_2 + OH^- \qquad [10]$$

Reactions [8]-[10] correspond to the so-called "dissociative electron attachment" or DEA process, which has been observed in amorphous solid water at ~20 K for electron energies between about 5 and 12 eV (ROWNTREE et al., 1991). It has been suggested that DEA to water was responsible, at least in part, for the yield of "nonscavengeable" molecular hydrogen observed experimentally in the radiolysis of liquid water at early times (PLATZMAN, 1962*b*; FARAGGI and DÉSALOS, 1969; GOULET and JAY-GERIN, 1989; KIMMEL et al., 1994; COBUT et al., 1996; MEESUNGNOEN et al., 2015). Recent experiments have sustained this proposed mechanism for the production of $H_2$, by showing that the previously accepted nonscavengeable yield of $H_2$ is due to precursors of $e^-_{aq}$ (*i.e.*, "dry" or "pre-hydrated" electrons) and it can be lowered with suitable scavengers in sufficiently high concentrations (PASTINA et al., 1999).

Excited water molecules may be produced directly in an initial act (reaction [4]) or by neutralization of an ion (reaction [7]). Very little is known about the decay channels for an excited water molecule in the liquid phase and the branching ratios associated with each of them. Fortunately, the contribution of the water excited states to the primary radical and molecular products in water radiolysis is of relatively minor importance in comparison with that of the ionization processes, so that the lack of information about their decomposition has only limited consequences. Hence, the competing de-excitation mechanisms of $H_2O^*$ are generally assumed to be essentially the same as those reported

for an isolated water molecule,[2] namely (for example, see: SWIATLA-WOJCIK and BUXTON, 1995; COBUT *et al.*, 1998; MEESUNGNOEN and JAY-GERIN, 2005*a*; SANGUANMITH et al., 2011*a*; KANIKE et al., 2015*b*),

$$H_2O^* \rightarrow H^\bullet + {}^\bullet OH \quad [11a]$$
$$H_2O^* \rightarrow H_2 + O(^1D) \quad [11b]$$
$$H_2O^* \rightarrow 2H^\bullet + {}^\bullet O^\bullet(^3P) \quad [11c]$$
$$H_2O^* \rightarrow H_2O + \text{release of thermal energy} \quad [11d]$$

where $O(^1D)$ and ${}^\bullet O^\bullet(^3P)$ represent the oxygen atom in its singlet $^1D$ first excited state and triplet $^3P$ ground state, respectively (see Figure 1.5). Specific to the liquid phase, the following dissociation reaction:

$$H_2O^* \rightarrow e^-_{aq} + H_2O^{\bullet+} \quad [11e]$$

also needs to be considered in the menu of possibilities that can lead to the decay of $H_2O^*$. Its threshold is at ~6.5 eV (NIKOGOSYAN et al., 1983; MIGUS et al., 1987; BERNAS et al., 1997).

It is believed that reaction [11*a*] is the main source of the "initial" (*i.e.*, at $\sim 10^{-12}$ s, prior to spur/track expansion) yield of hydrogen atoms. Note also that the $O(^1D)$ atoms produced in reaction [11*b*] react very efficiently with water to form $H_2O_2$ (or probably also $2{}^\bullet OH$) (TAUBE, 1957; BIEDENKAPP et al., 1970). By contrast, the ground-state $O(^3P)$ atoms in aqueous solution are rather inert to water but react with most additives (AMICHAI and TREININ, 1969). As for the values of the branching ratios (or decay probabilities) used for the different decay channels [11*a*-*e*], they are chosen in order to consistently match the observed picosecond *G*-values of the various spur species (MUROYA *et al.*, 2002; MEESUNGNOEN and JAY-GERIN, 2005*a*).

By ~1 ps following the passage of the radiation, the various initial radiolysis products are: $e^-_{aq}$, $H^\bullet$, $H_2$, ${}^\bullet OH$, $H_2O_2$, $H^+$ (or $H_3O^+$), $OH^-$, $O_2^{\bullet-}$ (or $HO_2^\bullet$, depending on the pH), ${}^\bullet O^\bullet(^3P)$, *etc*. At this time, these species begin to diffuse away from the position where they were originally produced. The result is that a fraction of them react together

[2] It should be noted that the same decay processes have been reported to occur for the electronically and vibrationally excited $H_2O$ molecules in the gas phase.

within the spurs/tracks as they develop in time while the remainder escape into the bulk solution in the chemical stage.

***(iii) The "chemical" stage***

The third or chemical stage consists of diffusion and reactions of the reactive species present at the end of the physicochemical stage and initially distributed nonhomogeneously with high concentrations in the center of spurs or along the axis of tracks. This stage is usually divided into two parts. The first part corresponds to the stage of "nonhomogeneous chemistry", which consists of the period after ~$10^{-12}$ s, during which spurs or tracks develop in time. A number of like radicals will combine to form the molecular products $H_2$ and $H_2O_2$; a number will combine to re-form $H_2O$, while the remainder will diffuse out into the bulk of the solution. At 25 °C, the spur/track expansion is essentially complete by ~$10^{-7}$-$10^{-6}$ s (for example, see: BUXTON et al., 1987; SANGUANMITH et al., 2012). At this time, the species that have escaped from spur or track reactions become homogeneously distributed throughout the bulk solution (*i.e.*, the system at large) (PLANTE et al., 2005; MUROYA et al., 2006). Beyond a few microseconds, the reactions which occur in the bulk solution can usually be described with conventional homogeneous chemistry methods. This is the second part of the chemical stage, the so-called stage of "homogeneous chemistry". The radical and molecular products which emerge from the spurs/tracks are then available for reaction with dissolved solutes (if any) present (in low or moderate concentrations) at the time of irradiation.

***(iv) The "biological" stage***

The biological stage is the final stage in a physiologic system, the cells responding to the damage resulting from the products formed in the preceding stages. During this stage (~$10^{-3}$ s or longer, depending very much upon the medium), the biological responses affecting the long-term consequences of radiation exposure are induced.

In air-saturated solutions (where the concentration of dissolved oxygen in the water is ~2.5 × $10^{-4}$ M at 25 °C), $e^-_{aq}$ and $H^\bullet$ atoms are rapidly (on a time scale of a few

tenths of a microsecond) converted to superoxide radical anion ($O_2^{\bullet-}$)/hydroperoxyl ($HO_2^{\bullet}$) radicals, according to:

$$e^-_{aq} + O_2 \rightarrow O_2^{\bullet-} \qquad k_{12} = 2.34 \times 10^{10}\ M^{-1}\ s^{-1} \qquad [12]$$

$$H^{\bullet} + O_2 \rightarrow HO_2^{\bullet} \qquad k_{13} = 1.31 \times 10^{10}\ M^{-1}\ s^{-1} \qquad [13]$$

where $k_{12}$ and $k_{13}$ are the rate constants for the two individual reactions (ELLIOT and BARTELS, 2009). Accordingly, in an aerobic cellular environment at pH 7, the major reactive species at homogeneity include $O_2^{\bullet-}$, $^{\bullet}OH$, and $H_2O_2$ (the other molecular product, $H_2$, is relatively inert and normally plays only little part in the radiolysis of aqueous solutions, most of it escaping from solution) (SPINKS and WOODS, 1990).

In biological systems, ionizing radiation can also stimulate inducible nitric oxide synthase (iNOS) activity in hit cells (MIKKELSEN and WARDMAN, 2003), thereby generating large amounts of nitric oxide $^{\bullet}NO$ (officially called nitrogen monoxide). Although $^{\bullet}NO$ is chemically inert toward most cellular constituents (except for heme), it reacts quickly with $O_2^{\bullet-}$ to form the peroxynitrite anion ($ONOO^-$) with a rate constant ($1.9 \times 10^{10}\ M^{-1}\ s^{-1}$) that is larger than that for the copper/zinc-superoxide dismutase (SOD)-catalyzed disproportionation of $O_2^{\bullet-}$ ($4 \times 10^9\ M^{-1}\ s^{-1}$) (KOPPENOL, 1998; JAY-GERIN and FERRADINI, 2000). Like $^{\bullet}OH$ radicals, $ONOO^-$ and its conjugate acid, peroxynitrous acid ONOOH ($pK_a = 6.8$ at 37 °C) (PRYOR and SQUADRITO, 1995), are powerful oxidizing agents. They are capable of attacking a wide range of cellular targets, including lipids, thiols, proteins, and DNA bases (for example, see: HALLIWELL and GUTTERIDGE, 2015).

### *1.1.3 Spurs/tracks are acidic*

The major reducing radical formed in neutral solutions during water radiolysis was shown experimentally to bear a unit negative charge (CZAPSKI and SCHWARZ, 1962; COLLINSON et al., 1962), a result that contributed to the discovery of the "hydrated electron" in 1962 (HART and ANBAR, 1970). This suggests that an ejected electron can escape from its parent $H_2O^{\bullet+}$ ion and that $H_2O^{\bullet+}$ ions temporarily exist in a spur. The formation of $H_3O^+$ via the proton transfer reaction [5] therefore renders the spur

more acid than the body of the solution (SPINKS and WOODS, 1990). Some experimental evidence for this acid pH effect has been reported by several authors. For example, SMITH and STEVENS (1963) irradiated aqueous solutions of 1,1-diethoxyethane [$CH_3CH(OC_2H_5)_2$] buffered at pH 7 with 50-$kV_p$ X-rays and showed that hydrolysis catalyzed by $H_3O^+$ ions formed during the primary radiolytic processes in water:

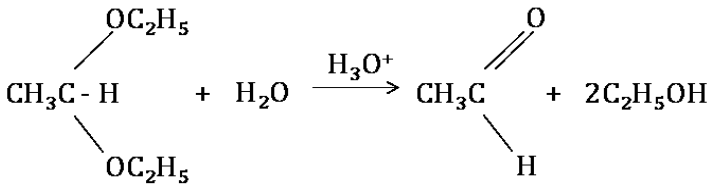

[14]

occurred. Assuming a spherically symmetric spur with a radius of 3 nm, the authors estimated that the pH in the spur would need to be ~1.4 to account for the observed hydrolysis. Another experiment indicative of an acid spur was the observation of a transient absorption attributed to $Cl_2^{\bullet-}$ in the pulse radiolysis of neutral aqueous sodium chloride solutions at $Cl^-$ concentrations of 0.1 M or greater (ANBAR and THOMAS, 1964). The formation of $Cl_2^{\bullet-}$ normally requires an acid medium. The results suggested the importance of $H_3O^+$ ions in the pH-dependent reaction of radiation-induced $^{\bullet}OH$ radicals with chloride ions (MATSUYAMA and NAMIKI, 1965):

$$Cl^- + {}^{\bullet}OH + H_3O^+ \rightarrow Cl^{\bullet} + 2H_2O \qquad [15]$$

followed by the combination of the $Cl^{\bullet}$ atom with $Cl^-$ to form $Cl_2^{\bullet-}$:

$$Cl^{\bullet} + Cl^- \rightarrow Cl_2^{\bullet-}. \qquad [16]$$

in the "spur" regions at early time.

Apart from these few experiments aiming at demonstrating this transient acid pH effect in a spur, there is only fragmentary information on its magnitude and time dependence following energy deposition. Moreover, the influence of the quality (or LET) of the radiation on the pH has not been investigated. In this work, our objective is to calculate quantitatively the pH values prevailing in the spur or track regions, using the general relationship:

$$C = \rho \, \mathcal{D} \, G \, , \qquad [17]$$

where $C$ is the concentration of species, $\rho$ is the density of the solution (1 g/cm$^3$ for liquid water at 25 °C), $\mathcal{D}$ is the radiation dose, and $G$ is the chemical yield (for example, see: HUMMEL, 1995). Note that with $C$ in mol/dm$^3$, $\mathcal{D}$ in J/kg (or Gy), and $G$ in mol/J, the density is to be expressed in kg/dm$^3$ in order to have a consistent set of units.

Keeping in mind that the pH is defined as the negative logarithm (base 10) of the concentration of $H_3O^+$ ions:

$$\mathrm{pH}(t) = -\log\left\{\left[\mathrm{H_3O^+}\right](t)\right\} \, , \qquad [18]$$

we thus need to estimate the concentration of hydronium ions generated *in situ* in the spur or track regions as a function of time as well as the time evolution of $G(H_3O^+)$ produced in the radiolysis of pure, deaerated water. As for the calculation of the radiation dose, we selected two different spatio-temporal models of a spur or track:

i. *An isolated "spherical" spur model* characteristic of low-LET radiation

ii. *An axially homogeneous "cylindrical" track model* for high-LET radiation

which are described below.

*Spherical spur model*

For low-LET radiation (for example, 300-MeV irradiating protons, LET ~ 0.3 keV/μm), we assume that the hydronium ions are produced evenly in an isolated spherical spur. The spur's initial radius $r_o$, prior to spur expansion, is equal to the average electron thermalization distance ($r_{th}$) obtained from our Monte Carlo simulations (~11.7 nm at 25 °C) (GOULET et al., 1990, 1996; MEESUNGNOEN and JAY-GERIN, 2005*a*). The low-LET spur concentrations of $H_3O^+$ are derived from

$$\left[\mathrm{H_3O^+}\right](t) = G\left(\mathrm{H_3O^+}\right)(t) \times \left( \frac{\text{Mean energy loss/event}}{\frac{4}{3}\pi \, r(t)^3} \right) , \qquad [19]$$

where the mean energy loss in a single energy deposition event (*i.e.*, the mean energy deposited in a spur) in liquid water is taken to be ~47 eV (COBUT, 1993; COBUT et al., 1998; AUTSAVAPROMPORN, 2006; MIRSALEH KOHAN et al., 2013) and

$$r(t)^2 = r_o^2 + 6\,D\,t \qquad [20]$$

represents the change with time of $r_o$ due to the three-dimensional diffusive expansion of the spur. Here, $t$ is time and $D$ is the diffusion coefficient of $H_3O^+$ in water ($D$ = 9.46 × $10^{-9}$ $m^2$ $s^{-1}$ at 25 °C) (FRONGILLO et al., 1998; TIPPAYAMONTRI et al., 2009).

Figure 1.6 shows the distribution of energy-loss events calculated for 150-keV incident electrons in liquid water at 25 °C using our Monte Carlo simulation code (AUTSAVAPROMPORN, 2006; MIRSALEH KOHAN et al., 2013). In the calculations, each simulation typically involved ~$10^4$-$10^5$ different primary tracks. The most probable energy loss in a single event was 15-20 eV, while the mean energy loss was ~47 eV/event. These values are in good agreement with those (22-23 and 56.8 eV, respectively) calculated previously for electrons with 1 MeV incident energy in liquid water (LAVERNE and PIMBLOTT, 1995).[3] They clearly indicate that most energy-loss events by fast electrons involve small transfers of energy (MOZUMDER, 1999). Note also that the various minima observed in the energy-loss distribution below 35 eV are associated with the abrupt changes in the total cross section due to the thresholds for electronic excitations and ionizations (or for multiple-scattering events involving these electronic energy losses) in this energy range (COBUT et al., 1998; MEESUNGNOEN et al., 2002*b*).

[3] It has been demonstrated that the probability of a given energy loss in a collision shows very little dependence on the incident electron energy from 10 keV to 1 MeV (for example, see: COBUT et al., 1998; PIMBLOTT et al., 1990; LAVERNE and PIMBLOTT, 1995).

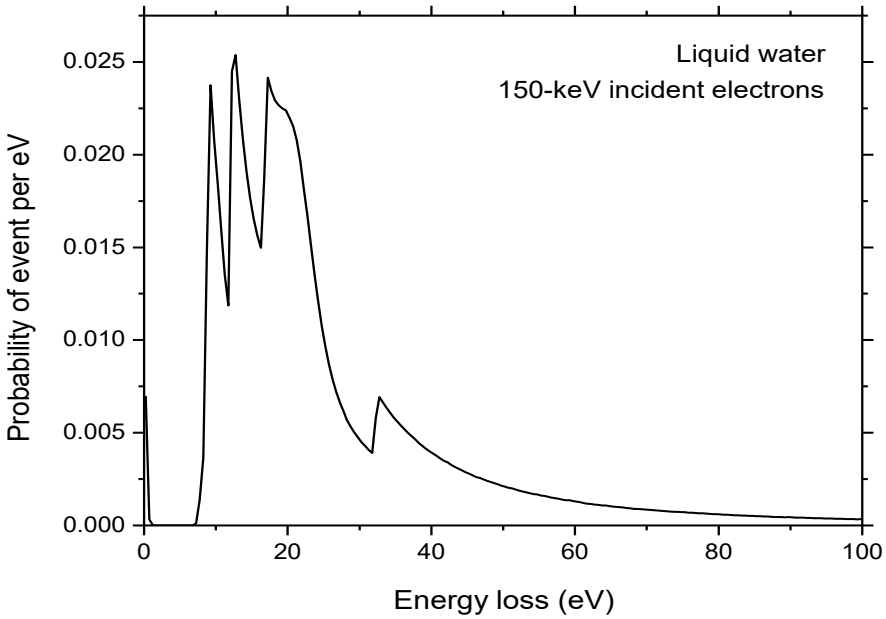


Figure 1.6 Frequency of a given energy loss for 150-keV incident electrons in liquid water at 25 °C. Electrons are followed over their whole track until their energy is lower than ~7.3 eV (threshold for electronic excitation). The corresponding average energy loss per event is ~47 eV. $10^4$-$10^5$ different track histories were used in the simulations.

*Cylindrical track model*

For high-LET radiation, we consider the track as being an axially homogeneous cylinder, of length $L$ = 1 µm and initial radius $r_c$ equal to the radius of the physical track "core" (which corresponds to the tiny radial region within the first few nanometers around the impacting ion trajectory). In this region the energy density of deposition is very high (CHATTERJEE and HOLLEY, 1993; MEESUNGNOEN and JAY-GERIN, 2011; MOZUMDER, 1999; MAGEE and CHATTERJEE, 1980, 1987). For the sake of illustration, we have considered track segments of three different high-LET irradiating ions: i) 150-keV protons (LET ~ 70 keV/µm), ii) 1.75-MeV/nucleon helium ions (LET ~ 70 keV/µm), and iii) 0.6-MeV/nucleon helium ions (LET ~ 146 keV/µm) in liquid water at 25 °C. The simulated track segments were calculated (at ~$10^{-13}$ s) with our Monte Carlo simulation code (KANIKE et al., 2015*b*, figures 5-7). In this case, the high-LET track concentrations of $H_3O^+$ are simply obtained from (MEESUNGNOEN and JAY-GERIN, 2011):

$$\left[H_3O^+\right](t) = G\left(H_3O^+\right)(t) \times \left(\frac{LET}{\pi\, r(t)^2}\right), \qquad [21]$$

where

$$r(t)^2 \;=\; r_c^{\,2} + 4\,D\,t \qquad [22]$$

represents the change with time of $r_c$ due to the two-dimensional diffusive expansion of the track. Here, $r_c$ was estimated directly from our simulations (KANIKE et al., 2015*b*).

Using equations [21] and [22] readily gives the concentrations of $H_3O^+$ as a function of time for axially homogeneous, cylindrically symmetric tracks. The pH in the corresponding track regions is then simply given by equation [18].

## 1.2 Many cellular processes critically depend on pH

The pH is a measure of the acidity (or alkalinity) of a solution. It is a measure of the concentration of hydrogen ions ($H^+$; proton). The $H^+$ ion concentration is one of the most important parameters which determine the rates and steady state concentrations in chemical and biochemical reactions. The higher the concentration of hydrogen ions in a solution the more acidic it is and the lower their concentration the more alkaline it is. A substance that donates $H^+$ to or accepts $OH^-$ ions from its environment is called an "acid", it lowers the pH. An acidic solution will have a pH below 7. A substance that accepts $H^+$ or donates $OH^-$ is called a "base" and it raises the pH. An alkaline solution will have a pH greater than 7. When acids and bases are brought together they may neutralize each other. Technically free protons ($H^+$) do not exist in water. They react with water molecules to form a hydronium ion ($H_3O^+$), which actually is a "hydrated" proton ($H^+_{aq}$). In the present work, we focus on the temporary acidic environment (pH < 7) due to the *in situ* radiolytic formation of $H_3O^+$ within the spurs and tracks of the radiolysis of water during and shortly after irradiation before homogeneity of the reacting species is attained.

Many cellular processes critically depend on pH, among which we can cite for example: (i) the *superoxide radical anion* ($O_2^{\bullet-}$), which is biologically quite toxic and is deployed by the immune system to kill invading microorganisms; (ii) the *nitric oxide* ($^{\bullet}NO$), which is an important cellular signalling molecule involved in many physiological and pathological processes; (iii) the *enzymes*, which are protein-based substances that

serve as catalysts in living organisms by regulating the rates of spontaneous chemical reactions. The rate of reaction does not solely depend on the free energy difference between the initial and final states, but also on the actual path through which the reactants are transformed into products; and (iv) the *abasic sites* in DNA, which correspond to the loss of purines (guanine, adenine) or pyrimidines (thymine, cytosine) by N-C bond cleavage from DNA. These are potentially mutagenic and lethal lesions that can block DNA replication and transcription. More information on all these points above is given in the Discussion section of this thesis.

### 1.3 pH in nuclear reactors

One of the most significant challenges in controlling the water chemistry of current (Generation III or less) water reactor systems (which operate in the ~250-330 °C temperature range and ~7-15 MPa pressure) and proposed more efficient Generation IV nuclear reactor designs with water under supercritical conditions (typically, ~300-625 °C and 25 MPa) is understanding and mitigating water radiolysis effects (COHEN, 1980; McCRACKEN et al., 1998; GUZONAS et al., 2010). Since the coolant water is circulated in the reactor core, it is irradiated by intense fluxes of ionizing radiations comprising low-LET γ-rays, fast neutrons whose energy is transferred to recoil protons and oxygen nuclei of high LET, and also much higher LET radiation (recoil of $^{7}Li$ ions and α-particles) associated with the nuclear reactions of thermal neutrons with boron-10 (used as a reactivity control chemical). This irradiation results in the chemical decomposition (radiolysis) of water and leads to the formation of a variety of oxidizing (transient and stable) products such as $^{\bullet}OH$, $H_2O_2$ and its decomposition product $O_2$, and $O_2^{\bullet-}$ (or its protonated form $HO_2^{\bullet}$, depending on the pH) that can cause corrosion, cracking and hydrogen pickup both in the core and in the associated piping components of the reactor (for example, see: COHEN, 1980; FÉRON and OLIVE, 2007). Problems from corrosion can affect the transport and deposition of both corrosion products and radionuclides, thereby influencing the long-term integrity and performance of reactors in addition to increasing radioactive contamination and radiation risk to personnel. In current pressurized water reactors, one commonly used chemical control measure to limit unwanted corrosion and degradation of materials by oxidizing species is to add a small

concentration of excess $H_2$ (~5 × $10^{-4}$-2 × $10^{-5}$ M) to the reactor coolant (ELLIOT and McCRACKEN, 1990; McCRACKEN et al., 1998; PASTINA et al., 1999; BARTELS et al., 2013; KANJANA et al., 2013; COOK and LISTER, 2014). This molecular hydrogen participates to a chain reaction, which is propagated by the $H^{\bullet}$ atom and the $^{\bullet}OH$ radical and which recombines $H^{\bullet}$, $^{\bullet}OH$, and $H_2O_2$ back to water:

$$^{\bullet}OH + H_2 \rightarrow H^{\bullet} + H_2O \quad [23]$$

$$H^{\bullet} + H_2O_2 \rightarrow {}^{\bullet}OH + H_2O\ , \quad [24]$$

the overall result being suppression of the net radiolytic production of oxidizing species.

For neutral water, there is an equilibrium established between the water molecules and the dissociation products $H^+$ (or $H_3O^+$) and $OH^-$ (called water's "autoprotolysis"), as follows:

$$2H_2O \rightleftharpoons H_3O^+ + OH^- \quad [25]$$

with the water autoprotolysis constant

$$K_w = [H_3O^+][OH^-] \quad [26]$$

equal to $10^{-14}$ at 25 °C (for example, see: MONK, 2004). Since in pure water $[H_3O^+] = [OH^-]$, then the concentrations of $H_3O^+$ and $OH^-$ can be determined by taking the square root of $K_w$. Hence, both $[H_3O^+]$ and $[OH^-]$ due to water's autoprotolysis equal $10^{-7}$ M in pure water at room temperature, indicating that only a very tiny fraction of water molecules are present as ions. According to the definition of pH in equation [18], the pH of pure water at equilibrium at 25 °C then equals -log ($10^{-7}$), which is 7.

The dissociation of water is dependent upon temperature (BANDURA and LVOV, 2006; ELLIOT and BARTELS, 2009). This is illustrated in Figure 1.7, which shows the temperature dependence of the pH of neutral water in the range of 25-350 °C. As can be seen from the figure, the pH is 7 at room temperature, decreases significantly to 5.69 at 250 °C before starting to increase again. The pH at 350 °C is about 6.19. This change in pH is solely a consequence of the effects of temperature change on water dissociation.

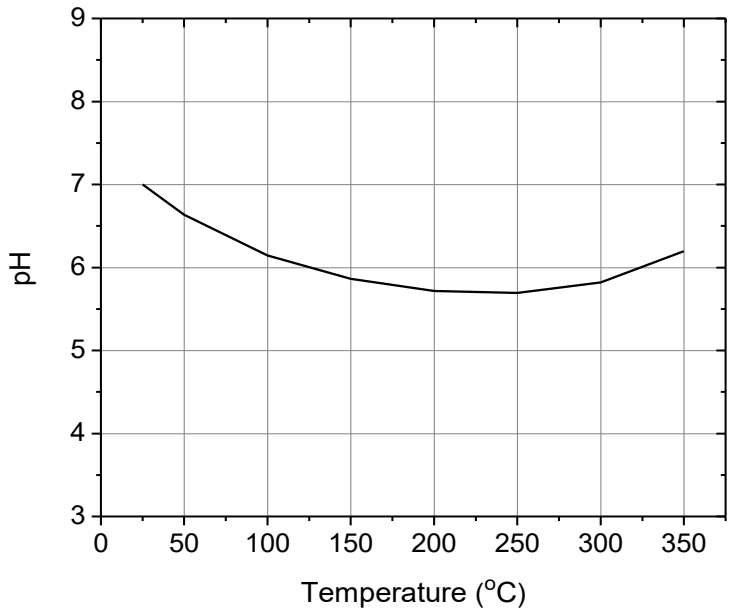


Figure 1.7 Temperature dependence of pH in pure water (ELLIOT and BARTELS, 2009).

Our most recent work is reported in Chapter 5 of this thesis, briefly mentioned in this section. In our work we calculated the time evolution of the pH values prevailing in spurs of the low-LET radiolysis of pure, deaerated water at elevated temperatures upto 350 °C (KANIKE et al., 2016). The total spur concentration of hydronium ions was obtained as the sum of the (time-dependent) concentration of $H_3O^+$ radiolytically produced *in situ* in these regions and of the (time-independent) non-radiolytic, pre-irradiation concentration of $H_3O^+$ that arises through water's autoprotolysis:

$$[H_3O^+]_{total}(t) = [H_3O^+]_{radiolytic}(t) + [H_3O^+]_{autoprotolysis} . \qquad [27]$$

The pH in the corresponding spur region is then simply given by the negative decimal logarithm of $[H_3O^+]_{total}(t)$:

$$pH(t) = -\log\{[H_3O^+]_{total}(t)\}. \qquad [28]$$

Direct observations or measurements of the chemistry in and around the core region of a nuclear reactor are extremely difficult, if not impossible. The extreme conditions of high temperature, pressure, and mixed radiation fields are not compatible

with normal chemical instrumentation. There are also problems of access to fuel channels in the reactor core. For these reasons, theoretical calculations and computer simulations have been used extensively by many investigators to model the radiation chemistry and reaction kinetics of transients under these conditions. A large amount of information on the reactivities, diffusion coefficients, and yields of the radiolytically-produced species, as well as on the physicochemical properties (viscosity, dielectric constant, $K_w$, etc.) of water and aqueous systems is needed in order to develop such models. A good summary of the present status of aqueous radiation chemistry at elevated temperatures (say, up to 350 °C) can be found in the literature (McCRACKEN et al., 1998; ELLIOT, 1994; CHRISTENSEN, 2006; TIPPAYAMONTRI et al., 2009; ELLIOT and BARTELS, 2009).

## 1.4 Research objectives

In this thesis, the aim of our work is to present simple spatio-temporal models of a spur or track to quantitatively show that the *in situ* formation of $H_3O^+$ in reaction [5], during the initial radiolytic processes in irradiated water, renders the spur/track regions temporarily more acid than the body of the solution. Although experimental evidence of this effect has already been reported by several authors in the literature, there is only fragmentary information on its magnitude and time dependence following energy deposition. Moreover, the influence of the quality (or LET) of the radiation has not been investigated. We use here Monte Carlo track chemistry simulations to calculate, at 25 °C, the time evolution of the yields of $H_3O^+$ produced in the radiolysis of pure, deaerated water from ~1 ps to 1 ms. As examples, simulations are carried out for four different impacting ions: (1) 300-MeV protons, which mimic $^{60}$Co γ/fast electron irradiation (LET ~ 0.3 keV/µm); (2) 150-keV protons (LET ~ 70 keV/µm); (3) 1.75-MeV per nucleon helium ions (LET ~ 70 keV/µm); and (4) 0.6-MeV per nucleon helium ions (LET ~ 146 keV/µm). The concentrations of $H_3O^+$ and the corresponding pH values for each ion considered are then obtained from our calculated yields of $H_3O^+$ using two different spur/track models depending on the LET of the radiation: (1) an isolated "spherical" spur model associated with low-LET radiation and (2) an axially homogeneous "cylindrical" track model associated with high-LET radiation. Finally, in the case of low-LET

radiolysis of water, the calculations are extended to examine whether this transient acid pH effect observed in spurs at 25 °C also exists at elevated temperatures (up to 350 °C). As we will see, this work raises a number of questions about the potential implications of this effect for radiobiology and water-cooled nuclear reactors.

# 2 - MONTE CARLO SIMULATIONS

The complex sequence of events that are generated in aqueous systems following the absorption of ionizing radiation can be modeled successfully by the use of Monte Carlo simulation methods.[4] Such methods are well suited to take into account the *stochastic* nature of the phenomena, provided that realistic probabilities and cross sections for all possible events are adequately known. Simulations then allow the reconstruction of the intricate action of radiation. It also offers a powerful tool for appraising the validity of different assumptions, for making a critical examination of proposed reaction mechanisms, and for estimating some unknown parameters. The accuracy of these calculations is best determined by comparing their predictions with experimental data on well-characterized chemical systems that have been examined with a wide variety of incident radiation particles and energies.

TURNER and his coworkers (1981, 1983, 1988*a*,*b*) at the Oak Ridge National Laboratory (Oak Ridge, Tennessee, USA) jointly with MAGEE and CHATTERJEE at Lawrence Berkeley Laboratory (Berkeley, California, USA) were the first to use Monte Carlo calculations to derive computer-plot representations of the chemical evolution of a few keV electron tracks in liquid water at times between ~$10^{-12}$ and $10^{-7}$ s. ZAIDER and BRENNER (1984) also used such an approach to simulate the fast reactions of radiolysis products in water, and their calculated time-dependent yields of $e^-_{aq}$ and $^{\bullet}OH$ radicals were somewhat similar to values measured or derived in pulse-radiolysis experiments. Following these pioneering works, stochastic simulation codes employing Monte Carlo procedures were developed independently by different researchers to study the relationship between the initial radiation track structure, the subsequent chemistry, and the stable end products formed by radiolysis (for reviews, see, for example: BALLARINI et al., 2000; UEHARA and NIKJOO, 2006; KREIPL et al., 2009; KARAMITROS et al., 2011; MEESUNGNOEN and JAY-GERIN, 2011).

---

[4] The "Monte Carlo method" is a general term (named after the famous European gambling center) used to describe any algorithm or computational method that employs random numbers. Simulation methods are used to estimate means of random variables or probabilistic features of models that we cannot compute analytically.

In a program begun in 1988, the Sherbrooke group also developed and progressively refined, with very high levels of detail, several Fortran-based Monte Carlo computer codes that simulate the nonhomogeneous distribution of reactive species initially produced in liquid water by the absorption of an incident radiation and all secondary electrons, as well as the subsequent chemical reactions of these species in time with one another or with available solutes (COBUT, 1993; COBUT et al., 1994, 1998; FRONGILLO et al., 1996, 1998; HERVÉ DU PENHOAT et al., 2000; MEESUNGNOEN et al., 2001, 2003, 2010; MEESUNGNOEN and JAY-GERIN, 2005*a*,*b*; MUROYA et al., 2002, 2006; PLANTE et al., 2005; AUTSAVAPROMPORN et al., 2007; PLANTE, 2009; TIPPAYAMONTRI et al., 2009; SANGUANMITH et al., 2011*a*,*b*; MIRSALEH KOHAN et al., 2013; BUTARBUTAR et al., 2014, 2016). Since their introduction in 1993, these codes have been continuously upgraded to take advantage of the availability of new experimental or theoretical advances from the literature, and also extended largely driven by practical applications. In the present work, we have used the most recent version of the Sherbrooke codes, known as IONLYS-IRT. A detailed description of the IONLYS-IRT program and its implementation have already been reported (MEESUNGNOEN and JAY-GERIN, 2005*a*, 2011; TIPPAYAMONTRI et al., 2009; SANGUANMITH et al., 2011*a*) and will not be reproduced here. Only a brief overview of the most essential features of the simulation methodology and reaction scheme, pertinent to the current calculations, is given below.

## 2.1 The IONLYS code

The IONLYS step-by-step simulation code is used to model the early physical and physicochemical events that take place in liquid water up to ~1 ps following irradiation. It is actually composed of two modules, one (named TRACPRO) for transporting the investigated incident radiation particle (proton or any other heavy ion projectile) and another one (named TRACELE) for transporting all secondary electrons that result from the ionization of the water molecules. The code models, event by event, all the fundamental physical interactions (energy deposition) and the subsequent establishment of thermal equilibrium in the system (conversion of the physical products created locally after completion of the physical stage into the various initial radical and molecular

products of radiolysis). For a description of these events as well as their time scales, see Sect. 1.1.2 (reactions [3]-[11]).

More specifically, IONLYS describes, in a 3D geometric environment, each primary physical event, recording the coordinates of each interaction, the actual amount of energy lost by the scattered particle, its angular deflection, and modification caused locally to the medium. If a secondary electron is produced through ionization, its initial physical parameters (starting point, energy, and direction of motion) are also recorded for further processing of its transport and action in the medium. The slowing-down of the irradiating charge particle and of all the secondary electrons that it has generated occurs via a variety of inelastic interactions (ionization, electronic and vibrational/rotational excitation of single water molecules, and excitation of plasmon-type collective modes) as well as elastic scattering processes. The energy-dependent cross-sections needed for these various elastic and inelastic processes, together with their angular distributions, are entered as input data in the code, based on direct measurements or on theoretical estimates (for example, see: COBUT et al., 1998; DINGFELDER and FRIEDLAND, 2001; NIKJOO *et al.*, 2006; UEHARA and NIKJOO, 2006; DINGFELDER *et al.*, 2008; ZIEGLER et al., 2015). These collision cross-sections are needed to follow the history of an energetic charged particle and its products, covering all ranges of energy transferred in individual collisions. Most importantly, they provide the particle's scattering mean free path used to determine the distance to the next interaction (the particle is assumed to move in straight free-flight-paths between collisions), the type of interaction at each event, energy loss, and the direction of the scattered particle. In practice, the stochastic selection of the scattering events is done with various sampling techniques (direct inversion, *etc*.) in accordance with the appropriate scattering cross-sections for each process (COBUT et al., 1998). These techniques all use pseudo-random numbers uniformly distributed on the interval between 0 and 1.

Unlike other simulation programs, IONLYS uses protons (or heavier ion projectiles) as the primary particles. This choice of proton impact was originally adopted by the Sherbrooke group because protons offer, by far, the most comprehensive database of collision cross-sections for "bare" (*i.e.*, fully ionized or stripped) ion projectiles (DINGFELDER et al., 2000; TOBUREN, 2004), and also because they can act, through

appropriate choices of their initial energies, as excellent model particles for studying LET effects on radiolytic yields (FRONGILLO et al., 1998). The simulations performed with IONLYS thus consist in the generation of short proton (or ion) track segments in water. The primary particle is simulated until it has penetrated the chosen length of the track segment into the medium. Due to its large mass, the proton (or the impacting heavy ion) is almost not deflected by collisions with the target electrons. The use of short track segments is useful as the instantaneous LET of the incident particle is nearly constant over such segments and can be varied simply by changing its energy. In this work, for example, to mimic the radiolysis with $^{60}$Co γ-radiation or fast electrons, we use short track segments (typically, ~150 μm) of 300-MeV protons, over which the average LET value obtained in the simulations remains essentially constant and equal to ~0.3 keV/μm at 25 °C (WATT, 1996; McCRACKEN et al., 1998).

A great advantage of the code is that, while it was devised for protons, it can also be used for heavier ion projectiles by assuming that the interaction cross-sections scale as $Z^2$, where $Z$ is the projectile charge number. In this scaling procedure, based on the lowest-order (or first Born) approximation of perturbation theories, the cross-sections for bare ion impact are approximately $Z^2$ times the cross-sections for proton impact *at the same velocity* (INOKUTI, 1971; McDANIEL et al., 1993; ICRU REPORT 55, 1996). This simple $Z^2$ scaling rule, which holds at sufficiently high impact energies (>1 MeV/nucleon) where the interactions are not too strong, is useful for providing cross-sections for ionization and excitation by ion projectiles, especially as there are only very limited experimental data available involving ions heavier than proton or helium in collision with water molecules.

At the incident ion energies considered in this work, interactions involving electron capture and loss by the moving ion (charge-changing collisions) have been neglected (LAVERNE, 2004; ZIEGLER et al., 2015).

All of the produced energetic secondary electrons are transported spatially from their initial energies until they reach the subexcitation energy region below ~7.3 eV, the threshold assumed for electronic excitations in liquid water (see Sect. 1.1.2). The time that a secondary electron takes to reach subexcitation energies is $<10^{-15}$ s. The thermalization of $e^-_{sub}$ is treated by IONLYS using the "distribution of thermalization

distances" ($r_{th}$) obtained from separate Monte Carlo simulations (GOULET and JAY-GERIN, 1989; GOULET et al., 1990, 1996) based on experimental scattering cross-sections of slow (1-100 eV) electrons in amorphous ice (MICHAUD et al., 2003) with corrections to account for the liquid phase. Given the initial position and energy of the subexcitation electron, its position is simply displaced in a randomly selected, isotropic direction [5] by the corresponding, energy-dependent mean $r_{th}$ value taken from this distribution (COBUT et al., 1998). At its new position, the electron is then regarded as thermalized and subsequently trapped and hydrated *where it is*, an approximation likely to be valid in a highly polar medium such as liquid water (MOZUMDER, 1999). Finally, it is worth recalling here that a certain proportion of $e^-_{sub}$ will actually never get thermalized, but will instead undergo prompt recombination with their positive parent ion $H_2O^{\bullet+}$ or dissociative attachment (DEA) onto a surrounding $H_2O$ molecule (see Sect. 1.1.2).

The complex spatial distribution of reactants [$e^-_{aq}$, $H^\bullet$, $H_2$, $^\bullet OH$, $H_2O_2$, $H^+$ (or $H_3O^+$), $OH^-$, $O_2^{\bullet-}$ (or $HO_2^\bullet$, depending on pH), $^\bullet O^\bullet(^3P)$, *etc.*] formed at the end of the physicochemical stage (~1 ps, time that is assumed to mark the beginning of diffusion), which is provided as an output of the IONLYS program, is then used directly as the starting point for the subsequent nonhomogeneous/homogeneous chemical stage, which is covered by the IRT program.

## 2.2 The IRT code

The IRT program models the chemical stage of radiation action during which the different species diffuse randomly at rates determined by their diffusion coefficients and react with one another, or competitively with any dissolved solutes present at the time of irradiation. It employs the "independent reaction times" (IRT) method, a computer-efficient stochastic simulation technique that is used to simulate reaction times without having to follow explicitly the trajectories of the diffusing species (TACHIYA, 1983; CLIFFORD et al., 1986; GREEN et al., 1990; PIMBLOTT et al., 1991; PIMBLOTT and

[5] As with other simulation programs, IONLYS uses a uniform continuum model of the aqueous medium, irrespective of the underlying molecular nature of the target.

GREEN, 1995; FRONGILLO et al., 1996, 1998). In essence, the IRT method relies on the approximation that the distances between pairs of reactants evolve independently of each other, and, therefore, the reaction times of the various potentially reactive pairs are independent of the presence of other reactants in the system.

The simulation begins by considering the initial (or "zero-time") spatial distribution of the reactants (given by the IONLYS program). The separations between all the pairs of reactants are first calculated. Overlapping pairs (*i.e.*, pairs formed in a reactive configuration) are assumed to combine immediately. For every remaining pair, a reaction time is stochastically sampled according to the reaction time probability distribution function (GREEN et al., 1990; GOULET and JAY-GERIN, 1992; FRONGILLO et al., 1998) that is appropriate to the type of reaction considered. This function depends on the initial separation of the pair of interacting species, the sum of their diffusion coefficients, their Coulomb interaction (for reactions between two charged species), their reaction distance, and the probability that those species react during one of their encounters. The competition between the various reactions is taken into account by realizing them in ascending temporal order of sampled reaction times. In other words, the first reaction time is found by taking the minimum of the resulting ensemble of reaction times and allowing the corresponding pair of species to react at this time. Of course, when a reaction occurs, the reactants become unavailable for the subsequent reactions in which they were scheduled to be involved, but one must then consider the possible reactions of the newly formed products with the species that have survived up to that point. The minimum of the new ensemble of reaction times is the next reaction time. This procedure for modeling reaction is continued either until all reactions are completed or until a predefined cut-off time is reached.

Since the principle of the IRT method consists in generating reaction times rather than the explicit trajectories of the diffusing species, the model must therefore be supplemented by including a procedure which allows the sampling of the positions of the reaction products after a reaction has been sampled to occur at a certain time and a new product is formed, and of the species with which newly formed products can in turn react. Several alternative procedures, which incorporate varying degrees of spatial information about the system, have been devised and discussed in detail previously (CLIFFORD et

al., 1986; GREEN et al., 1990). The procedure adopted in our IRT code to account for the subsequent reactions of the newly formed products is the one originally given by FRONGILLO et al. (1998).

The IRT program also allows one to incorporate, in a simple way, pseudo first-order reactions of the radiolytic products with various scavengers that are homogeneously distributed in the solution, such as $H^+$, $OH^-$, and $H_2O$ itself, or more generally any solutes for which the relevant reaction rates are known. Similarly, the truly first-order fragmentations of the species are easily simulated. Finally, the IRT method is very well suited for the description of reactions that are only partially diffusion-controlled,[6] in which the species do not react instantaneously on encounter but experience, on the average, many encounters and separations before they actually react with each other.

The ability of the IRT method to give accurate time-dependent chemical yields under different irradiation conditions has been well validated by comparison with full random flight (or "step-by-step") Monte Carlo simulations[7] that do follow the reactant trajectories in detail (PIMBLOTT et al., 1991; GOULET et al., 1998; PLANTE, 2009). Its implementation has been described in detail (FRONGILLO et al., 1998). Finally, the IRT program can also be successfully used to describe the reactions that take place in the homogeneous chemical stage, *i.e.*, when the radiolytic products are homogeneously distributed in the bulk solution after spur/track expansion is complete, in the time domain beyond a few microseconds (BĚGUSOVÁ and PIMBLOTT, 2002; HARRIS and PIMBLOTT, 2002; AUTSAVAPROMPORN et al., 2007; MEESAT et al., 2012*a*; MIRSALEH KOHAN et al., 2013; MUSTAREE et al., 2014).

---

[6] Most reactions that occur in irradiated water are not diffusion-controlled even at room temperature.

[7] The full step-by-step Monte Carlo description of the diffusion and encounters of the various species of the system is certainly the most reliable and is generally considered as a measure of reality. The major limitation of this method is that it is inherently a time consuming calculation. The IRT method was devised to achieve much faster (of the order of at least two orders of magnitude faster, depending on the studied system) realizations than are possible with the full Monte Carlo model while at the same time sacrificing very little accuracy.

## 2.3 Simulation of the effects of temperature

Of basic and applied interest is knowledge of the effects of temperature on the primary yields of the radiolytic products $e^-_{aq}$, $H^\bullet$, $H_2$, $^\bullet OH$, and $H_2O_2$, as well as on the rate constants of their reactions. When the temperature is increased from ambient up to 350 °C, measurements using low-LET radiation made in different laboratories with many scavenger systems or directly by using pulse radiolysis (for example, see: KENT and SIMS, 1992*a*,*b*; ELLIOT et al., 1993, 1996; ELLIOT, 1994; SUNARYO et al., 1995; ISHIGURE et al., 1995; KATSUMURA et al., 1998; ŠTEFANIĆ and LAVERNE, 2002; JANIK et al., 2007; ELLIOT and BARTELS, 2009; STERNICZUK and BARTELS, 2016) have shown that $g(e^-_{aq})$, $g(^\bullet OH)$, $g(H^\bullet)$, and $g(H_2)$ continuously increase, while $g(H_2O_2)$ decreases. The general trend of yields of free radicals increasing with temperature is readily explained by the fact that most important recombination reactions in the spur are not diffusion-controlled and therefore have rates that increase *less* with temperature than the diffusion of the individual species out of the spur (ELLIOT et al., 1990; HERVÉ DU PENHOAT et al., 2000; JANIK et al., 2007). In other words, as the temperature rises, diffusion of free radical species out of spurs becomes more important than recombination, resulting in less molecular recombination products. This conclusion, of course long been known, was recently corroborated by picosecond time-resolved pulse radiolysis experiments on the decay kinetics of the hydrated electron in liquid water at different temperatures up to 350 °C and also beyond the thermodynamic critical point of water[8] (BALDACCHINO et al., 2006; MUROYA et al., 2010). The molecular hydrogen yield is, however, an exception to this general pattern. Indeed, although $H_2$ is a molecular

[8] In the past 5-10 years, measurements of the radical and molecular yields of the radiolysis of water have been extended up to 450 °C, *i.e.*, above the temperature of the critical point of water ($t_c$ = 373.95 °C, $P_c$ = 22.06 MPa or 217.7 atm, and $\rho_c$ = 0.322 g/cm$^3$) in the so-called "supercritical regime" (for example, see: LIN and KATSUMURA, 2011). Note that supercritical water is of particular interest nowadays because of its possible use as the heat transport medium in the next-generation ("Generation IV") technologies of nuclear reactors aimed at supplying future worldwide needs for electricity, hydrogen, and other products (for example, see: OKA and KOSHIZUKA, 1998; GUZONAS et al., 2012). However, this range of elevated temperatures (and pressures) is beyond the scope of the present study.

product, $g(H_2)$ is observed to increase with temperature, particularly above 200 °C. Although this *in situ* radiolytic production of $H_2$ is of particular importance in the management of reactor water chemistry (since it could affect the minimum concentration of excess $H_2$ to be added to the primary coolant water to suppress the net radiolysis of water; see Sect. 1.3), no definitive mechanism has been established at present to account for this anomalous increase in $g(H_2)$ at high temperature and some debate currently exists in the literature on the subject (PLATZMAN, 1962; FARAGGI and DÉSALOS, 1969; BURNS and MARSH, 1981; COBUT et al., 1996; SWIATLA-WOJCIK and BUXTON, 2005, 2010; JANIK et al., 2007; BARTELS, 2009; MEESUNGNOEN et al., 2015; STERNICZUK and BARTELS, 2016). Based on a critical review of the radiolysis data available in 2008, ELLIOT and BARTELS (2009) have recommended the following equations for the temperature dependences of the *g*-values (in molecule per 100 eV) for the radical and molecular species formed in the low-LET radiolysis of water over the range of 20-350 °C:

$$g(e^-_{aq}) = 2.641 + 4.162 \times 10^{-3}\, t + 9.093 \times 10^{-6}\, t^2 - 4.717 \times 10^{-8}\, t^3 \qquad [29]$$

$$g(^\bullet OH) = 2.531 + 1.134 \times 10^{-2}\, t - 1.269 \times 10^{-5}\, t^2 + 3.513 \times 10^{-8}\, t^3 \qquad [30]$$

$$g(H^\bullet) = 0.556 + 2.198 \times 10^{-3}\, t - 1.184 \times 10^{-5}\, t^2 + 5.223 \times 10^{-8}\, t^3 \qquad [31]$$

(equation developed from material balance considerations)

$$g(H_2) = 0.419 + 8.721 \times 10^{-4}\, t - 4.971 \times 10^{-6}\, t^2 + 1.503 \times 10^{-8}\, t^3 \qquad [32]$$

$$g(H_2O_2) = 0.752 - 1.620 \times 10^{-3}\, t\,, \qquad [33]$$

where $t$ is the temperature in °C. These observed temperature dependences of the *g*-values have been reproduced satisfactorily by deterministic diffusion-kinetic modeling of spur/track processes (KABAKCHI and BUGAENKO, 1992; LAVERNE and PIMBLOTT, 1993; SWIATLA-WOJCIK and BUXTON, 1995, 1998, 2000, 2001; SWIATLA-WOJCIK, 2008) and Monte Carlo track chemistry simulations (HERVÉ DU PENHOAT et al., 2000, 2001; TIPPAYAMONTRI et al., 2009; SANGUANMITH et al., 2011*a*,*b*; MIRSALEH KOHAN et al., 2013; BUTARBUTAR et al., 2014, 2016; MEESUNGNOEN et al., 2015).

In this study, we used an extended version of the IONLYS-IRT code which was originally developed by HERVÉ DU PENHOAT et al. (2000, 2001) to include the effects of elevated temperature on low- and high-LET water radiolysis. This code was recently

revised (SANGUANMITH et al., 2011*a*; MUROYA et al., 2012; MEESUNGNOEN et al., 2015) using newly measured or re-assessed experimental data up to 350 °C. Much of these data were drawn from the self-consistent radiolysis database (including rate constants, diffusion coefficients, and *g*-values) recommended by ELLIOT and BARTELS (2009) as the best values to use to model water radiolysis over the temperature range of 20-350 °C. Comparisons between model predictions and experiment resulted in the re-evaluation of the temperature dependence of certain parameters intervening in the early physicochemical stage of the radiolysis. These parameters include, in particular, the thermalization distance ($r_{th}$) and the dissociative attachment (DEA) of subexcitation electrons, as well as the branching ratios of the excited water molecule decay channels (see Sect. 1.1.2). Of particular relevance to the present study, the temperature dependence of $r_{th}$ was determined from comparing the computed time-dependent $e^-_{aq}$ yield data to recent picosecond pulse radiolysis measurements of the decay kinetics of $e^-_{aq}$ at several different temperatures between 25 and 350 °C (MUROYA et al., 2012). A remarkable agreement was obtained between experiment and simulation if $r_{th}$ were assumed to decrease with increasing temperature by a factor of ~2.5 at 300 °C (Figure 2.1).[9] This observed "shrinkage" of spur sizes at high temperatures was attributed to an increase in the scattering cross-sections of subexcitation electrons, originating from a decrease in the degree of structural order of water molecules (caused by an increasing breaking of hydrogen bonds) as the temperature is increased[10] (SANGUANMITH et al., 2011*a*; MUROYA et al., 2012). The knowledge of the temperature dependence of $r_{th}$ is important as it gives, under low-LET irradiation, a measure of the variation of the spur's initial radius ($r_o$) (prior to spur expansion) as the temperature is varied. As seen from Eqs. [19] and [20], $r_o$ is actually one of the key parameters in determining the pH inside a spur.

---

[9] A similar conclusion was obtained previously by HOCHANADEL and GHORMLEY (1962), who suggested that, at higher temperature, "subexcitation electrons are thermalized more rapidly".

[10] Low-energy electrons in their subexcitation energy range (< 7.3 eV) are known to be sensitive to the structural order of the surrounding medium, owing to their non-negligible delocalized quantum character (their associated de Broglie wavelength actually exceeds atomic dimensions).

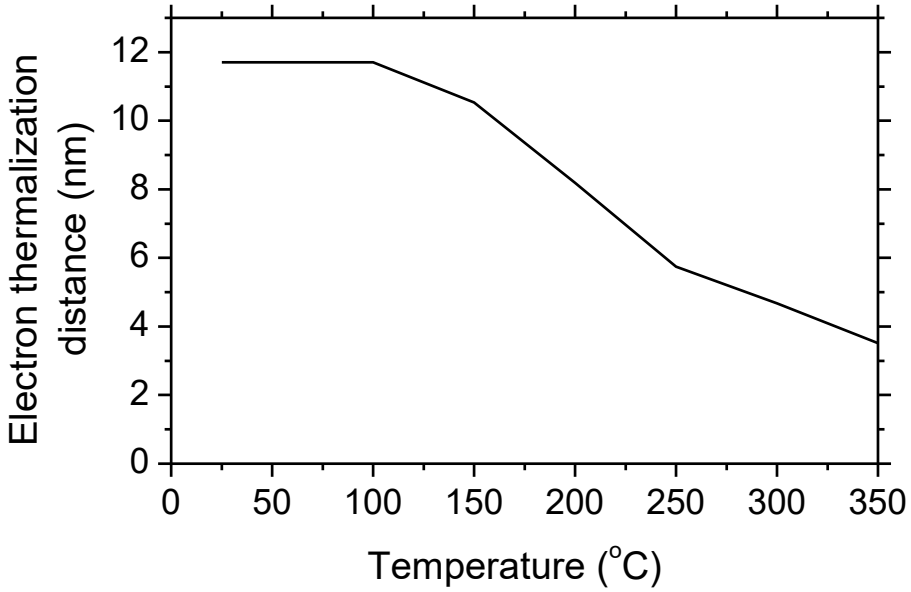


Figure 2.1 Temperature dependence of the (average) electron thermalization distance ($r_{th}$) of subexcitation electrons in liquid water over the range of 25-350 °C used in this study (MEESUNGNOEN and JAY-GERIN, 2005; SANGUANMITH et al., 2011; MUROYA et al., 2012).

Some chemical reactions can take place *before* any diffusion of the species occurs because they are already in contact at the end of the physicochemical stage (COBUT et al., 1998; FRONGILLO et al., 1998). For simplicity, in the simulations, those "contact reactions" are considered to occur at ~1 ps (*i.e.*, at the starting point of the nonhomogeneous kinetics).

The influence of temperature on the diffusion coefficients ($D$) depends on the actual species considered. Values of $D$ of the reactive species involved in the simulations and their temperature dependences are given in Table 1 of HERVÉ DU PENHOAT et al. (2000). Figure 2.2 shows, for the sake of illustration, the temperature dependences of the diffusion coefficients for $H_3O^+$, $OH^-$, and $H_2O$ in water that are used in this work, represented by polynomial fits to the experimental data (ELLIOT and BARTELS, 2009). For the species whose diffusion coefficients are unknown at elevated temperatures, the following scaling procedure was adopted:

$$D_{\mathrm{I}}(t) = D_{\mathrm{I}}(25°\mathrm{C})\,\frac{D_{\mathrm{H2O}}(t)}{D_{\mathrm{H2O}}(25°\mathrm{C})}, \qquad [34]$$

where $t$ denotes the temperature in degrees Celsius. In this procedure, the temperature dependence for diffusion of a given reactant (I) is assumed to be the same as that for the self-diffusion of water ($D_{H_2O}$) above room temperature (ELLIOT et al., 1990, 1996; ELLIOT, 1994; HERVÉ DU PENHOAT et al., 2000; ELLIOT and BARTELS, 2009).

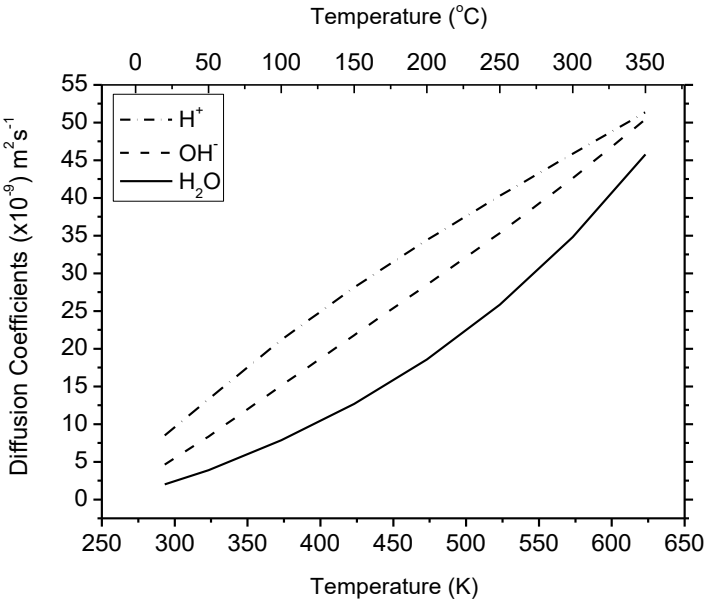


Figure 2.2 Temperature dependence of $D_{H_3O^+}$, $D_{OH^-}$, and $D_{H_2O}$ used in the simulations over the range of 25-350 °C (ELLIOT and BARTELS, 2009).

The reaction scheme for the radiolysis of pure liquid water used in IONLYS-IRT is given in Table 1. This set of reactions, initially assembled by ELLIOT (1994), FRONGILLO et al. (1998), and HERVÉ DU PENHOAT et al. (2000), now includes the recently compiled reaction rates by ELLIOT and BARTELS (2009).

All Monte Carlo simulations reported in this study were performed along the liquid-vapor coexistence curve, the density of the pressurized water decreasing from 1 g/cm$^3$ (1 bar or 0.1 MPa) at 25 °C to 0.575 g/cm$^3$ (~16.5 MPa) at 350 °C (LINSTROM and MALLARD, 2005). For this temperature range, calculations show that radiation chemical yields of transient species, to a large extent, depend relatively little on the applied pressure.

Table 1 Main spur/track reactions and rate constants ($k$ in $M^{-1}$ $s^{-1}$; for first-order reactions, the value of $k$ is given in $s^{-1}$) used in our simulations of the radiolysis of pure liquid water in the temperature range of 25-350 °C (ELLIOT and BARTELS, 2009).

| Temperature (°C) | 25 | 100 | 200 | 300 | 350 |
|---|---|---|---|---|---|
| Reactions | | | | | |
| 1) $H^{\bullet} + H^{\bullet} \rightarrow H_2$ | 5.20E+09 | 1.83E+10 | 5.25E+10 | 1.04E+11 | 1.36E+11 |
| 2) $H^{\bullet} + {}^{\bullet}OH \rightarrow H_2O$ | 1.61E+10 | 3.37E+10 | 6.26E+10 | 9.36E+10 | 1.09E+11 |
| 3) $H^{\bullet} + H_2O_2 \rightarrow {}^{\bullet}OH + H_2O$ | 3.60E+07 | 1.99E+08 | 8.39E+08 | 2.14E+09 | 3.05E+09 |
| 4) $H^{\bullet} + e^-_{aq} \rightarrow H_2 + OH^-$ | 2.76E+10 | 9.33E+10 | 2.48E+11 | 3.14E+11 | 3.17E+11 |
| 5) $H^{\bullet} + OH^- \rightarrow e^-_{aq} + H_2O$ | 2.44E+07 | 4.99E+08 | 2.86E+09 | 8.03E+09 | 1.32E+10 |
| 6) $H^{\bullet} + O_2 \rightarrow HO_2^{\bullet}$ | 1.31E+10 | 3.03E+10 | 4.93E+10 | 6.07E+10 | 6.42E+10 |
| 7) $H^{\bullet} + HO_2^{\bullet} \rightarrow H_2O_2$ | 1.12E+10 | 3.85E+10 | 1.09E+11 | 2.13E+11 | 2.75E+11 |
| 8) $H^{\bullet} + O_2^{\bullet-} \rightarrow HO_2^-$ | 1.12E+10 | 3.85E+10 | 1.09E+11 | 2.13E+11 | 2.75E+11 |
| 9) $H^{\bullet} + HO_2^- \rightarrow {}^{\bullet}OH + OH^-$ | 1.47E+09 | 1.17E+10 | 6.61E+10 | 2.03E+11 | 2.27E+11 |
| 10) $H^{\bullet} + O(^3P) \rightarrow {}^{\bullet}OH$ | 2.02E+10 | 7.14E+10 | 2.07E+11 | 4.13E+11 | 5.37E+11 |
| 11) $H^{\bullet} + O^{\bullet-} \rightarrow OH^-$ | 2.00E+10 | 6.84E+10 | 1.62E+11 | 3.04E+11 | 3.99E+11 |
| 12) $H^{\bullet} + O_3 \rightarrow O_2 + {}^{\bullet}OH$ | 3.67E+10 | 9.24E+10 | 1.79E+11 | 2.67E+11 | 3.12E+11 |
| 13) $H^{\bullet} + H_2O \rightarrow e^-_{aq} + H^+$ | 4.58E-05 | 1.43E-01 | 1.24E+02 | 1.00E+04 | 5.36E+04 |
| 16) $H^{\bullet} \rightarrow e^-_{aq} + H^+$ | 1.07E-01 | 2.45E+01 | 9.50E+02 | 4.16E+03 | 2.78E+03 |
| 17) ${}^{\bullet}OH + {}^{\bullet}OH \rightarrow H_2O_2$ | 6.31E+09 | 1.15E+10 | 1.42E+10 | 1.30E+10 | 1.18E+10 |
| 18) ${}^{\bullet}OH + H_2O_2 \rightarrow HO_2^{\bullet} + H_2O$ | 2.94E+07 | 8.99E+07 | 2.30E+08 | 4.24E+08 | 5.35E+08 |
| 19) ${}^{\bullet}OH + H_2 \rightarrow H^{\bullet} + H_2O$ | 3.95E+07 | 1.72E+08 | 6.11E+08 | 7.83E+08 | 6.19E+08 |
| 20) ${}^{\bullet}OH + e^-_{aq} \rightarrow OH^-$ | 3.55E+10 | 8.50E+10 | 2.01E+11 | 3.72E+11 | 4.77E+11 |
| 21) ${}^{\bullet}OH + OH^- \rightarrow O^{\bullet-} + H_2O$ | 1.33E+10 | 4.04E+10 | 8.27E+10 | 1.36E+11 | 1.68E+11 |
| 22) ${}^{\bullet}OH + HO_2^{\bullet} \rightarrow O_2 + H_2O$ | 9.00E+09 | 1.54E+10 | 2.41E+10 | 3.23E+10 | 3.61E+10 |
| 23) ${}^{\bullet}OH + O_2^{\bullet-} \rightarrow O_2 + OH^-$ | 1.08E+10 | 2.61E+10 | 5.49E+10 | 8.91E+10 | 1.07E+11 |
| 24) ${}^{\bullet}OH + HO_2^- \rightarrow HO_2^{\bullet} + OH^-$ | 8.32E+09 | 2.95E+10 | 8.53E+10 | 1.70E+11 | 2.22E+11 |
| 25) ${}^{\bullet}OH + O(^3P) \rightarrow HO_2^{\bullet}$ | 2.02E+10 | 7.14E+10 | 2.07E+11 | 4.13E+11 | 5.37E+11 |
| 26) ${}^{\bullet}OH + O^{\bullet-} \rightarrow HO_2^-$ | 1.00E+09 | 1.87E+09 | 3.16E+09 | 4.45E+09 | 5.06E+09 |
| 27) ${}^{\bullet}OH + O_3^{\bullet-} \rightarrow O_2^{\bullet-} + HO_2^{\bullet}$ | 8.50E+09 | 1.55E+10 | 1.92E+10 | 2.10E+10 | 2.15E+10 |
| 28) ${}^{\bullet}OH + O_3 \rightarrow HO_2^{\bullet} + O_2$ | 1.11E+08 | 3.93E+08 | 1.14E+09 | 2.28E+09 | 2.96E+09 |
| 29) ${}^{\bullet}OH + H_2O \rightarrow O^{\bullet-} + H^+$ | 1.70E-03 | 5.74E-02 | 4.12E-01 | 6.39E-01 | 2.58E-01 |
| 30) $H_2O_2 + e^-_{aq} \rightarrow {}^{\bullet}OH + OH^-$ | 1.10E+10 | 3.91E+10 | 1.14E+11 | 2.29E+11 | 2.98E+11 |
| 31) $H_2O_2 + OH^- \rightarrow HO_2^- + H_2O$ | 1.33E+10 | 4.04E+10 | 8.27E+10 | 1.36E+11 | 1.68E+11 |

| Temperature (°C) | 25 | 100 | 200 | 300 | 350 |
|---|---|---|---|---|---|
| Reactions | | | | | |
| 32) $H_2O_2 + O(^3P) \rightarrow {}^{\bullet}OH + HO_2^{\bullet}$ | 1.60E+09 | 6.73E+09 | 2.25E+10 | 4.93E+10 | 6.64E+10 |
| 33) $H_2O_2 + O^{\bullet-} \rightarrow HO_2^{\bullet} + OH^-$ | 5.55E+08 | 1.97E+09 | 5.69E+09 | 1.14E+10 | 1.48E+10 |
| 34) $H_2O_2 + H_2O \rightarrow H^+ + HO_2^-$ | 1.70E-03 | 5.74E-02 | 4.12E-01 | 6.39E-01 | 2.58E-01 |
| 35) $H_2 + O(^3P) \rightarrow H^{\bullet} + {}^{\bullet}OH$ | 4.77E+03 | 8.07E+04 | 8.70E+05 | 4.09E+06 | 7.36E+06 |
| 36) $H_2 + O^{\bullet-} \rightarrow H^{\bullet} + OH^-$ | 1.28E+08 | 3.63E+08 | 8.74E+08 | 1.55E+09 | 1.92E+09 |
| 37) $e^-_{aq} + e^-_{aq} \rightarrow H_2 + 2OH^-$ | 7.26E+09 | 3.85E+10 | 1.50E+10 | 5.92E+06 | 5.53E+04 |
| 38) $e^-_{aq} + H^+ \rightarrow H^{\bullet}$ | 2.13E+10 | 5.40E+10 | 1.54E+11 | 7.14E+11 | 1.93E+12 |
| 39) $e^-_{aq} + O_2 \rightarrow O_2^{\bullet-}$ | 2.34E+10 | 5.99E+10 | 1.32E+11 | 2.21E+11 | 2.69E+11 |
| 40) $e^-_{aq} + HO_2^{\bullet} \rightarrow HO_2^-$ | 1.30E+10 | 3.73E+10 | 9.03E+10 | 1.61E+11 | 2.00E+11 |
| 41) $e^-_{aq} + O_2^{\bullet-} \rightarrow H_2O_2 + 2OH^-$ | 1.30E+10 | 3.73E+10 | 9.03E+10 | 1.61E+11 | 2.00E+11 |
| 42) e-aq + $HO_2^- \rightarrow O^{\bullet-} + OH^-$ | 3.51E+09 | 1.22E+10 | 3.49E+10 | 6.91E+10 | 8.96E+10 |
| 43) $e^-_{aq} + O(^3P) \rightarrow O^{\bullet-}$ | 1.98E+10 | 6.29E+10 | 1.54E+11 | 2.66E+11 | 3.26E+11 |
| 44) $e^-_{aq} + O^{\bullet-} \rightarrow OH^- + OH^-$ | 2.31E+10 | 4.39E+10 | 7.52E+10 | 1.07E+11 | 1.22E+11 |
| 45) $e^-_{aq} + O_3 \rightarrow O_3^{\bullet-}$ | 3.57E+10 | 1.13E+11 | 2.77E+11 | 4.79E+11 | 5.87E+11 |
| 46) $e^-_{aq} + H_2O \rightarrow H^{\bullet} + OH^-$ | 1.58E+01 | 2.01E+02 | 7.30E+02 | 2.01E+03 | 3.55E+03 |
| 47) $H^+ + OH^- \rightarrow H_2O$ | 1.18E+11 | 3.22E+11 | 6.05E+11 | 1.13E+12 | 1.63E+12 |
| 48) $H^+ + O_2^{\bullet-} \rightarrow HO_2^{\bullet}$ | 5.02E+10 | 1.27E+11 | 2.71E+11 | 5.69E+11 | 8.22E+11 |
| 49) $H^+ + HO_2^- \rightarrow H_2O_2$ | 5.02E+10 | 1.27E+11 | 2.71E+11 | 5.69E+11 | 8.22E+11 |
| 50) $H^+ + O^{\bullet-} \rightarrow {}^{\bullet}OH$ | 5.02E+10 | 1.27E+11 | 2.71E+11 | 5.69E+11 | 8.22E+11 |
| 51) $H^+ + O_3^{\bullet-} \rightarrow {}^{\bullet}OH + O_2$ | 9.00E+10 | 2.36E+11 | 4.87E+11 | 9.03E+11 | 1.25E+12 |
| 52) $OH^- + HO_2^{\bullet} \rightarrow O_2^{\bullet-} + H_2O$ | 1.33E+10 | 4.04E+10 | 8.27E+10 | 1.36E+11 | 1.68E+11 |
| 53) $OH^- + O(^3P) \rightarrow HO_2^-$ | 4.20E+08 | 4.24E+08 | 4.25E+08 | 4.26E+08 | 4.26E+08 |
| 54) $O_2 + O(^3P) \rightarrow O_3$ | 4.00E+09 | 5.19E+09 | 5.59E+09 | 5.74E+09 | 5.78E+09 |
| 55) $O_2 + O^{\bullet-} \rightarrow O_3^{\bullet-}$ | 3.72E+09 | 9.23E+09 | 1.98E+10 | 3.25E+10 | 3.93E+10 |
| 56) $HO_2^{\bullet} + HO_2^{\bullet} \rightarrow H_2O_2 + O_2$ | 1.94E+08 | 3.31E+08 | 5.19E+08 | 6.96E+08 | 7.78E+08 |
| 57) $HO_2^{\bullet} + O_2^{\bullet-} \rightarrow O_2 + HO_2^-$ | 9.70E+07 | 1.95E+08 | 3.49E+08 | 5.11E+08 | 5.90E+08 |
| 58) $HO_2^{\bullet} + O(^3P) \rightarrow O_2 + OH$ | 2.02E+10 | 7.14E+10 | 2.07E+11 | 4.13E+11 | 5.37E+11 |
| 59) $HO_2^{\bullet} + H_2O \rightarrow O_2^{\bullet-} + H^+$ | 1.40E+04 | 4.49E+04 | 2.95E+04 | 3.92E+03 | 8.78E+02 |
| 60) $O_2^{\bullet-} + O^{\bullet-} \rightarrow O_2 + 2OH^-$ | 6.00E+08 | 6.55E+08 | 6.97E+08 | 8.10E+08 | 1.03E+09 |
| 61) $O_2^{\bullet-} + O_3 \rightarrow O_3^{\bullet-} + O_2$ | 1.50E+09 | 3.73E+09 | 7.99E+09 | 1.31E+10 | 1.59E+10 |
| 62) $O_2^{\bullet-} + H_2O \rightarrow HO_2^{\bullet} + {}^{\bullet}OH^-$ | 1.55E-01 | 2.09E+01 | 1.20E+03 | 2.87E+04 | 6.10E+04 |
| 63) $HO_2^- + O(^3P) \rightarrow {}^{\bullet}OH + O_2^{\bullet-}$ | 5.30E+09 | 7.84E+09 | 8.85E+09 | 9.26E+09 | 9.38E+09 |
| 64) $HO_2^- + O^{\bullet-} \rightarrow OH^- + O_2^{\bullet-}$ | 8.02E+08 | 5.75E+09 | 3.01E+10 | 8.85E+10 | 1.33E+11 |

| Temperature (°C) | 25 | 100 | 200 | 300 | 350 |
|---|---|---|---|---|---|
| Reactions | | | | | |
| 65) $HO_2^- + H_2O \rightarrow H_2O_2 + OH^-$ | 1.27E+06 | 1.63E+07 | 8.56E+07 | 1.76E+08 | 2.08E+08 |
| 66) $O(^3P) + O(^3P) \rightarrow O_2$ | 2.20E+10 | 7.80E+10 | 2.26E+11 | 4.51E+11 | 5.86E+11 |
| 67) $O(^3P) + H_2O \rightarrow {}^{\bullet}OH + {}^{\bullet}OH$ | 1.90E+03 | 5.31E+04 | 8.74E+05 | 5.41E+06 | 1.08E+07 |
| 68) $O^{\bullet-} + O^{\bullet-} \rightarrow H_2O_2 + 2OH^-$ | 1.00E+08 | 1.19E+08 | 1.21E+08 | 1.20E+08 | 1.19E+08 |
| 69) $O^{\bullet-} + O_3^{\bullet-} \rightarrow 2O_2^{\bullet-}$ | 7.00E+08 | 7.78E+08 | 8.44E+08 | 1.04E+09 | 1.51E+09 |
| 70) $O^{\bullet-} + H_2O \rightarrow {}^{\bullet}OH + OH^-$ | 1.27E+06 | 1.63E+07 | 8.56E+07 | 1.76E+08 | 2.08E+08 |
| 71) $O_3^{\bullet-} + H_2O \rightarrow O^{\bullet-} + O_2$ | 4.65E+01 | 2.05E+03 | 5.29E+04 | 4.99E+05 | 1.34E+06 |
| 72) $H_2O \rightarrow H^+ + OH^-$ | 2.12E-05 | 3.14E-03 | 4.58E-02 | 6.53E-02 | 2.04E-02 |

Finally, it should be noted that, for the low-LET radiolysis of pure liquid water, the time ($\tau_s$) at which spurs have dissipated (*i.e.*, when the radiolytic products are homogeneously distributed in the bulk solution) is dependent on temperature. SANGUANMITH et al. (2012) have shown that $\tau_s$ decreases monotonically by about an order of magnitude over the 25-350 °C temperature range, going from ~2 × $10^{-7}$ s at 25 °C to ~3.5 × $10^{-8}$ s at 350 °C (Figure 2.3).

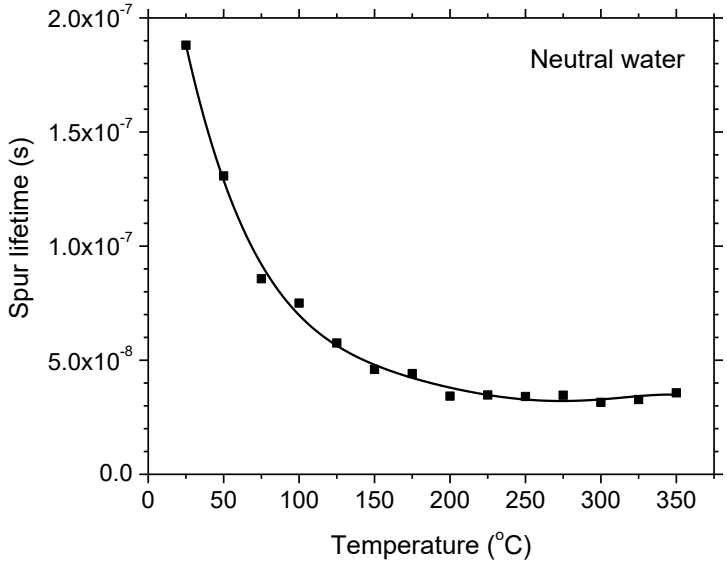


Figure 2.3 Temperature dependence of the spur lifetime ($\tau_s$) for the low-LET radiolysis of pure liquid water in the range of 25-350 °C (SANGUANMITH et al., 2012).

In the simulations reported here, the effect of temperature on the *in situ* formation of $H_3O^+$ ions and the corresponding abrupt transient "acid spike" response has been followed over the interval of ~1 ps to 1 ms after the initial energy deposition (KANIKE et al., 2016).

# 3 - ARTICLE No. 1

## Transient acid pH effect in tracks in the radiolysis of water: Does this effect contribute to biological damage caused by ionizing radiation?

**Authors**: **Vanaja Kanike**, Jintana Meesungnoen and Jean-Paul Jay-Gerin

**Status**: Published in ***Austin Journal of Nuclear Medicine and Radiotherapy***, ***2015, Vol. 2, No. 1, 1011*** (6 pages).

**Foreword**: In this first article, we present some preliminary results of our work demonstrating the "acid spike" effect. Using Monte Carlo track chemistry simulations, we quantitatively show that the in situ formation of $H_3O^+$ in the radiolysis of pure, deaerated water renders the spur/track regions temporarily more acid than the body of the solution. Two track models are considered depending on the quality (LET) of the radiation: a "spherical" isolated spur model (300-MeV incident protons, which mimic $^{60}$Co γ-irradiation; LET ~ 0.3 keV/μm) and a "cylindrical" track model (0.15-MeV irradiating protons; LET ~ 70 keV/μm), at 25 °C. In both cases, an abrupt transient acid pH effect is observed at times immediately after the initial energy release. This effect, which we call an "acid spike" effect, is found to be greatest for times shorter than ~1 ns: equal to ~3.3 in isolated spurs and ~2.5 in cylindrical tracks. At longer times, the pH increases gradually, ultimately reaching a value of 7 (neutral pH) at ~1 μs for the spherical geometry and ~0.1 ms for the cylindrical geometry.

**Résumé** : Ce premier article présente certains résultats préliminaires de nos travaux démontrant l'effet de "pic acide". À l'aide de simulations Monte Carlo de la chimie intervenant dans les trajectoires, nous y montrons que la formation *in situ* d'ions hydronium ($H_3O^+$) dans la radiolyse de l'eau pure désaérée rend la région des grappes ou des trajectoires du rayonnement temporairement plus acide que le milieu environnant. Deux modèles de grappe et de trajectoire sont considérés, à 25 °C, selon la qualité (TEL) du rayonnement : un modèle de grappe isolée "sphérique" (trajectoires de protons de 300 MeV, de faible LET : ~0,3 keV/μm) et un modèle de trajectoire "cylindrique" (protons incidents de 150 keV, de LET élevé : ~70 keV/μm). Dans les deux cas, un effet de pH acide brusque transitoire, ou effet de "pic acide", est observé aux temps courts immédiatement après le dépôt initial d'énergie (< 1 ns) : égal à ~3,3 dans les grappes isolées et ~2,5 dans les trajectoires cylindriques. À temps plus longs, le pH augmente progressivement, atteignant la valeur 7 (pH neutre) à ~1 μs pour la géométrie sphérique et ~0,1 ms pour la géométrie cylindrique.

# Transient acid pH effect in tracks in the radiolysis of water: Does this effect contribute to biological damage caused by ionizing radiation?

**V. Kanike, J. Meesungnoen and J.-P. Jay-Gerin***

Department of Nuclear Medicine and Radiobiology, Université de Sherbrooke, Canada

***Corresponding author**: Prof. Jean-Paul Jay-Gerin, Department of Nuclear Medicine and Radiobiology, Faculty of Medicine and Health Sciences, Université de Sherbrooke, 3001, 12th Avenue North, Sherbrooke, QC J1H 5N4, Canada. Tel: (1) 819-821-8000, ext. 74682; Email: jean-paul.jay-gerin@USherbrooke.ca

*Austin J Nucl Med Radiother 2(1):1011 (2015)* (6 pages)

Open Access

Received: December 16, 2014
Accepted: February 13, 2015
Published: February 16, 2015

**ABSTRACT**

We present a model calculation, using Monte Carlo track chemistry simulations, which quantitatively shows that the formation of $H_3O^+$ during the primary radiolysis processes in water renders the spur/track regions more acid than the surrounding solution. Although experimental evidence for this effect has already been reported, there is only fragmentary information on its magnitude and time dependence. Here, we compare our calculated yields of $H_3O^+$ and the corresponding pH values for both low-LET ("spherical" spur model) and high-LET ("cylindrical" track model) radiation. Our calculated time evolution of $G(H_3O^+)$ in the radiolysis of pure deaerated water by 300-MeV incident protons (which mimic $^{60}$Co γ/fast electron irradiation) is in very good agreement with available experimental data. For both studied cases, an abrupt transient acid pH effect is observed at times immediately after the initial energy release. This effect, which we call an "acid spike", is found to be greatest for times shorter than ~1 ns. In this time range, the pH remains nearly constant: ~3.3 in spherical spurs and ~2.5 in cylindrical tracks. Beyond ~1 ns, the pH increases gradually, ultimately reaching a value of 7 at ~1 μs for the spherical spur and at a somewhat longer time (~0.1 ms) for the cylindrical track. It does not appear that the acid spike described here has been explored in water or in a cell subject to the action of ionizing radiation. In this regard, this work raises a number of questions, some of which are briefly evoked.

*Keywords*: liquid water; aqueous solution; radiolysis; linear energy transfer (LET); low- and high-LET radiation; spur; track; hydronium ion ($H_3O^+$); radiation chemical yield; pH; biological damage; radiobiology; radiotherapy; hyperthermia.

## Introduction

Water is the major (about 70-85%) constituent of living cells. A thorough knowledge of the radiolysis of water is therefore critical for understanding radiobiological effects. The absorption of energetic radiations by water leads to the production of reactive chemical species that can damage all biomolecules, including lipids, proteins, and DNA; DNA is considered to be the most important molecule in

defining the radiobiological response. Lesions randomly induced in cellular DNA by ionizing radiation can be repaired or can result in cytotoxic and mutagenic effects and chromosomal instability, all of which can contribute to tumorigenesis [1-5].

It has been customary to separate the complex succession of events that follow the irradiation of water into four, more or less clearly delineated, consecutive, temporal stages [6-9]. Briefly, the first or "physical" stage consists of the phenomena by which energy is transferred from the incident radiation to the water. Its duration is of the order of $10^{-16}$ s or less. This energy absorption gives rise, along and around the path of the radiation, to a large number of ionized ($H_2O^{\bullet+}$) and electronically excited ($H_2O^*_{elec}$) water molecules distributed in a specific, highly non-homogeneous track structure which depends on the type and energy of the radiation used. Secondary electrons generated in the ionization events have a wide range of energies. Generally, they have enough energy to ionize or excite one or more other water molecules in the vicinity. The second or "physicochemical" stage consists of the re-establishment of thermal equilibrium in the bulk medium with reactions and the reorganization of initial products to give new chemical species such as stable molecules and water free radicals. It lasts about $10^{-12}$ s. During this stage, secondary electrons slow down to thermal energy ($e^-_{th}$) and, following thermalization, they become trapped ($e^-_{tr}$) and hydrated ($e^-_{aq}$). By ~$10^{-12}$ s, the radiolysis of water can be simply described by the following reactions [8,9]:

$$H_2O \rightsquigarrow H_2O^{\bullet+} + e^- \quad (1)$$

$$H_2O \rightsquigarrow H_2O^*_{elec} \quad (2)$$

$$H_2O^{\bullet+} + H_2O \rightarrow H_3O^+ + {}^{\bullet}OH \quad (3)$$

$$e^- \rightarrow e^-_{th} \rightarrow e^-_{tr} \rightarrow e^-_{aq} \quad (4)$$

$$H_2O^*_{elec} \rightarrow H^{\bullet} + {}^{\bullet}OH \quad (5)$$

where $H_3O^+$ (or equivalently, $H_{aq}^+$) represents the hydrated proton. In addition to the two radical species $e^-_{aq}$ and ${}^{\bullet}OH$ (hydroxyl radical), a small quantity of $H^{\bullet}$ atoms and the molecular products $H_2$ and $H_2O_2$ are produced. The third or "chemical" stage consists of diffusion and reactions of the reactive species leading to the re-establishment of chemical equilibrium. During this stage, the various radiolytic products present at the end of the physicochemical stage diffuse away from the site where they were originally produced

and then either react within the tracks as they develop in time or escape into the bulk solution. At 25 °C, all intra-track reactions are essentially complete by ~$10^{-6}$ s after the initial energy deposition. At this time, the species that have escaped from track reactions become homogeneously distributed throughout the bulk of the solution (also referred to as the "background") and the radiation track no longer exists. The radical and molecular products, considered as additions to the background, are then available for reaction with dissolved solutes (if any) present (in moderate concentrations) at the time of irradiation. On a quantitative basis, the species produced in the radiolysis of pure deaerated (air-free) water at homogeneity are $e^-_{aq}$, $H_3O^+$, $H^\bullet$, $^\bullet OH$, $OH^-$, $H_2$, $H_2O_2$, $O_2^{\bullet-}$ [or its protonated form $HO_2^\bullet$, depending on the pH; p$K_a(HO_2^\bullet/O_2^{\bullet-})$ = 4.8 in water at 25 °C], *etc*. In air-saturated solutions (the concentration of oxygen is ~0.25 m*M*), $e^-_{aq}$ and $H^\bullet$ atoms are rapidly (on a time scale of a few tenths of a microsecond) converted to superoxide anion/hydroperoxyl radicals. Thus, in an aerobic cellular environment at pH 7, the major reactive species at homogeneity include $O_2^{\bullet-}$, $^\bullet OH$, and $H_2O_2$ ($H_2$ plays only a limited role in the radiolysis of aqueous solutions, and most of it escapes from solution). Finally, in a physiological system, there follows a "biological" stage in which the cells respond to the damage resulting from the products formed in the preceding stages (~$10^{-3}$ s or longer, depending very much upon the medium). A good summary of the present status of aqueous radiation chemistry is given in [9-13].

Many experimental and theoretical studies have shown that the yields in the radiolysis of water are strong functions of the *quality* of the incident radiation, a measure of which is given by the "linear energy transfer" (LET) (also called "stopping power" by physicists) that represents the nonhomogeneity of the energy deposition on a sub-microscopic scale, commonly referred to as the "track structure" [8,9,14]. (Throughout this article, radiation chemical yields are given as *G*-values, in units of radicals, ions or molecules per 100 eV of energy deposited; for conversion into SI units, 1 molecule/100 eV ≈ 0.10364 μmol/J.) At the lowest LET (*e.g.*, for sparsely ionizing radiation such as γ-rays from $^{60}$Co, fast electrons or ~300 MeV protons generated by a particle accelerator, LET ~ 0.3 keV/μm), tracks are formed initially by well-separated Magee-type "spurs" [15,16] (spherical in shape) that develop independently in time (without interference from the neighboring spurs). In this case, the predominant effect is radical production. As LET

increases, the mean separation distance between the spurs decreases and the isolated spur structure changes to a situation in which the spurs overlap and form a dense continuous column (cylinder shape). This permits more radicals to be formed in close proximity with correspondingly greater probability of reacting with one another to produce molecular products or to reform water. High-LET, densely ionizing radiation therefore tends to produce high yields of molecular products, at the expense of free-radical yields [9,17]. To illustrate this point, Fig. 1 shows typical two-dimensional representations of the track segments of 300- and 0.15-MeV irradiating protons (LET ~ 0.3 and 70 keV/μm, respectively) on liquid water at 25 °C, calculated with our IONLYS Monte Carlo simulation code (see below).

Herein, we present a model calculation, using Monte Carlo track chemistry simulations, which quantitatively shows that the formation of $H_3O^+$ in reaction (3) during the primary radiolytic processes in water renders the spur/track regions temporarily more acid than the body of the solution. Although experimental evidence for this transient acid pH effect has already been reported [10,19,20], there is only fragmentary information on its magnitude and time dependence following energy deposition. Moreover, the influence of the quality (or LET) of the radiation on $G(H_3O^+)$ has not been investigated. In this work, we compare the calculated yields of $H_3O^+$ and the corresponding pH values for both low-LET ("spherical" spur model) and high-LET ("cylindrical" track model) radiation.

**Monte Carlo Track Chemistry Simulations of Water Radiolysis**

Monte Carlo simulations of the complex succession of events that are generated in pure, deaerated liquid water following the absorption of ionizing radiation were performed using our IONLYS-IRT code. This program simulates, in a three-dimensional geometrical environment, the nonhomogeneous distribution of reactive species initially produced by the absorption of the incident radiation and all of the energetic secondary electrons, as well as the subsequent chemical reactions of these species. A detailed description of the code has been reported previously [9,17,21-23]. Briefly, the IONLYS program is used to model the early physical and physicochemical stages of radiation action up to ~$10^{-12}$ s in the track development. It actually models, event by event, all the

basic physical interactions (energy deposition) and the radical and molecular products of the radiolysis, distributed in a highly nonhomogeneous track structure. The complex spatial distribution of reactants at the end of the physicochemical stage, which is provided as an output of the IONLYS program, is then used directly as the starting point for the subsequent nonhomogeneous/homogeneous chemical stage. Our IRT program models this stage during which the different species diffuse randomly at rates determined by their diffusion coefficients and react with one another, or competitively with any dissolved solutes present at the time of irradiation. This program employs the "independent reaction times" (IRT) method [22,24,25], a computer-efficient stochastic simulation technique that is used to simulate reaction times without having to follow the trajectories of the diffusing species. The IRT method relies on the approximation that the reaction time of each pair of reactants is independent of the presence of other reactants in the system. Its implementation has been described in detail [22], and its ability to give accurate time-dependent chemical yields under different irradiation conditions has been well validated by comparison with full random flights (or "step-by-step") Monte Carlo simulations, which do follow the reactant trajectories in detail [26,27].

The reaction scheme for the radiolysis of pure, deaerated liquid water at 25 °C used in IONLYS-IRT is the same as used previously (see Table 1 of [28]). Values for the diffusion coefficients of the reactive species involved in the simulations are listed in Table 6 of [17].

To reproduce the effects of low-LET radiation, which predominantly produces spherical spurs separated by large distances, we used short segments of 300 MeV incident proton tracks (Fig. 1), over which the average LET value obtained in the simulations was nearly constant and equal to ~0.3 keV/μm at 25 °C. (Such model calculations thus gave "track segment" yields at a well-defined LET [14].) The influence of the LET of the radiation on the yields of $G(H_3O^+)$ was investigated by performing a series of simulations with protons of different initial energies and therefore different LET. In this study, we limited ourselves to the incident proton energy of 0.15 MeV, corresponding to a LET value of ~70 keV/μm [29]. In this case, spurs are formed so close to each other along the path of the irradiating proton that they merge to form a cylindrical region of high LET

(see Fig. 1). In either case, at low dose rates (so that no track overlap occurs), each spherical spur or cylindrical track can be treated independently from all others.

The simulations consist of following the transport and energy loss of an incident proton until it has penetrated the chosen length (~20-150 μm) of the track segment into the medium. Due to its large mass, the impacting proton is almost not deflected by collisions with the target electrons. Typically, about 5000 to 35 000 reactive chemical species are generated in the chemical development of such simulated track segments (depending on the LET). The number of proton histories (usually ~30-150, depending on the proton energy) was chosen to permit averaging of chemical yields with acceptable statistical confidence.

In the s

imulations reported here, the time evolution of $G(H_3O^+)$ has been followed until ~1 ms.

**Results and Discussion**

Figure 2 shows the time evolution of $G(H_3O^+)$ as obtained from our simulations of the radiolysis of pure deaerated liquid water by 300- and 0.15-MeV incident protons (LET ~ 0.3 and 70 keV/μm, respectively) at ambient temperature. For the sake of comparison, available experimental data for $^{60}$Co γ/fast electron irradiation [30-34] are also included in the figure. As can be seen, our simulated values agree very well with the measured $H_3O^+$ yields. The sharp decrease of $G(H_3O^+)$ observed at times longer than ~10 μs for 300-MeV irradiating protons is mainly due to $H_3O^+$ reacting with $OH^-$ and, to a lesser extent, with the hydrated electrons escaping the spurs, according to:

$$H_3O^+ + OH^- \rightarrow 2H_2O \qquad k_6 = 1.18 \times 10^{11}\ M^{-1}\ s^{-1} \qquad (6)$$

$$H_3O^+ + e^-_{aq} \rightarrow H^\bullet + H_2O \qquad k_7 = 2.13 \times 10^{10}\ M^{-1}\ s^{-1} \qquad (7)$$

where $k_6$ and $k_7$ are the rate constants for the two individual reactions [13,28]. The time dependence of the cumulative yield variations $\Delta G(H_3O^+)$ for the different reactions that contribute to $G(H_3O^+)$ (data not shown here) confirms that the decrease of $G(H_3O^+)$ at long times is predominantly due to reaction (6) in the stage of homogeneous chemistry. To our knowledge, there are no experimental data of $G(H_3O^+)$ available for 0.15-MeV

irradiating protons with which to compare our results. In this case, our simulations show that the decay of $H_3O^+$ with time still largely results from reactions (6) and (7), although there is also a relatively small contribution due to the following reactions [13,28]:

$$H_3O^+ + O^{\bullet -} \rightarrow {}^{\bullet}OH + H_2O \qquad k_8 = 5 \times 10^{10}\ M^{-1}\ s^{-1} \tag{8}$$

$$H_3O^+ + HO_2^- \rightarrow H_2O_2 + H_2O \qquad k_9 = 5 \times 10^{10}\ M^{-1}\ s^{-1} \tag{9}$$

However, as shown in Fig. 2, the decrease in $G(H_3O^+)$ occurs as early as ~$10^2$ picoseconds up to microseconds, which is clearly different from what is observed for irradiation with 300-MeV incident protons (which mimic $^{60}$Co γ/fast electron irradiation). As expected, this is consistent with differences in the initial spatial distribution of primary transient species (*i.e.*, in the track structure). As mentioned earlier, in the track (columnar) geometry of the higher-LET 0.15-MeV irradiating protons, the reactive intermediates are formed locally in much closer initial proximity than in the spur (spherical) geometry, which favours the incidence, at shorter time scales, of an increased amount of intervening intra-track reactions.

With the objective of calculating the pH values prevailing in the spur/track regions, we now need to estimate the concentrations of $H_3O^+$ generated *in situ* in these regions as a function of time. Two models are considered depending on the quality (LET) of the radiation.

For 300-MeV incident protons (LET ~ 0.3 keV/μm), we assume that the hydronium ions are produced evenly in an isolated *spherical* spur whose initial radius $r_o$ (prior to spur expansion) is equal to the average electron thermalization distance obtained from our simulations ($r_o$ = 11.7 nm) [23]. The low-LET spur concentrations of $H_3O^+$ are derived from

$$[H_3O^+](t) = G(H_3O^+)(t) \times \left( \frac{\text{Mean energy loss/event}}{\frac{4}{3}\pi r(t)^3} \right) \tag{10}$$

where the mean energy loss in a single event (*i.e.*, the mean energy deposited in a spur) is taken to be ~47 eV [21,28,35] and

$$r(t)^2 = r_o^2 + 6Dt \tag{11}$$

represents the change with time of $r_o$ due to the (three dimensional) diffusive expansion of the spur. Here, $t$ is time and $D$ is the diffusion coefficient of $H_3O^+$ in water ($D = 9.46 \times 10^{-9}$ m$^2$ s$^{-1}$ at 25 °C) [17,22].

For 0.15-MeV irradiating protons (LET ~ 70 keV/μm), we consider the track as being a *cylinder*, homogeneous along its axis, of length $L$ = 1 μm and initial radius $r_c$ equal to the radius of the physical track "core" (which corresponds to the tiny radial region within the first few nanometers around the impacting ion path, at ~$10^{-13}$ s) [8,36]. In this case, the high-LET track concentrations of $H_3O^+$ can be obtained from [9]

$$[H_3O^+](t) = G(H_3O^+)(t) \times \left(\frac{\text{LET}}{\pi r(t)^2}\right), \tag{12}$$

where

$$r(t)^2 = r_c^2 + 4\,D\,t \tag{13}$$

represents the change with time of $r_c$ due to the (two dimensional) diffusive expansion of the track. Here, $r_c$ was obtained from our simulations [29] and is taken to be ~25 nm.

Using Eqs. (10) and (12) readily gives the concentrations of $H_3O^+$ as a function of time for both isolated "spherical" spurs and axially homogeneous "cylindrical" tracks. The pH in the corresponding spur/track regions is then simply given by the negative logarithm of $[H_3O^+]$:

$$\text{pH}(t) = -\log\{[H_3O^+](t)\}\,. \tag{14}$$

The time evolution of the pH values calculated as indicated above for 300- and 0.15-MeV incident protons in pure, deaerated liquid water (LET ~ 0.3 and 70 keV/μm, respectively) using the spherical spur and cylindrical track models at 25 °C is shown in Fig. 3. As can be seen, for both radiations considered, there is an abrupt transient *acid* pH effect at times immediately after the initial energy release. This effect, which we call an "acid spike" in analogy with the "thermal spike" used in radiation chemistry to describe the formation of a transient excess temperature region around the tracks of high-LET accelerated heavy ions [14,37], is found to be greatest for times shorter than ~1 ns. In this time range, the pH remains nearly constant, equal to ~3.3 in spherical spurs and ~2.5 in

cylindrical tracks. Beyond ~1 ns, the pH increases gradually for the two cases studied, ultimately reaching a value of 7 (neutral pH) at ~1 μs for the spherical spur geometry (corresponding to the end of spur expansion and the beginning of homogeneous chemistry [9-12]) and at a somewhat longer time (~0.1 ms) for the cylindrical track geometry.

To the best of our knowledge, the acid-spike effect described above has not been explored in water or in a cell subject to the action of ionizing radiation, especially high-LET radiations (*e.g.*, α-particles, high charge and high energy particles). In this respect, this work raises a number of questions. For example, in radiation chemistry, does the generation of strongly acidic regions, which extend over spatial dimensions of the order of tens of nanometers, have any noticeable influence on the final product formation by affecting all pH-dependent species and reaction rates [37,38]? In radiation- and free radical-biology, as many cellular processes depend on pH[39,40], is this transient acid pH, which is well outside the physiological range, toxic to cells (*e.g.*, by attacking DNA, by causing oxidative injury, by modifying normal biochemical reactions, or by triggering different signalling cascades that respond to these stress conditions [5]),and could it contribute to the initial events that lead to cell damage, enhanced lethality, "bystander" responses (where stressful effects are propagated from irradiated cells to non-targeted neighbours) [41-43], or genomic instability in progeny of irradiated cells and their neighbouring bystanders [44,45]? In the development of effective therapies for malignant diseases, do these spikes of acidity have any adverse effect on the response of cells to conventional anticancer drugs and possibly influence the outcome of tumour therapy [39]? Finally, it has been demonstrated that cells in an acid pH environment are more sensitive to the lethal effect of heat [46]. Thus, this work also raises the question of whether the highly acidic environment generated in the spurs/tracks of the radiation could explain, at least partly, why the combination of hyperthermia and radiotherapy is synergistic (in other words, why hyperthermia is a very effective radiosensitizer) and works best when the two are applied *simultaneously* [39,47-49].

## Conclusion

In this work, Monte Carlo track chemistry simulations have been used in an attempt to quantify the "acid spike" effect that is generated *in situ* in tracks in the radiolysis of water during the primary radiolytic processes. Two track models were considered depending on the quality (LET) of the radiation: an isolated "spherical" spur model (associated with 300-MeV irradiating protons, LET ~ 0.3 keV/μm) and an axially homogeneous "cylindrical" track model (corresponding to 0.15-MeV incident protons, LET ~ 70 keV/μm). For times shorter than ~1 ns, the pH was found to be nearly constant in both cases: equal to ~3.3 in isolated spurs and ~2.5 in cylindrical tracks. Beyond ~1 ns, the pH increased gradually for both studied cases, ultimately reaching a value of 7 (neutral pH) at ~1 μs (corresponding to the lifetime of the spur) for the spherical geometry and ~0.1 ms for the cylindrical geometry.

We should also emphasize here the very good agreement of our calculated time evolution of $G(H_3O^+)$ in the radiolysis of pure deaerated water by 300-MeV incident protons (which mimic $^{60}$Co γ/fast electron irradiation) with available experimental data at 25 °C.

It does not appear that the transient acid pH effect that we have described has been explored in water or in a cell subject to the action of ionizing radiation, especially high-LET radiation. In this regard, this work raises a number of questions, some of which have been briefly evoked.

## Acknowledgment

We thank Professor Edouard I. Azzam of New Jersey Medical School Cancer Center for his valuable comments. The financial assistance of the Natural Sciences and Engineering Research Council of Canada (Grant No. 9020-2010) is gratefully acknowledged.

## References

1. von Sonntag C. Free-Radical-Induced DNA Damage and its Repair. A Chemical Perspective. Berlin: Springer-Verlag. 2006.

2. Becker D, Sevilla MD. The chemical consequences of radiation damage to DNA. Adv. Radiat. Biol. 1993; 17: 121-180.

3. Cadet J, Berger M, Douki T, Ravanat J-L. Oxidative damage to DNA : Formation, measurement, and biological significance. Rev. Physiol. Biochem. Pharmacol.1997; 131: 1-87.

4. O'Neill P. Radiation-induced damage in DNA. Jonah CD, Rao BSM, editors. In: Radiation Chemistry: Present Status and Future Trends. Amsterdam: Elsevier. 2001; 585-622.

5. Azzam EI, Jay-Gerin J-P, Pain D. Ionizing radiation-induced metabolic oxidative stress and prolonged cell injury. Cancer Lett.2012; 327: 48-60.

6. Platzman RL. The physical and chemical basis of mechanisms in radiation biology. Claus WD, editor. In: Radiation Biology and Medicine. Selected Reviews in the Life Sciences. Reading: Addison-Wesley. 1958; 15-72.

7. Kuppermann A. Theoretical foundations of radiation chemistry.J. Chem. Ed. 1959; 36: 279-285.

8. Chatterjee A, Holley WR. Computer simulation of initial events in the biochemical mechanisms of DNA damage. Adv. Radiat. Biol. 1993; 17: 181-226.

9. Meesungnoen J, Jay-Gerin J-P. Radiation chemistry of liquid water with heavy ions: Monte Carlo simulation studies. Hatano Y, Katsumura Y, Mozumder A, editors. In: Charged Particle and Photon Interactions with Matter: Recent Advances, Applications, and Interfaces. Boca Raton: Taylor & Francis. 2011; 355-400.

10. Spinks JWT, Woods RJ. An Introduction to Radiation Chemistry. 3rd edn. New York: Wiley. 1990.

11. Ferradini C, Jay-Gerin J-P. La radiolyse de l'eau et des solutions aqueuses: historique et actualité. Can. J. Chem. 1999; 77: 1542-1575.

12. Buxton GV. Radiation chemistry of the liquid state: (1) Water and homogeneous aqueous solutions. Farhataziz, Rodgers MA, editors. In: Radiation Chemistry: Principles and Applications. New York: VCH Publishers. 1987; 321-349.

13. Elliot AJ, Bartels DM. The reaction set, rate constants and *g*-values for the simulation of the radiolysis of light water over the range 20 to 350 °C based on information available in 2008. Report AECL-153-127160-450-001. Atomic Energy of Canada Limited, Chalk River, Ontario, Canada. 2009.

14. LaVerne JA. Track effects of heavy ions in liquid water. Radiat.Res. 2000; 153: 487-496.

15. Magee JL. Radiation chemistry.Annu. Rev. Nucl. Sci. 1953; 3: 171-192.

16. Mozumder A, Magee JL. Model of tracks of ionizing radiations for radical reaction mechanisms.Radiat.Res. 1966; 28: 203-214.

17. Tippayamontri T, Sanguanmith S, Meesungnoen J, Sunaryo GR, Jay-Gerin J-P. Fast neutron radiolysis of the ferrous sulfate (Fricke) dosimeter: Monte Carlo simulations. Recent Res.Devel.Physical Chem. 2009; 10: 143-211.

18. Watt DE. Quantities for Dosimetry of Ionizing Radiations in Liquid Water. London: Taylor & Francis. 1996.

19. Smith DR, Stevens WH. Radiation-induced hydrolysis of acetal: Evidence for the reaction of $H_3O^+$ ions in spurs in the radiolysis of water. Nature 1963; 200: 66-67.

20. Anbar M, Thomas JK. Pulse radiolysis studies of aqueous sodium chloride solutions. J. Phys. Chem. 1964; 68: 3829-3835.

21. Cobut V, Frongillo Y, Patau JP, Goulet T, Fraser M-J, Jay-Gerin J-P. Monte Carlo simulation of fast electron and proton tracks in liquid water. I. Physical and physicochemical aspects. Radiat.Phys. Chem. 1998; 51: 229-243.

22. Frongillo Y, Goulet T, Fraser M-J, Cobut V, Patau JP, Jay-Gerin J-P. Monte Carlo simulation of fast electron and proton tracks in liquid water. II. Nonhomogeneous chemistry. Radiat.Phys. Chem. 1998; 51: 245-254.

23. Meesungnoen J, Jay-Gerin J-P. High-LET radiolysis of liquid water with $^{1}H^{+}$, $^{4}He^{2+}$, $^{12}C^{6+}$, and $^{20}Ne^{9+}$ ions: Effects of multiple ionization. J. Phys. Chem. A. 2005; 109: 6406-6419.

24. Tachiya M. Theory of diffusion-controlled reactions: Formulation of the bulk reaction rate in terms of the pair probability. Radiat.Phys. Chem. 1983; 21: 167-175.

25. Pimblott SM, Pilling MJ, Green NJB. Stochastic models of spur kinetics in water. Radiat. Phys. Chem. 1991; 37: 377-388.

26. Goulet T, Fraser M-J, Frongillo Y, Jay-Gerin J-P. On the validity of the independent reaction times approximation for the description of the nonhomogeneous kinetics of liquid water radiolysis. Radiat. Phys. Chem. 1998; 51: 85-91.

27. Plante I. Développement de codes de simulation Monte-Carlo de la radiolyse de l'eau et de solutions aqueuses par des électrons, ions lourds, photons et neutrons. Applications à divers sujets d'intérêt expérimental. PhD Thesis. Université de Sherbrooke, Sherbrooke, Québec, Canada, 2009.

28. Mirsaleh Kohan L, Sanguanmith S, Meesungnoen J, Causey P, Stuart CR, Jay-Gerin J-P. Self-radiolysis of tritiated water. 1. A comparison of the effects of $^{60}Co$ γ-rays and tritium β-particles on water and aqueous solutions at room temperature. RSC Adv. 2013; 3: 19282-19299.

29. Muroya Y, Plante I, Azzam EI, Meesungnoen J, Katsumura Y, Jay-Gerin J-P. High-LET ion radiolysis of water: Visualization of the formation and evolution of ion tracks and relevance to the radiation-induced bystander effect. Radiat.Res. 2006; 165: 485-491.

30. Pikaev AK, Kabakchi SA, Zansokhova AA. Yields and reactions of hydrogen ions on radiolysis of water and aqueous solutions. Faraday Disc. Chem. Soc. 1977; 63: 112-123.

31. Čerček B, Kongshaug. Hydrogen ion yields in the radiolysis of neutral aqueous solutions. J. Phys. Chem. 1969; 73: 2056-2058.

32. Anderson RF, Vojnovic B, Michael BD. The radiation-chemical yields of $H_3O^+$ and $OH^-$ as determined by nanosecond conductimetric measurements. Radiat.Phys. Chem. 1985; 26: 301-303.

33. Barker GC, Fowles P, Sammon DC, Stringer B. Pulse radiolytic induced transient electrical conductance in liquid solutions. 1. Technique and the radiolysis of water. Trans. Faraday Soc. 1970; 66: 1498-1508.

34. Schmidt KH, Ander SM. Formation and recombination of $H_3O^+$ and hydroxide in irradiated water. J. Phys. Chem. 1969; 73: 2846-2852.

35. Autsavapromporn N. The effects of pH and radiation quality (LET) on the radiolysis of liquid water and aqueous solutions: A study by using Monte Carlo simulations. MSc Thesis. Burapha University, Bangsaen, Chonburi, Thailand, 2006.

36. Magee JL, Chatterjee A. Track reactions of radiation chemistry. Freeman GR, editor. In: Kinetics of Nonhomogeneous Processes. New York: Wiley. 1987; 171-214.

37. Draganić IG, Draganić ZD. The Radiation Chemistry of Water. New York: Academic Press. 1971.

38. Ferradini C, Jay-Gerin J-P. The effect of pH on water radiolysis: A still open question. A minireview. Res. Chem. Intermed.2000; 26: 549-565.

39. Tannock IF, Rotin D. Acid pH in tumors and its potential for therapeutic exploitation. Cancer Res. 1989; 49: 4373-4384.

40. Errera M, Forssberg A. Mechanisms in Radiobiology: Multicellular Organisms. Burlington: Elsevier. 2013.

41. Nagasawa H, Little JB. Induction of sister chromatid exchanges by extremely low doses of α-particles. Cancer Res. 1992; 52: 6394-6396.

42. Buonanno M, de Toledo SM, Pain D, Azzam EI. Long-term consequences of radiation-induced bystander effects depend on radiation quality and dose and correlate with oxidative stress. Radiat. Res. 2011; 175: 405-415.

43. Ponnaiya B, Suzuki M, Tsuruoka C, Uchihori Y, Wei Y, Hei TK. Detection of chromosomal instability in bystander cells after Si490-ion irradiation. Radiat. Res. 2011; 176: 280-290.

44. Azzam EI, Little JB. The radiation-induced bystander effect: Evidence and significance. Hum. Exp. Toxicol. 2004; 23: 61-65.

45. Morgan WF. Non-targeted and delayed effects of exposure to ionizing radiation: II. Radiation-induced genomic instability and bystander effects *in vivo*, clastogenic factors and transgenerational effects. Radiat. Res. 2003; 159: 581-596.

46. Hall EJ, Giaccia AJ. Radiobiology for the Radiologist. 6th edn. Philadelphia: Lippincott Williams &Wilkins. 2006.

47. Horsman MR, Overgaard J. Hyperthermia: A potent enhancer of radiotherapy. Clin. Oncol. (R. Coll. Radiol.) 2007; 19: 418-426.

48. Kampinga HH. Cell biological effects of hyperthermia alone or combined with radiation or drugs: A short introduction to newcomers in the field. Int. J. Hyperthermia 2006; 22: 191-196.

49. Hainfeld JF, Lin L, Slatkin DN, Dilmanian FA, Vadas TM, Smilowitz HM. Gold nanoparticle hyperthermia reduces radiotherapy dose. Nanomedicine 2014; 10: 1609-1617.

**Figure 1**: Projections over the *XY*-plane of track segments of 300 (a) and 0.15 (b) MeV protons (LET ~ 0.3 and 70 keV/μm, respectively) incident on liquid water at 25 °C, calculated (at ~$10^{-13}$ s) with our IONLYS Monte Carlo track-structure simulation code (see text). The two irradiating protons are generated at the origin and start traveling along the *Y*-axis. Dots represent the energy deposited at points where an interaction occurred. Note that the penetration range of $^{1}H^{+}$ in liquid water, at the considered energy of 0.15 MeV, amounts to ~2.3 μm (ref. 18).

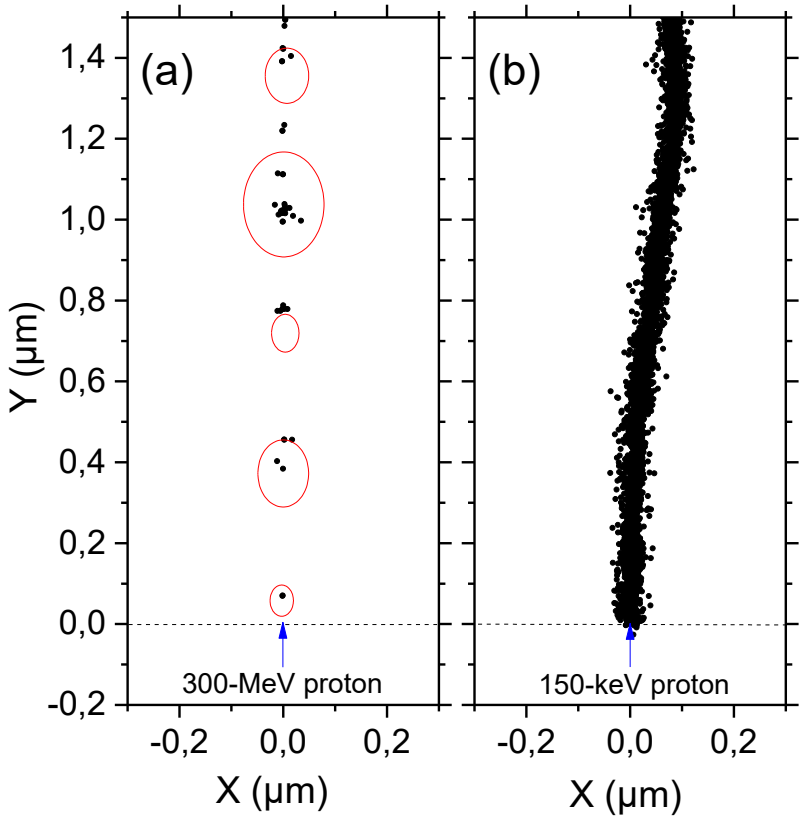

**Figure 2**: Time evolution of the yield (in molecule/100 eV) of hydrogen ions for the radiolysis of pure, deaerated liquid water by 300- and 0.15-MeV incident protons (LET ~ 0.3 and 70 keV/μm, respectively) at 25 °C from ~1 ps to 1 ms. The solid and dashed lines show the corresponding values of $G(H_3O^+)$ obtained from our Monte Carlo simulations (see text). Experimental data for $^{60}$Co γ/fast electron (~0.3 keV/μm) irradiation: (□) ref. 30, (▼) ref. 31, (Δ) ref. 32, (●) ref. 33, and (○) ref. 34. There are no experimental data available for 0.15-MeV irradiating protons with which to compare our results.

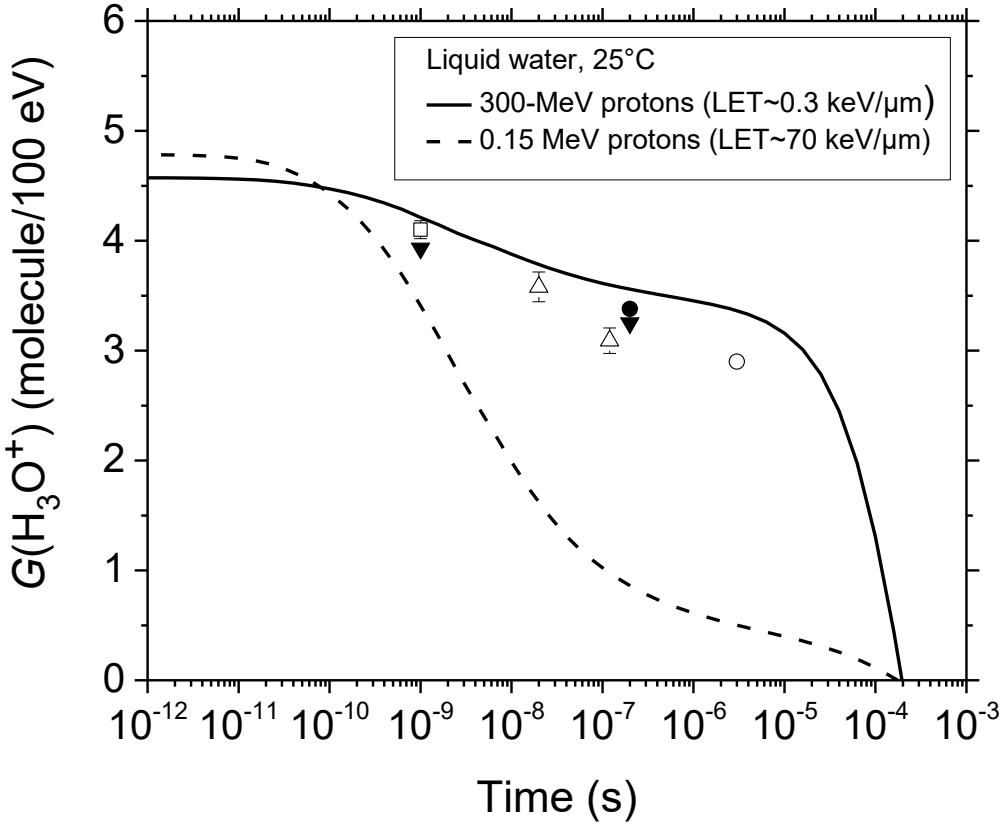

**Figure 3**: Variation of pH with time calculated for 300-MeV incident protons (LET ~ 0.3 keV/μm) using the isolated "spherical" spur model (solid line), characteristic of low-LET radiation, and for 0.15-MeV incident protons (LET ~ 70 keV/μm) using the axially homogeneous "cylindrical" track model (dashed line), characteristic of high-LET radiation, at 25 °C from ~1 ps to 1 ms (see text).

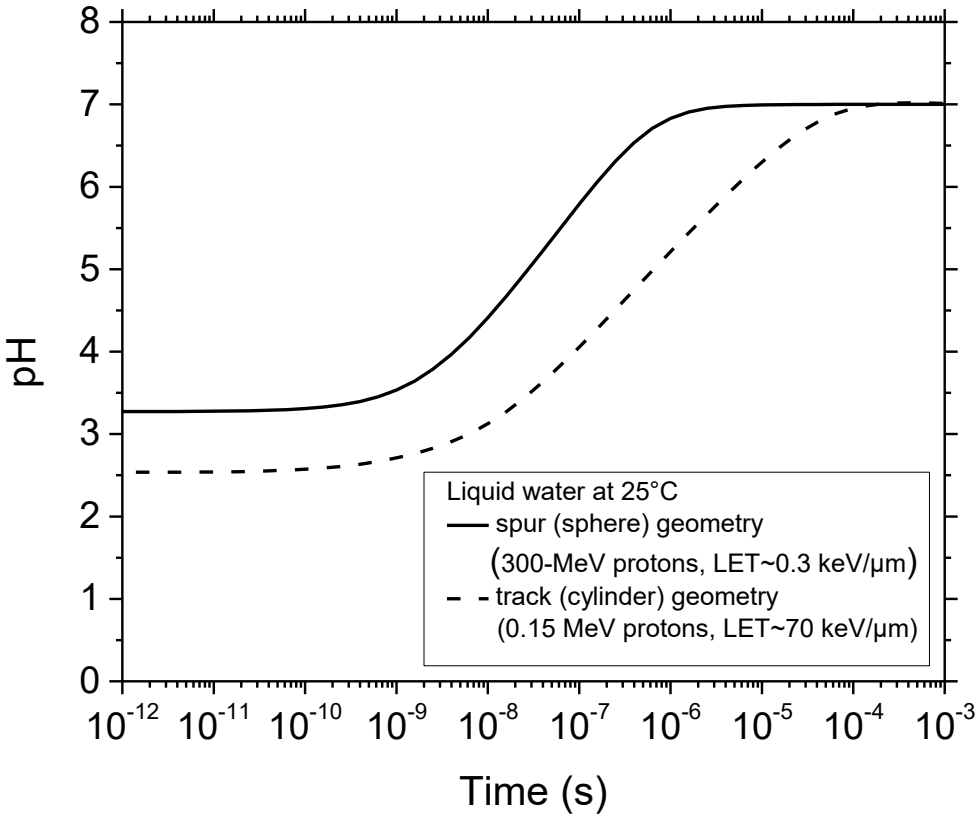

# 4 - ARTICLE No. 2

## Acid-spike effect in spurs/tracks of the low/high linear energy transfer radiolysis of water: potential implications for radiobiology

**Authors:** **Vanaja Kanike,** Jintana Meesungnoen and Jean-Paul Jay-Gerin

**Status**: Published in ***Royal Society of Chemistry Advances, 2015, Vol. 5, No. 54, pp. 43361-43370*** (10 pages).

**Foreword**: In this second article, we present a detailed study of the "acid-spike" effect that is generated *in situ* in spurs/tracks in the low/high-LET radiolysis of pure, deaerated water shortly after irradiation at room temperature. Monte Carlo track chemistry simulations are used, along with two different space-time track models, to calculate the yields of $H_3O^+$ and the corresponding spur/track pH values as a function of time from ~1 ps to ~1 ms. These models include a "spherical" spur model (characteristic of low-LET radiation) and a "cylindrical" track model (for high-LET radiation), and are illustrated by four different selected impacting ions: 300-MeV protons (which mimic $^{60}$Co γ-irradiation; LET ~ 0.3 keV/μm); 150-keV protons (~70 keV/μm); 1.75-MeV per nucleon helium ions (~70 keV/μm); and 0.6-MeV per nucleon helium ions (~146 keV/μm). For all cases studied, an acid spike response to ionizing radiation is observed. For the three high-LET, cylindrically symmetric irradiating ion tracks considered, however, the acid-spike effect is far more intense than that for the spherical spur geometry, with pH around 0.5 on a time scale of ~100 ps. This work, in many respects, raises a number of questions about the potential implications of this effect for radiobiology, some of which are briefly evoked.

**Résumé** : Dans ce second article, nous présentons l'étude détaillée de l'effet de "pic acide" qui se manifeste *in situ* dans les grappes/trajectoires du rayonnement lors de la radiolyse de l'eau pure désaérée à faible/haut TEL immédiatement après le dépôt initial d'énergie, à 25 °C. L'évolution temporelle des concentrations en ions $H_3O^+$ et des valeurs de pH correspondantes est calculée à l'aide de simulations Monte Carlo de la chimie intervenant dans les trajectoires et en utilisant deux modèles spatio-temporels de grappe/trajectoire : un modèle de grappe isolée "sphérique" (faible TEL) et un modèle de trajectoire "cylindrique" (TEL élevé). Quatre ions incidents de TEL variés ont été sélectionnés : des protons de 300 MeV (qui miment une irradiation γ de $^{60}$Co; ~0,3 keV/μm), des protons de 150 keV (~70 keV/μm), des ions hélium de 1,75 MeV/nucléon (~70 keV/μm) et des ions hélium de 0,6 MeV/nucléon (~146 keV/μm). Dans tous les cas, nous observons une réponse marquée de pic acide aux temps courts. Cet effet est cependant beaucoup plus intense dans les trajectoires cylindriques que dans les grappes sphériques, avec des pH avoisinant ~0,5 sur une échelle de temps de ~100 ps. Cette étude, à bien des égards, soulève de nombreuses questions quant aux implications potentielles de cet effet de pic acide en radiobiologie. Certaines d'entre elles sont évoquées brièvement.

# Acid-spike effect in spurs/tracks of the low/high linear energy transfer radiolysis of water: Potential implications for radiobiology

**V. Kanike, J. Meesungnoen and J.-P. Jay-Gerin***

Département de Médecine Nucléaire et Radiobiologie, Faculté de Médecine et des Sciences de la Santé, Université de Sherbrooke, Sherbrooke, Québec J1H 5N4, Canada

***Corresponding author**: Prof. Jean-Paul Jay-Gerin, Department of Nuclear Medicine and Radiobiology, Faculty of Medicine and Health Sciences, Université de Sherbrooke, 3001, 12th Avenue North, Sherbrooke, QC J1H 5N4, Canada. Tel: (1) 819-821-8000, ext. 74682; Email: jean-paul.jay-gerin@USherbrooke.ca ca

*RSC Adv 5(54):43361-43370 (2015)* (10 pages)

Impact Factor: 3.289

Received: April 20, 2015
Accepted: May 7, 2015
Published: May 15, 2015

## ABSTRACT

Monte Carlo track chemistry simulations have been used to calculate the yields of hydronium ions ($H_3O^+$) that are formed within spurs/tracks of the low/high linear energy transfer (LET) radiolysis of pure, deaerated water during and shortly after irradiation. The *in situ* formation of $H_3O^+$ renders the spur/track regions temporarily more acid than the surrounding medium. Although experimental evidence for an acid spur has already been reported, there is only fragmentary information on its magnitude and time dependence. Here, spur/track $H_3O^+$ concentrations and the corresponding pH values are obtained from our calculated yields of $H_3O^+$ as a function of time (in the interval of ~1 ps to 1 ms). We selected four impacting ions and we used two different spur/track models: 1) an isolated "spherical" spur model characteristic of low-LET radiation (such as 300-MeV protons, which mimic $^{60}$Co γ/fast electron irradiation, LET ~ 0.3 keV/μm) and 2) an axially homogeneous "cylindrical" track model for high-LET radiation (such as 150-keV protons, LET ~ 70 keV/μm; 1.75-MeV/nucleon helium ions, LET ~ 70 keV/μm; and 0.6-MeV/nucleon helium ions, LET ~ 146 keV/μm). Very good agreement is found between our calculated time evolution of $G(H_3O^+)$ in the radiolysis of pure, deaerated water by 300-MeV incident protons and the available experimental data at 25 °C. For all cases studied, an abrupt transient acid pH effect is observed at times immediately after the initial energy release. This effect, which we call an "acid spike", is found to be greatest for times shorter than ~1 ns in isolated spurs. In this time range, the pH remains nearly constant at ~3.3. For cylindrical tracks, the acid spike response to ionizing radiation is far more intense than that for the spherical spur geometry. For the three high-LET irradiating ions considered, the pH is around 0.5 on a time scale of ~100 ps. At longer times, the pH increases gradually for all cases, ultimately reaching a value of 7 (neutral pH) at ~1 μs for the spherical geometry and ~0.1 ms for the cylindrical geometry. It does not appear that the transient acid-spike effect described here has been explored in water or in a cellular environment subject to the action of ionizing radiation, especially high-LET radiation. In this regard, this work raises a number of questions about the potential implications of this effect for radiobiology, some of which are briefly evoked.

## 1. Introduction

All biological systems are damaged by ionizing radiation. Since living cells and tissues consist mainly of water (~70-85% by weight), a thorough knowledge of the radiation chemistry of water is critical to our understanding of early stages in the complicated chain of radiobiological events that follow the absorption of radiation. Indeed, in a cellular environment, reactive species generated by water radiolysis are likely to cause chemical modifications and changes in cells, which subsequently may act as triggers of signaling or damaging effects.[1-3] Ultimately, this can lead to observable biological responses.

Although damage can be randomly induced in all biomolecules (*e.g.*, DNA, membrane lipids, and proteins), DNA and its associated water molecules are considered to be the critical target in defining the radiobiological response. Exposure to ionizing radiation is known to cause a plethora of DNA damage. This includes single- and double-strand breaks, base damage, abasic sites, destruction of sugars, tandem lesions, cross-links, defects in mitochondrial functions, and clustered damage.[4-15] Clustered damage is the most biologically-relevant DNA damage induced by radiation because it is less readily repaired by the cell. Damage is caused either directly or indirectly through chemical attack by radiolytic products as the radiation track passes through and deposits energy near to (mostly bulk water) or in the DNA. If unrepaired or mis-repaired, this damage may lead to mutations and promote tumorigenesis, cell death, or long-term stressful effects in surviving cells. A goal of radiobiology research is to understand how radiation exposure deregulates molecular pathways that are important in maintaining genomic integrity.

It is noteworthy that the extent and nature of cellular radiobiological damage depend not only on the absorbed dose but also on the quality of radiation. The “linear energy transfer” (LET) (also called “stopping power” by physicists) represents, to a first approximation, the nonhomogeneity of energy deposition on a sub-microscopic scale. High-LET radiation (*e.g.*, α-particles, high-energy charged nuclei) has a high potential to kill cells with little oxygen and cell cycle dependence. It is thought that the enhanced biological severity of high-LET heavy ions reflects the increased ionization density of high-LET radiation. Therefore, a full understanding is essential of 1) the early physicochemical

track structure (*i.e.*, the physical and chemical events that occur in the "native" radiation track) and 2) the spatio-temporal development of the track. Using this information, we can develop a realistic description of all the reactive fragment species created at early times and involved as precursors to radiobiological damage.[1,3,7,10,16-18] It is also important to know how the initial, spatially nonhomogeneous distribution of reactive species relaxes in time toward a homogeneous distribution. This knowledge is critical to unravel the fundamental biochemical mechanisms leading to the biological consequences of ionizing radiation.

While fundamental biological processes are numerous and complex, they are triggered in aqueous environments. Low-LET, sparsely ionizing radiation includes γ-rays from $^{60}$Co and $^{137}$Cs, hard X-rays, and high-energy charged particles, such as fast electrons or ~300-MeV protons (LET ~ 0.3 keV/μm). From the viewpoint of pure aqueous radiation chemistry, tracks are formed initially by well-separated clusters of reactive species. These are commonly known as "spurs"[19,20] (spherical in shape). During the physicochemical stage of radiation action in Platzman's classification[21,22] (from ~$10^{-16}$ to $10^{-12}$ s after the initial energy deposition), the radiolysis of liquid water can be described by the following reactions:[17,23-25]

$$H_2O \rightsquigarrow H_2O^{\bullet+} + e^- \text{ (ionization)} \quad (1)$$

$$H_2O \rightsquigarrow H_2O^* \text{ (excitation)} \quad (2)$$

$$H_2O^{\bullet+} + H_2O \rightarrow H_3O^+ + {}^{\bullet}OH \text{ (proton transfer reaction, ~200 fs)}[26] \quad (3)$$

$$H_2O^{\bullet+} + M \rightarrow M^{\bullet+} + H_2O \quad (4)$$
(scavenging of the radical cation $H_2O^{\bullet+}$ in highly concentrated solutions)[27]

$$e^- \rightarrow e^-_{sub} \rightarrow e^-_{th} \rightarrow e^-_{tr} \rightarrow e^-_{aq} \text{ (~240 fs to 1 ps)}[28,29] \quad (5)$$
(slowing down to subexcitation energies (< 7.3 eV), thermalization, trapping and hydration)[30]

$$e^- + H_2O^{\bullet+} \rightarrow H_2O^* \text{ (electron-cation geminate recombination)}[31-33] \quad (6)$$

$$e^- + H_2O \rightarrow H_2O^{\bullet-} \rightarrow H^- + {}^{\bullet}OH, \quad (7)$$
(resonant dissociative electron attachment, or DEA process)[33-37]

followed by

$$H^- + H_2O \rightarrow H_2 + OH^- \quad (8)$$

$$\{e^-, e^-_{sub}, e^-_{th} \text{ or } e^-_{tr}\} + M \rightarrow M^{\bullet-} \quad (9)$$

("dry" or "pre-hydrated" electron capture by a suitable scavenger in sufficiently high concentrations)[38-42]

$H_2O^* \rightarrow e^-_{aq} + H_2O^{\bullet+}$ (threshold at ~6.5 eV)[43] (10)

$H_2O^* \rightarrow H^\bullet + {}^\bullet OH$ (11)

$H_2O^* \rightarrow H_2 + O(^1D)$ (oxygen atom in its singlet $^1D$ first excited state) (12)

followed by

$O(^1D) + H_2O \rightarrow H_2O_2$ (or possibly also $2\,{}^\bullet OH$)[44] (13)

$H_2O^* \rightarrow 2\,H^\bullet + {}^\bullet O^\bullet(^3P)$ (oxygen atom in its triplet $^3P$ ground state, rather inert to water but reacts with most additives)[45] (14)

By ~1 ps, the various "initial" radiolysis products are the hydrated electron ($e^-_{aq}$), $H^\bullet$, ${}^\bullet OH$, $H_2$, $H_2O_2$, $H^+$ (or equivalently, $H_3O^+$ or $H^+_{aq}$), $OH^-$, $O_2^{\bullet-}$ [or $HO_2^\bullet$, depending on the pH; $pK_a(HO_2^\bullet/O_2^{\bullet-}) = 4.8$ in water at 25 °C],[46] ${}^\bullet O^\bullet(^3P)$, *etc.*[17,23-25] At this time, these species begin to diffuse away from the site where they were originally produced. The result is that a fraction of them react together within the spurs as they develop in time while the remainder escape into the bulk solution. At ambient temperature, the spur expansion is essentially complete by ~0.2 μs.[47] At this time, the species that have escaped from spur reactions become homogeneously distributed throughout the bulk of the solution (*i.e.*, the system at large) and the radiation track structure no longer exists.[1,48]

The yields per 100 eV of absorbed energy of the species, which emerge from the spurs at the end of the nonhomogeneous chemical stage,[21,22] are the so-called "primary" (or "escape") yields. They are denoted by $g(e^-_{aq})$, $g(H^\bullet)$, $g({}^\bullet OH)$, $g(H_2)$, $g(H_2O_2)$, *etc.*[17,23-25,49,50] For $^{60}$Co γ-irradiated neutral solution at 25 °C, $g(e^-_{aq}) = 2.65$, $g(H^\bullet) = 0.6$, $g({}^\bullet OH) = 2.8$, $g(H_2) = 0.45$, and $g(H_2O_2) = 0.68$ molecules/100 eV.[50,51] The radical and molecular products are then available for reaction with dissolved solutes (if any) present (in low or moderate concentrations) at the time of irradiation. In the presence of air or oxygen, $e^-_{aq}$ and $H^\bullet$ atoms are rapidly converted to superoxide anion ($O_2^{\bullet-}$)/hydroperoxyl ($HO_2^\bullet$) radicals, according to:

$e^-_{aq} + O_2 \rightarrow O_2^{\bullet-}$ $\quad k_{15} = 2.11 \times 10^{10}\ M^{-1}\ s^{-1}$ (15)

$H^\bullet + O_2 \rightarrow HO_2^\bullet$ $\quad k_{16} = 1.2 \times 10^{10}\ M^{-1}\ s^{-1}$ (16)

where $k_{15}$ and $k_{16}$ are the rate constants for the two individual reactions.[50] Thus, in an aerobic cellular environment at pH 7, the major reactive species at homogeneity (~0.2 μs) include $O_2^{\bullet-}$, $^{\bullet}OH$, and $H_2O_2$.[3]

In biological systems, ionizing radiation can also stimulate inducible nitric oxide synthase (iNOS) activity in hit cells,[52] thereby generating large amounts of nitrogen monoxide (or "nitric oxide", $^{\bullet}NO$). Although $^{\bullet}NO$ is chemically inert toward most cellular constituents (except for heme), it reacts with $O_2^{\bullet-}$ to form the peroxynitrite anion ($ONOO^-$) with a rate constant ($1.9 \times 10^{10}$ $M^{-1}$ $s^{-1}$) that is larger than that for the copper/zinc-superoxide dismutase (SOD)-catalyzed disproportionation of $O_2^{\bullet-}$.[53] Like $^{\bullet}OH$ radicals, $ONOO^-$ and its conjugate acid, peroxynitrous acid ONOOH ($pK_a$ = 6.8 at 37 °C),[54] are powerful oxidizing agents. They are capable of attacking a wide range of cellular targets, including lipids, thiols, proteins, and DNA bases.[3,53-55]

The yield of all the radiolytic species and free radical intermediates and their initial geometric distributions along the tracks are strongly dependent on the radiation type and energy. For the chemical properties of spurs, the predominant effect of $^{60}$Co γ/fast electron radiolysis is radical production.[23-25] However, the chemistry of water and aqueous solutions is very different after irradiation with high-LET, densely ionizing radiation.[1,17,48,56,57] Indeed, with increasing LET, the mean separation distance between the spurs decreases. Further, the isolated spur structure changes to a situation in which the spurs eventually overlap and form (initially) a dense continuous column (cylindrical in shape) of species.[1,30,58,59] This leads to an increased amount of intra-track chemistry, favoring radical-radical reactions in the diffusing tracks. Under these conditions, the free-radical yields tend to diminish as the LET is increased, whereas the molecular yields increase.[17,24,25,56]

Herein, we present simple space-time model calculations. They quantitatively show that the formation of $H_3O^+$ in reaction (3), during the initial radiolytic processes in irradiated water, renders the spur/track regions temporarily more acid than the body of the solution. Although experimental evidence for this transient acid pH effect has already been reported,[24,60,61] there is only fragmentary information on its magnitude and time dependence following energy deposition. In this work, we use Monte Carlo track chemistry simulations to calculate, at 25 °C, the yields of $H_3O^+$ produced by water radiolysis as a function of time from ~1 ps to 1 ms. We carry out simulations for four different impacting

ions: 1) 300-MeV protons (which mimic $^{60}$Co γ/fast electron irradiation; LET ~ 0.3 keV/μm); 2) 150 keV protons (LET ~ 70 keV/μm); 3) 1.75-MeV/nucleon helium ions (LET ~ 70 keV/μm); and 4) 0.6-MeV/nucleon helium ions (LET ~ 146 keV/μm). The results are compared with available experimental data. The concentrations of $H_3O^+$ and the corresponding pH values for each ion considered are obtained from our calculated yields of $H_3O^+$ using a "spherical" spur model for low-LET radiation and a "cylindrical" track model for high-LET radiation.

A brief preliminary report of this work has been presented elsewhere.[62]

## 2. Monte Carlo track chemistry simulations of water radiolysis

Monte Carlo simulation methods are well suited to take into account the stochastic nature of the complex sequence of events that are generated in aqueous systems following the absorption of ionizing radiation. Simulations allow the reconstruction of the intricate action of radiation. This is a powerful tool for studying the relationship between the initial radiation track structure, the ensuing chemical processes, and the stable end products formed by radiolysis. In previous studies,[17,33,63-66] we provided a detailed description of our IONLYS-IRT Monte Carlo code. This program simulates, in a 3D geometrical environment, the nonhomogeneous distribution of reactive species initially produced by the absorption of incident radiation and all of the energetic secondary electrons, as well as the subsequent diffusion and chemical reactions of these species. Briefly, the IONLYS step-by-step simulation program covers the early physical and physicochemical stages of radiation action up to ~1 ps in track development. It models all the basic physical interactions (energy deposition). It also models the subsequent conversion of the physical products created locally into the various initial radical and molecular products of radiolysis [see reactions (1)-(14)], which are distributed in a highly nonhomogeneous track structure. The complex spatial distribution of reactants at the end of the physicochemical stage is provided as an output of the IONLYS program. It is then used directly as the starting point for the subsequent nonhomogeneous chemical stage.[21,22] The different species now diffuse randomly at rates determined by their diffusion coefficients. They react, or compete, with one another as well as with any added solutes present at the time of irradiation until all spur/track reactions are complete (typically, on the time scale from ~1 ps to ~0.2-1 μs). We

simulate this stage using the "independent reaction times" (IRT) method.[64,67,68] This is a computer-efficient stochastic simulation technique that is used to simulate reaction times without having to follow the trajectories of the diffusing species. The IRT method relies on the approximation that the reaction time of each pair of reactants is independent of the presence of other reactants in the system. Its implementation has been described in detail previously.[64] The IRT method gives accurate time-dependent chemical yields over a wide range of irradiation conditions. This has been well validated by comparison with full random flight Monte Carlo simulations, which do follow the reactant trajectories on an event-by-event basis.[69,70] This IRT program can also be used to efficiently describe the reactions that occur in the bulk solution during the homogeneous chemical stage[21,22] (*i.e.*, in the time domain beyond a few microseconds).

The reaction scheme and reaction parameters used in our IRT program for pure liquid water at 25 °C are the same as used previously (see Table 1 of ref. 71). This set of reactions, initially compiled in ref. 17 and 44, now includes some newly measured or recently re-assessed reaction rates by Elliot and Bartels.[50] Values for the diffusion coefficients of the various reactive species involved in the simulations are listed in Table 6 of ref. 72.

To reproduce the effects of $^{60}$Co γ/fast electron radiolysis, we used short segments of 300-MeV incident proton tracks (see Fig. 1, panel a, of ref. 62 and 73). The average LET value obtained in the simulations was nearly constant and equal to ~0.3 keV/μm at 25 °C. Such model calculations thus gave "track segment" yields at a well-defined LET.[56,64,74] The influence of the LET of the radiation on the $H_3O^+$ yields was investigated by performing a series of similar simulations, but using different types of impacting ions of various initial energies. In this study, we limited ourselves to the following cases: 1) 150-keV protons and 1.75-MeV/nucleon helium ions, which have the same LET (~70 keV/μm),[1] and 2) 0.6-MeV/nucleon helium ions, corresponding to a LET value of ~146 keV/μm.[75] In these cases, spurs are formed so close to each other along the path of the irradiating ions that they merge to form a cylindrical region of high LET (see below). At low dose rates (so that no track overlap occurs), each spherical spur or cylindrical track can be treated independently from the others.

The simulations consist of following the transport and energy loss of the incident ion (proton or helium ion) until it has penetrated the chosen length (~1-150 μm) of the track segment into the medium. At the incident ion energies considered here, interactions involving electron capture and loss by the moving ion (charge-changing collisions) have been neglected. Due to its large mass, the impacting ion is almost not deflected by collisions with the target electrons.[1,17,63] Typically, about 5000 to $10^5$ reactive chemical species are generated in these simulated track segments (depending on the type and energy of the irradiating ions). This ensures only small statistical fluctuations in the determination of averaged chemical yields.

## 3. Results and discussion

Figure 1 shows the time evolution of $G(H_3O^+)$ as obtained from our simulations of the radiolysis of pure, deaerated liquid waterby 300-MeV incident protons (LET ~ 0.3 keV/μm) at ambient temperature, over the interval of ~1 ps to 1 ms. For comparison, experimental data obtained by several groups[76-80] for $^{60}$Co γ/fast electron irradiation are also shown in the figure. As can be seen, our computed values (red solid line) are in very good agreement with the measured $H_3O^+$ yields.

The sharp decrease of $G(H_3O^+)$ observed at times longer than ~10 μs for 300-MeV irradiating protons is mainly due to $H_3O^+$ reacting with $OH^-$ and, to a lesser extent, with the hydrated electrons escaping the spurs, according to:

$$H_3O^+ + OH^- \rightarrow 2H_2O \qquad k_{17} = 1.18 \times 10^{11}\, M^{-1}\, s^{-1} \qquad (17)$$

$$H_3O^+ + e^-_{aq} \rightarrow H^\bullet + H_2O \qquad k_{18} = 2.13 \times 10^{10}\, M^{-1}\, s^{-1} \qquad (18)$$

where $k_{17}$ and $k_{18}$ are the rate constants for the two individual reactions.[17,71] This is clearly seen in Fig. 2 where we show the time profiles of $\Delta G(H_3O^+)$ for each of the reactions that contribute to $G(H_3O^+)$, calculated from our Monte Carlo simulations in the time interval ~1 ps to 1 ms.

Figure 3 shows the effect of LET on the temporal variation of the yield of $H_3O^+$ at 25 °C for pure, deaerated liquid water irradiated by 300-MeV (LET ~ 0.3 keV/μm) and 150-keV (LET ~ 70 keV/μm) incident protons, and with 1.75-MeV/nucleon (LET ~ 70 keV/μm) and 0.6-MeV/nucleon (LET ~ 146 keV/μm) helium ions. As can be seen, the

decrease in $G(H_3O^+)$ in high-LET ion tracks occurs as early as ~100 ps up to microseconds, which is clearly different from what is observed for irradiation with 300-MeV incident protons (which mimic $^{60}$Co γ/fast electron irradiation). As expected on physical grounds, this is consistent with differences in the initial spatial distribution of primary transient species (*i.e.*, in the track structure). As mentioned earlier, in the track (cylindrical) geometry of the three high-LET irradiating ions used, the reactive intermediates are formed locally in much closer initial proximity than in the spur (spherical) geometry. This favors, at shorter time scales, an increased amount of intervening intra-track reactions. In this case, the results in Fig. 3 show that, as the LET is increased, the decrease in $G(H_3O^+)$ becomes more pronounced as a function of time, and begins at shorter times. It is also shown that the temporal variations of $G(H_3O^+)$ for 150-keV protons and 1.75-MeV/nucleon helium ions, which have nearly equal LET (~70 keV/μm), are little affected by the differences in track structure between these two irradiating ions.[1] To our knowledge, there is no experimental information available in the literature, unfortunately, with which to compare our results on the time dependences of the yield of $H_3O^+$ at high LET.

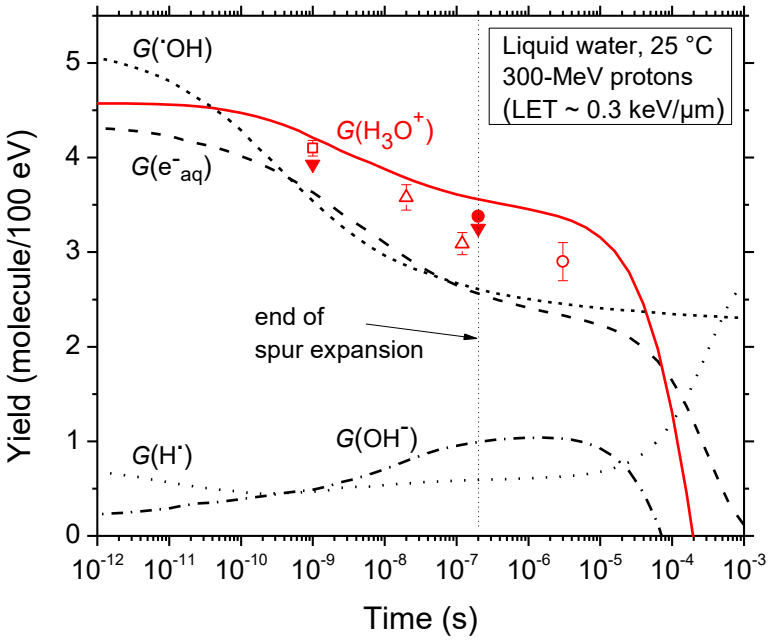


**Fig. 1** Time evolution of $G(H_3O^+)$ (in molecule/100 eV) for the radiolysis of pure, deaerated liquid water by 300-MeV incident protons (LET ~ 0.3 keV/μm) at 25 °C from ~1 ps to 1 ms. The red solid line shows the hydrogen ion yield values obtained from our Monte Carlo simulations (see text). Experimental data for $^{60}$Co γ/fast electron irradiation are: (□)

ref. 76, (▼) ref. 77, (Δ) ref. 78, (●) ref. 79, and (○) ref. 80. For the sake of reference, our simulated time-dependent yields of $e^-_{aq}$ and $^\bullet OH$ (see ref. 81), $H^\bullet$ and $OH^-$ are also included in the figure. Note that the hydroxide ion $OH^-$, which is formed largely by the reaction: $e^-_{aq} + {}^\bullet OH \rightarrow OH^-$ ($k = 3.55 \times 10^{10}\ M^{-1}\ s^{-1}$) as the spur expands, contributes to an alkaline spur and consequently counteracts the acid-spike effect discussed in this work. However, as we can see from the figure, $G(OH^-)$ remains much smaller than $G(H_3O^+)$ over the time range of interest. As a result, its effect only slightly modifies the quantitative features of the pH and can be ignored to a good approximation. Finally, the (dotted) line shown at ~0.2 μs indicates the end of spur expansion (ref. 47), *i.e.*, the time required to observe the transition from nonhomogeneity to homogeneity in the distribution of the radiolytic species.

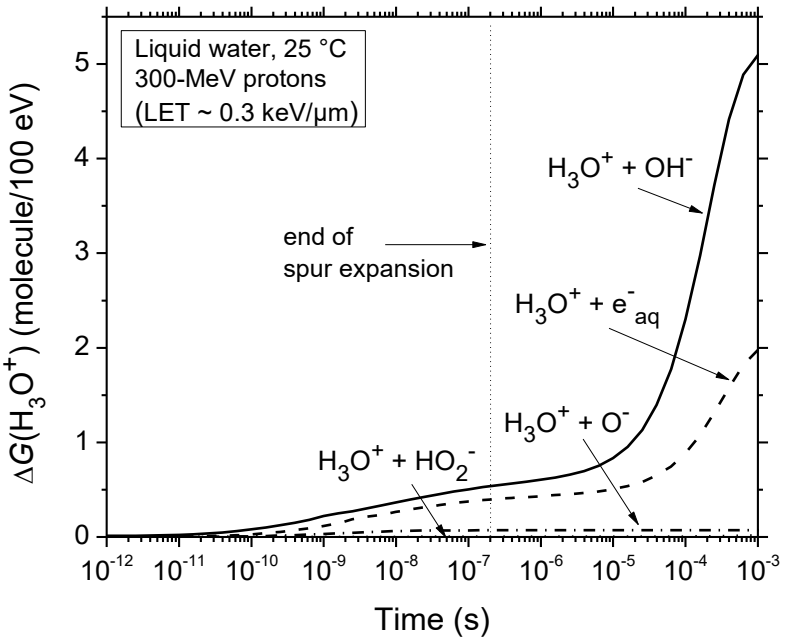


**Fig. 2** Time dependence of the extents $\Delta G(H_3O^+)$ (in molecule/100 eV) of the different reactions that are involved in the decay of $H_3O^+$, calculated from our Monte Carlo simulations of the radiolysis of pure, deaerated water by 300-MeV incident protons (LET ~ 0.3 keV/μm) at 25 °C, in the interval of ~1 ps to 1 ms. Other reactions, such as $H_3O^+ + O^{\bullet -} \rightarrow {}^\bullet OH + H_2O$ ($k = 5 \times 10^{10}\ M^{-1}\ s^{-1}$) and $H_3O^+ + HO_2^- \rightarrow H_2O_2 + H_2O$ ($k = 5 \times 10^{10}\ M^{-1}\ s^{-1}$), contribute only little to the decay of $G(H_3O^+)$. The (dotted) line shown at ~0.2 μs indicates the end of spur expansion (ref. 47).

With the objective of calculating the pH values prevailing in the spur or track regions, we now need to estimate the concentrations of $H_3O^+$ generated *in situ* in these regions as a

function of time. Two simple models are considered here depending on the quality (or LET) of the radiation.

1) For 300-MeV incident protons (LET ~ 0.3 keV/μm), we assume that the hydronium ions are produced evenly in an isolated *spherical* spur. The spur's initial radius $r_o$, prior to spur expansion, is equal to the average electron thermalization distance obtained from our simulations ($r_o$ ~ 11.7 nm).[31,33,82] The low-LET spur concentrations of $H_3O^+$ are derived from[62,83]

$$[H_3O^+](t) = G(H_3O^+)(t) \times \left( \frac{\text{Mean energy loss per event}}{\frac{4}{3}\pi r(t)^3} \right) \quad (19)$$

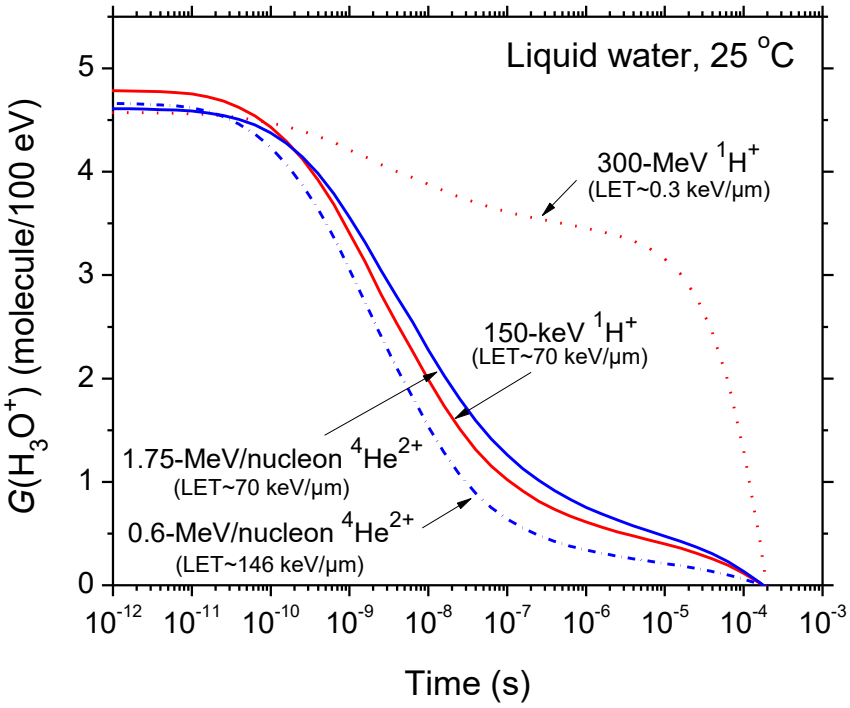


**Fig. 3** Time dependences of $H_3O^+$ yields (in molecule/100 eV) calculated from our Monte Carlo simulations of the radiolysis of pure, deaerated liquid water at 25 °C and in the interval of ~1 ps to 1 ms, for impacting 300-MeV (~0.3 keV/μm) and 150-keV (~70 keV/μm) protons, and 1.75-MeV/nucleon (~70 keV/μm) and 0.6-MeV/nucleon (~146 keV/μm) $^4He^{2+}$ ions. It is worth noting here that $G(OH^-)$, in all high-LET ion tracks considered, remains at a nearly constant level well below 1 *G*-unit, and therefore much smaller than $G(H_3O^+)$, during the lifetime of the tracks (not shown in the figure). Consequently, as mentioned in the caption of Fig. 1, the formation of $OH^-$ ions only slightly modifies the quantitative features of the pH and can simply be ignored.

where the mean energy loss in a single energy deposition event (*i.e.*, the mean energy deposited in a spur) in liquid water is taken to be ~47 eV[63,71,84,85] and

$$r(t)^2 = r_o^2 + 6\,D\,t \qquad (20)$$

represents the change with time of $r_o$ due to the three-dimensional diffusive expansion of the spur. Here, $t$ is time and $D$ is the diffusion coefficient of $H_3O^+$ in water ($D = 9.46 \times 10^{-9}$ $m^2$ $s^{-1}$ at 25 °C).[64]

Using a consistent set of units,[83] Eqs. (19) and (20) readily give the concentration of $H_3O^+$ as a function of time. The pH in the corresponding spur region is then simply given by the negative logarithm (to the base 10) of $[H_3O^+]$:

$$pH(t) = - \log \{[H_3O^+](t)\} . \qquad (21)$$

The time evolution of the pH values calculated for 300-MeV incident protons in pure, deaerated liquid water (LET ~ 0.3 keV/μm) using the spherically symmetric spur model is shown by the solid curve in Fig. 4. As can be seen, there is an abrupt transient *acid* pH

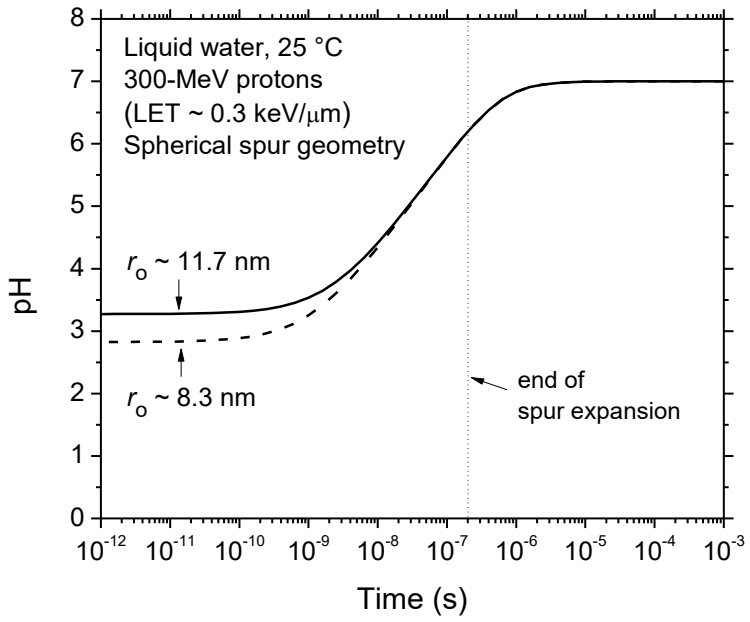


**Fig. 4** Time evolution of pH in a spur calculated for 300-MeV incident protons in pure, deaerated liquid water (LET ~ 0.3 keV/μm) using the isolated "spherical" spur model, characteristic of low-LET radiation, at 25 °C (see text). The solid and dashed lines show the pH values obtained for two different spur radii $r_o$ = 11.7 and 8.3 nm, respectively. The (dotted) line shown at ~0.2 μs indicates the end of spur expansion (ref. 47).

effect at times immediately after the initial energy release. This "acid spike" is greatest for times shorter than ~1 ns. The "acid spike" term arises from an analogy with the "thermal spike" used in radiation chemistry to describe the formation of a transient excess temperature region around the high-LET tracks of heavy ions in water.[56,86-88] In this time range, the pH remains nearly constant, equal to ~3.3. Beyond ~1 ns, the pH increases gradually, ultimately reaching a value of 7 (neutral pH) at ~1 μs (*i.e.*, slightly longer than the end of spur expansion and the beginning of homogeneous chemistry).[17,23-25] Figure 4 also shows the sensitivity of our calculated pH results to the choice of the radius of the initial spatial distribution of $e^-_{aq}$ ($r_o$), which is not precisely known. Using a smaller value of $r_o$ (~8.3 nm instead of 11.7 nm)[82] results in an increased acid-spike effect at early times (pH ~ 2.8 instead of 3.3), but has little impact on the temporal variation of the pH beyond ~1 ns (dashed curve in Fig. 4). This is expected since a decrease in the spur radius, all other parameters being constant, leads to an increase in the concentration of $H_3O^+$ ions formed in the spur and, hence, to a more acidic pH response.

2) For high-LET radiation, we consider the track as being an axially homogeneous *cylinder*, of length $L$ = 1 μm and initial radius $r_c$ equal to the radius of the physical track "core". The core corresponds to the tiny radial region within the first few nanometers around the impacting ion trajectory. In this region the energy density of deposition is very high.[16,17,30,59] For the sake of illustration, Figs. 5-7 show typical two-dimensional representations of 1-μm track segments of, respectively, a 150-keV (LET ~ 70 keV/μm) proton, a 1.75-MeV/nucleon (LET ~ 70 keV/μm) helium ion, and a 0.6-MeV/nucleon (LET ~ 146 keV/μm) helium ion in liquid water at 25 °C. They were calculated (at ~$10^{-13}$ s) with our IONLYS Monte Carlo simulation code. In this case, the high-LET track concentrations of $H_3O^+$ can be obtained from[17,62,83]

$$[H_3O^+](t) = G(H_3O^+)(t) \times \left(\frac{\text{LET}}{\pi r(t)^2}\right), \tag{22}$$

where[59]

$$r(t)^2 = r_c^2 + 4\,D\,t \tag{23}$$

represents the change with time of $r_c$ due to the two-dimensional diffusive expansion of the track. Here, $r_c$ was estimated directly from our simulations (see Figs. 5-7).

Using Eq. (22) and (23) readily gives the concentrations of $H_3O^+$ as a function of time for axially homogeneous, cylindrically symmetric tracks. The pH in the corresponding track regions is then simply given by Eq. (21).

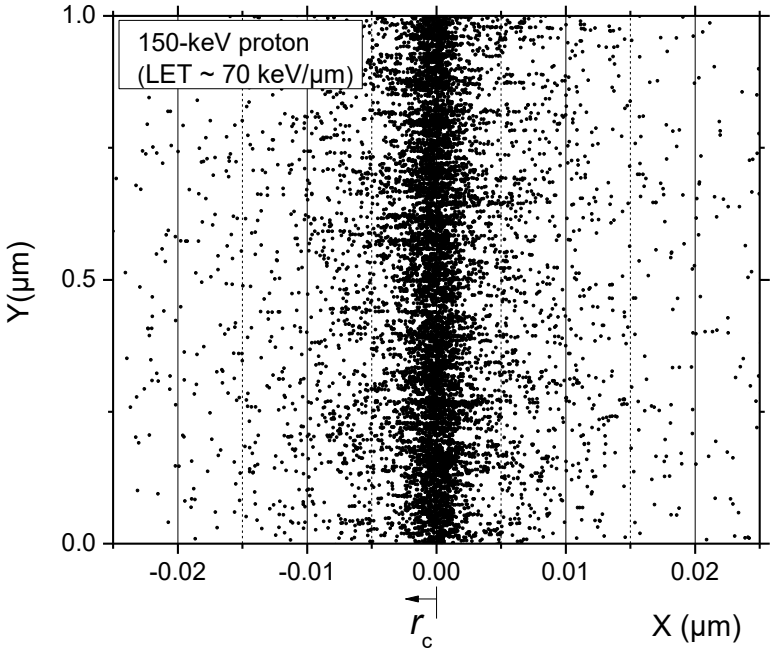


**Fig. 5** Simulated track history (at ~$10^{-13}$ s, projected into the *XY*-plane of figure) of a 150-keV proton (LET ~ 70 keV/μm) traversing through liquid water at 25 °C. The irradiating proton is generated at the origin and starts traveling along the *Y*-axis. Dots represent the energy deposited at points where an interaction occurred. The track can be described as two coaxial cylindrical volumes centered on the path of the proton. The inner cylindrical volume (*i.e.*, the region adjacent to the trajectory) is the track "core" with radius $r_c$. Surrounding the core is a much larger region called the "penumbra" where all of the energy is deposited by energetic secondary electrons (δ-rays) created in knock-on collisions by the primary proton. The total time for penumbra formation may be as long as ~1 ps, and its radius extends to the limit of the range of knock-on electrons.

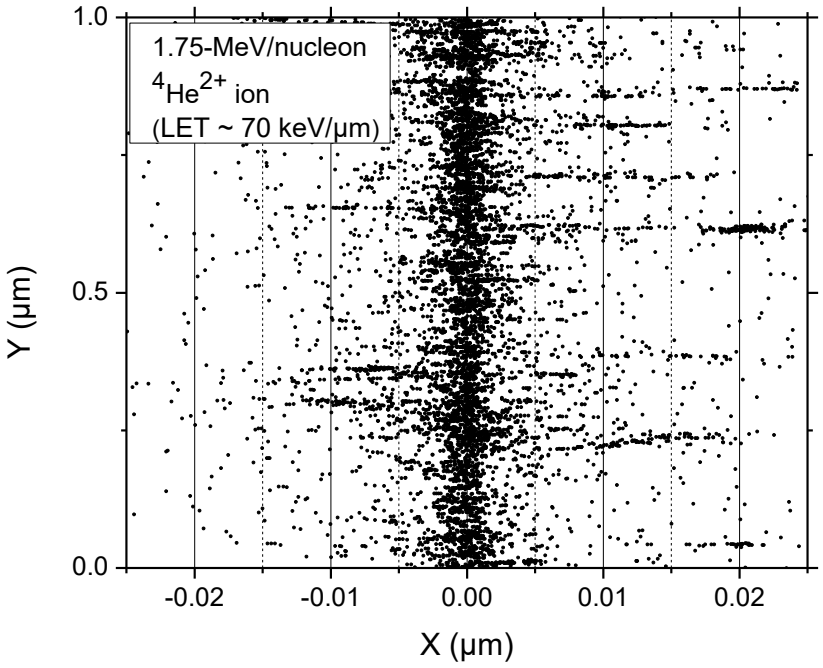


**Fig. 6** Simulated track history (at ~$10^{-13}$ s, projected into the *XY*-plane of figure) of a 1.75-MeV/nucleon helium ion (LET ~ 70 keV/μm) incident on liquid water at 25 °C. Irradiating conditions are the same as in Fig. 5.

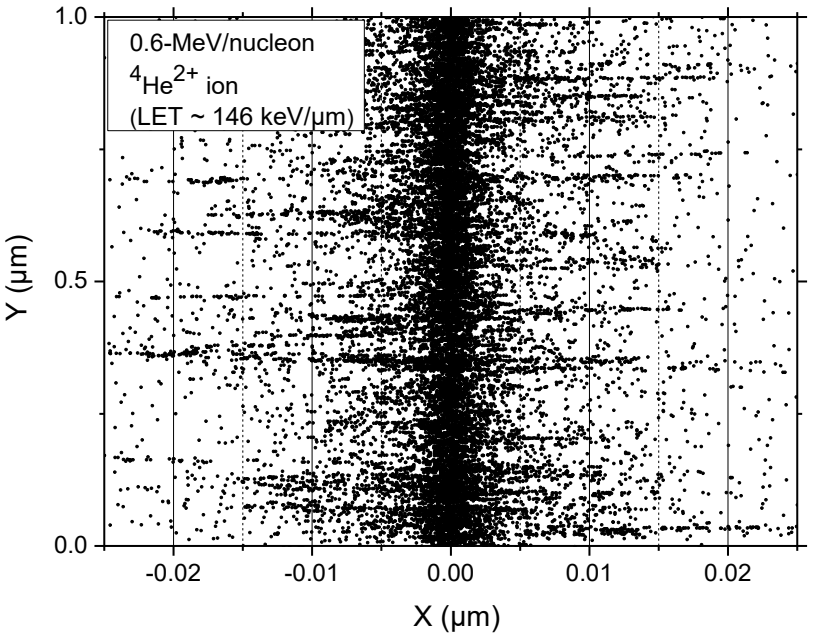


**Fig. 7** Simulated track history (at ~$10^{-13}$ s, projected into the *XY*-plane of figure) of a 0.6-MeV/nucleon helium ion (LET ~ 146 keV/μm) incident on liquid water at 25 °C. Irradiating conditions are the same as in Fig. 5.

Figure 8 shows the time evolution of the pH values calculated as indicated above for 150-keV incident protons in pure, deaerated liquid water (LET ~ 70 keV/μm) using the cylindrical track model at 25 °C for different values of $r_c$ in the range of 2-25 nm. Quite similarly to the spherical spur case for low-LET radiation, there is an abrupt temporary *acid* pH effect at early times. Its magnitude and duration strongly depend on the value chosen for $r_c$. If we adopt $r_c$ = 2 nm (which is the most pertinent value for $r_c$ according to Fig. 5), the pH is equal to ~0.35 at times less than ~100 ps and then increases gradually with time. Ultimately, it reaches a value of 7 (pH of the body of the solution) at ~100 μs.

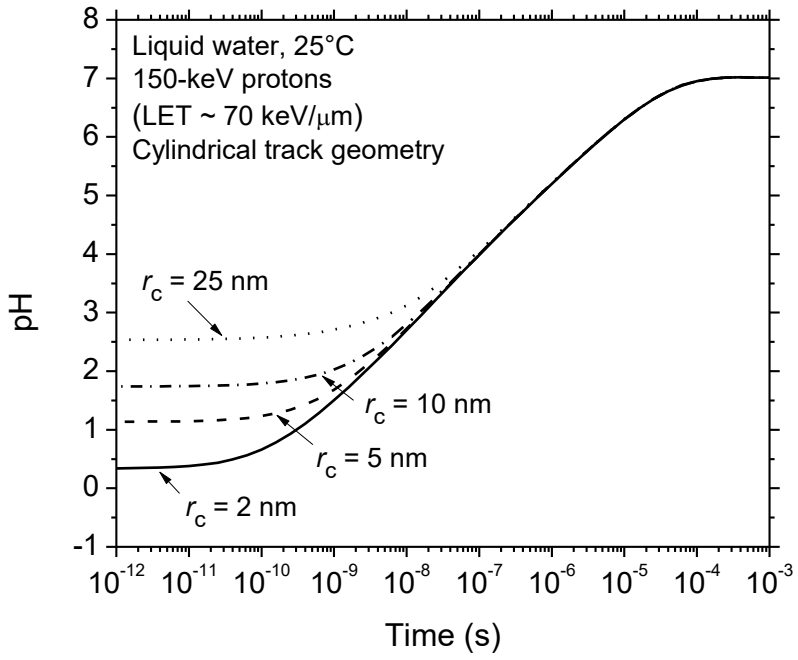


**Fig. 8** Variation of pH with time calculated for 150-keV incident protons (LET ~ 70 keV/μm) using the axially homogeneous cylindrical track model, characteristic of high-LET radiation, for different physical core radii between 2 and 25 nm, at 25 °C from ~1 ps to 1 ms (see text).

However, even if the curves shown in Fig. 8 have shapes closely resembling those of Fig. 4, *the acid spike for the cylindrical track is clearly far more intense than that found for isolated spherical spurs*. This is also well illustrated in Fig. 9, where we show the effect of LET of the incident radiation on the variation of pH with time. Calculations were carried out for pure, deaerated liquid water irradiated by four impacting ions: 1) 300-MeV protons

(which mimic $^{60}$Co γ/fast electron irradiation; LET ~ 0.3 keV/μm); 2) 150-keV protons (LET ~ 70 keV/μm); 3) 1.75-MeV/nucleon helium ions (LET ~ 70 keV/μm); and 4) 0.6-MeV/nucleon helium ions (LET ~ 146 keV/μm). The different curves were obtained by using Eqs. (19)-(21) for the spherical spur model (low-LET radiation) and Eqs. (21)-(23) for the cylindrical track model (high-LET radiation) along with our calculated yields of $H_3O^+$ shown in Fig. 3.

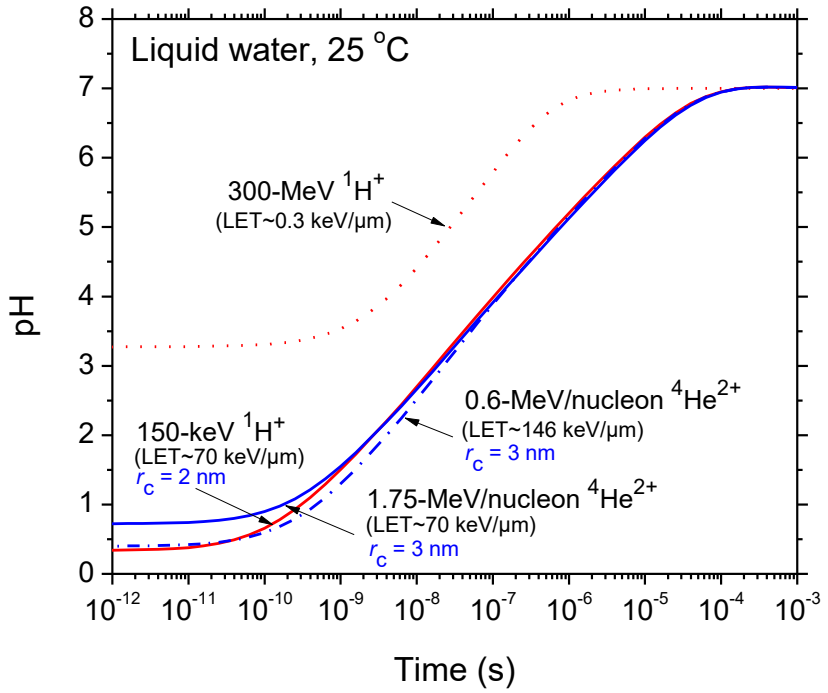


**Fig. 9** Variation of pH with time calculated for pure, deaerated liquid water at 25 °C and in the interval of ~1 ps to 1 ms, for irradiating 300-MeV protons (LET ~ 0.3 keV/μm) (dotted line) using the isolated spherical spur model (characteristic of low-LET radiation) and for impacting 150-keV protons (LET ~ 70 keV/μm), and 1.75-MeV/nucleon (LET ~ 70 keV/μm) and 0.6-MeV/nucleon (LET ~ 146 keV/μm) helium ions using the axially homogeneous cylindrical track model (characteristic of high-LET radiation) (see text).

To the best of our knowledge, the early-time, acid-spike effect described above has never been explored in water or in living cells subject to ionizing radiation, especially high-LET radiations (*e.g.*, α-particles, high charge and high energy particles). In this context, this work prompts a number of important questions not only in radiation chemistry, but also in radiation- and free-radical-biology[2,62,89] as many cellular processes critically depend on

pH.[90-92] Any significant change in the early time, transient kinetics/chemistry would provoke important new insights into our understanding of many aspects of the biological action of radiation. This should stimulate novel predictions that can then be tested through new measurements. We mention a few of these questions below.

For example, in radiation chemistry, does the generation of strongly acidic regions, which extend over spatial dimensions of the order of tens of nanometers, have any noticeable influence on final product formation by affecting all pH-dependent species, protonation/deprotonation reactions, and reaction rates?[11,51,93] In radiation- and free-radical-biology, is this transient acid pH, which is well outside the physiological range, toxic to cells (*e.g.*, by attacking DNA, by causing oxidative injury, by modifying normal biochemical reactions, or by triggering different signaling cascades that respond to these stress conditions)?[3] Moreover, could these *in situ* changes in acidity contribute to the initial events that lead to cell damage, enhanced lethality, "bystander" responses (where stressful effects are propagated from irradiated cells to non-targeted neighbors),[94-97] or genomic instability in progeny of irradiated cells and their neighboring bystanders?[98,99] In the development of effective therapies for malignant diseases, do these spikes of acidity have any adverse effect on the response of cells to conventional anticancer drugs and possibly influence the outcome of tumor therapy?[90]

Finally, it has been demonstrated that cells in an acid pH environment are more sensitive to the lethal effect of heat (in the clinically relevant temperature range of 39-45 °C).[12,100] We have described the highly acidic environment that is generated temporarily in the spurs/tracks of the radiation. Thus, could this phenomenon explain, at least partly, why the combination of hyperthermia with radiotherapy ("thermoradiotherapy") is synergistic (or, in other words, why hyperthermia is a very effective radiation sensitizer) and works best when the two are applied simultaneously?[90,100-103]

## 4. Conclusion

In this work, Monte Carlo track chemistry simulations have been used in an attempt to quantify the "acid spike" effect that is generated *in situ* in spurs/tracks in the radiolysis of pure, deaerated water during and shortly after irradiation. Two track models were

considered depending on the quality (LET) of the radiation: 1) an isolated "spherical" spur model associated with low-LET radiation, such as ~300-MeV irradiating protons (LET ~ 0.3 keV/μm) and 2) an axially homogeneous "cylindrical" track model associated with high-LET radiation, such as 150-keV protons (LET ~ 70 keV/μm), 1.75-MeV/nucleon helium ions (LET ~ 70 keV/μm), and 0.6-MeV/nucleon helium ions (LET ~ 146 keV/μm). For times shorter than ~1 ns, the pH was found to be nearly constant and equal to ~3.3 in isolated spurs. For cylindrical tracks, however, the acid spike response to the ionizing radiation was far more intense than that for the spherical spur geometry. Indeed, on a time scale of ~100 ps, the pH was found to be around 0.5 for the three cases of high-LET radiation considered. At longer times, the pH increased gradually for all cases, ultimately reaching a value of 7 (neutral pH) at ~1 μs for the spherical geometry and ~0.1 ms for the cylindrical geometry.

We should also emphasize here the very good agreement of our calculated time evolution of $G(H_3O^+)$ in the radiolysis of pure, deaerated water by 300-MeV incident protons (which mimic $^{60}$Co γ/fast electron irradiation) with available experimental data at 25 °C.

The transient acid pH effect that we have described does not appear to have been explored in water or in a cellular environment subject to the action of ionizing radiation, especially high-LET radiation. In this regard, this work raises a number of questions about the potential implications of this effect for radiobiology, some of which have been briefly evoked.

**Acknowledgments**

We thank Professor Edouard I. Azzam (New Jersey Medical School Cancer Center, USA) and Professor Yusa Muroya (Osaka University, Japan) for valuable comments. The financial assistance of the Natural Sciences and Engineering Research Council of Canada (RGPIN-2015-06100) is gratefully acknowledged.

**Notes and references**


1 Y. Muroya, I. Plante, E.I. Azzam, J. Meesungnoen, Y. Katsumura and J.-P. Jay-Gerin, *Radiat. Res.*, 2006, **165**, 485.

2 P. O'Neill and P. Wardman, *Int. J. Radiat. Biol.*, 2009, **85**, 9; P. Wardman, *Brit. J. Radiol.*, 2009, **82**, 89.

3 E.I. Azzam, J.-P. Jay-Gerin and D. Pain, *Cancer Lett.*, 2012, **327**, 48.

4 J.F. Ward, *Prog. Nucleic Acid Res. Mol. Biol.*, 1988, **35**, 95.

5 P. O'Neill and E.M. Fielden, *Adv. Radiat. Biol.*, 1993, **17**, 53.

6 M. Faraggi, C. Ferradini and J.-P. Jay-Gerin, *J. Chim. Phys.*, 1996, **93**, 78.

7 D. Becker and M.D. Sevilla, *Adv. Radiat. Biol.*, 1993, **17**, 121; D. Becker, A. Adhikary and M.D. Sevilla, in *Charged Particle and Photon Interactions with Matter: Recent Advances, Applications, and Interfaces*, ed. Y. Hatano, Y. Katsumura and A. Mozumder, Taylor & Francis, Boca Raton, 2011, p. 503.

8 D.T. Goodhead, *Int. J. Radiat. Biol.*, 1994, **65**, 7.

9 J. Cadet, M. Berger, T. Douki and J.-L. Ravanat, *Rev. Physiol. Biochem. Pharmacol.*, 1997, **131**, 1; T. Douki and J. Cadet, in *Radiation Chemistry: From Basics to Applications in Material and Life Sciences*, ed. M. Spotheim-Maurizot, M. Mostafavi, T. Douki and J. Belloni, EDP Sciences, Les Ulis Cedex A, 2008, p. 177;J. Cadet, J.-L. Ravanat, M. Taverna Porro, H. Menoni and D. Angelov, *Cancer Lett.*, 2012, **327**, 5; J. Cadet, T. Douki, D. Gasparutto, J.-L. Ravanat and J.R. Wagner, in *Encyclopedia of Radicals in Chemistry, Biology, and Materials*, ed. C. Chatgilialoglu and A. Studer, Wiley, Chichester, UK, 2012, p. 1319.

10 P. O'Neill, in *Radiation Chemistry: Present Status and Future Trends*, ed. C.D. Jonah and B.S.M. Rao, Elsevier, Amsterdam, 2001, p. 585.

11 C. von Sonntag, *Free-Radical-Induced DNA Damage and its Repair. A Chemical Perspective*, Springer-Verlag, Berlin, 2006.

12 E.J. Hall and A.J. Giaccia, *Radiobiology for the Radiologist*, Lippincott Williams & Wilkins, Philadelphia, 6th edn, 2006.

13 W.A. Bernhard and D.M. Close, in *Charged Particle and Photon Interactions with Matter: Chemical, Physicochemical, and Biological Consequences with Applications*, ed. A. Mozumder and Y. Hatano, Marcel Dekker, New York, 2004, p. 431.

14 S. Lehnert, *Biomolecular Action of Ionizing Radiation*, Taylor & Francis, Boca Raton, 2008.

15 M. Tubiana *et al.*(14 authors), *Radiobiologie*, Hermann, Paris, 2008.

16 A. Chatterjee and W.R. Holley, *Adv. Radiat. Biol.*, 1993, **17**, 181.

17 J. Meesungnoen and J.-P. Jay-Gerin, in *Charged Particle and Photon Interactions with Matter: Recent Advances, Applications, and Interfaces*, ed. Y. Hatano, Y. Katsumura and A. Mozumder, Taylor & Francis Group, Boca Raton, 2011, p. 355. See also J. Meesungnoen, *Ph.D. thesis*, Université de Sherbrooke, Sherbrooke, Québec, Canada, 2007.

18 V. Malka, J. Faure and Y.A. Gauduel, *Mutat. Res.*, 2010, **704**, 142.

19 A.H. Samuel and J.L. Magee, *J. Chem. Phys.*, 1953, **21**, 1080; J.L. Magee, *Annu. Rev. Nucl. Sci.*, 1953, **3**, 171.

20 G.R. Freeman, in *Proceedings of the Workshop on the Interface between Radiation Chemistry and Radiation Physics*, Report ANL-82-88, ed. M.A. Dillon, R.J. Hanrahan, R. Holroyd, Y.-K. Kim, M.C. Sauer, Jr. and L.H. Toburen, Argonne National Laboratory, Argonne, 1983, p. 9.

21 R.L. Platzman, in *Radiation Biology and Medicine. Selected Reviews in the Life Sciences*, ed. W.D. Claus, Addison-Wesley, Reading, 1958, p. 15.

22 A. Kuppermann, *J. Chem. Ed.*, 1959, **36**, 279.

23 G.V. Buxton, in *Radiation Chemistry: Principles and Applications*, ed. Farhataziz and M.A.J. Rodgers, VCH Publishers, New York, 1987, p. 321.

24 J.W.T. Spinks and R.J. Woods, *An Introduction to Radiation Chemistry*, Wiley, New York, 3rd edn, 1990.

25 C. Ferradini and J.-P. Jay-Gerin, *Can. J. Chem.*, 1999, **77**, 1542.

26 J. Li, Z. Nie, Y.Y. Zheng, S. Dong and Z.-H. Loh, *J. Phys. Chem. Lett.*, 2013, **4**, 3698.

27 J. Ma, U. Schmidhammer, P. Pernot and M. Mostafavi, *J. Phys. Chem. Lett.*, 2014, **5**, 258.

28 C.-R. Wang, T. Luo and Q.-B. Lu, *Phys. Chem. Chem. Phys.*, 2008, **10**, 4463.

29 C. Pépin, T. Goulet, D. Houde and J.-P. Jay-Gerin, *J. Phys. Chem. A*, 1997, **101**, 4351.

30 A. Mozumder, *Fundamentals of Radiation Chemistry*, Academic Press, San Diego, 1 1999.

31 T. Goulet, J.P. Patau and J.-P. Jay-Gerin, *J. Phys. Chem.*, 1990, **94**, 7312.

32 D.M. Bartels, D. Gosztola and C.D. Jonah, *J. Phys. Chem. A*, 2001, **105**, 8069.

33 J. Meesungnoen and J.-P. Jay-Gerin, *J. Phys. Chem. A*, 2005, **109**, 6406; J. Meesungnoen, J.-P. Jay-Gerin, A. Filali-Mouhim and S. Mankhetkorn, *Radiat. Res.*, 2002, **158**, 657.

34 R.L. Platzman, in *Abstracts of Papers, Second International Congress of Radiation Research, Harrogate, England, 1962*, p. 128.

35 T. Goulet and J.-P. Jay-Gerin, *Radiat. Res.*, 1989, **118**, 46.

36 P. Rowntree, L. Parenteau and L. Sanche, *J. Chem. Phys.*, 1991, **94**, 8570.

37 V. Cobut, J.-P. Jay-Gerin, Y. Frongillo and J.P. Patau, *Radiat. Phys. Chem.*, 1996, **47**, 247.

38 J.W. Hunt, in *Advances in Radiation Chemistry*, Vol. 5, ed. M. Burton and J.L. Magee, Wiley-Interscience, New York, 1976, p. 185.

39 G. Duplâtre and C.D. Jonah, *Radiat. Phys. Chem.*, 1985, **24**, 557.

40 B. Pastina, J.A. LaVerne and S.M. Pimblott, *J. Phys. Chem. A*, 1999, **103**, 5841.

41 C.-R. Wang, J. Nguyen and Q.-B. Lu, *J. Am. Chem. Soc.*, 2009, **131**, 11320.

42 M. Farren-Dai, E. Awoonor-Williams, C.S. MacNeil, Z. Mahimwalla and K. Ghandi, *Chem. Phys. Lett.*, 2014, **610-611**, 331.

43 D.N. Nikogosyan, A.A. Oraevsky and V.I. Rupasov, *Chem. Phys.*, 1983, **77**, 131; A. Migus, Y. Gauduel, J.L. Martin and A. Antonetti, *Phys. Rev. Lett.*, 1987, **58**, 1559; A. Bernas, C. Ferradini and J.-P. Jay-Gerin, *Chem. Phys.*, 1997, **222**, 151.

44 D. Biedenkapp, L.G. Hartshorn and E.J. Bair, *Chem. Phys. Lett.*, 1970, **5**, 379.

45 O. Amichai and A. Treinin, *Chem. Phys. Lett.*, 1969, **3**, 611.

46 B.H.J. Bielski, D.E. Cabelli, R.L. Arudi and A.B. Ross, *J. Phys. Chem. Ref. Data*, 1985, **14**, 1041.

47 S. Sanguanmith, J. Meesungnoen, Y. Muroya, M. Lin, Y. Katsumura and J.-P. Jay-Gerin, *Phys. Chem. Chem. Phys.*, 2012, **14**, 16731.

48 I. Plante, A. Filali-Mouhim and J.-P. Jay-Gerin, *Radiat. Phys. Chem.*, 2005, **72**, 173.

49 In the study of the radiation chemistry of water, the main goal is to determine the yields (or *G*-values) of the radicals and molecules produced by the irradiation. Throughout this paper, radiation chemical yields are quoted in units of molecules per 100 eV, as *g*(X) for "primary" (or "escape") yields and *G*(X) for experimentally measured yields. Recall here that the so-called "primary" radical and molecular yields are defined, in the case of low-LET radiation, as the numbers of species formed or destroyed per 100 eV of absorbed energy that remain after "spurs" have dissipated. For conversion into SI units (mol/J), 1 molecule per 100 eV ≈ 0.10364 μmol/J.

50 A.J. Elliot and D.M. Bartels, *The reaction set, rate constants and g-values for the simulation of the radiolysis of light water over the range 20 °C to 350 °C based on information available in 2008*, Report AECL No. 153-127160-450-001, Atomic Energy of Canada Limited, Chalk River, Ontario, 2009.

51 C. Ferradini and J.-P. Jay-Gerin, *Res. Chem. Intermed.*, 2000, **26**, 549.

52 R.B. Mikkelsen and P. Wardman, *Oncogene*, 2003, **22**, 5734.

53 J.-P. Jay-Gerin and C. Ferradini, *Biochimie*, 2000, **82**, 161.

54 W.A. Pryor and S.L. Squadrito, *Am. J. Physiol. Lung Cell. Mol. Physiol.*, 1995, **268**, L699.

55 S. Burney, J.L. Caulfield, J.C. Niles, J.S. Wishnok and S.R. Tannenbaum, *Mutat. Res.*, 1999, **424**, 37; J.C. Niles, J.S. Wishnok and S.R. Tannenbaum, *Nitric Oxide*, 2006, **14**, 109.

56 J.A. LaVerne, in *Charged Particle and Photon Interactions with Matter: Chemical, Physicochemical, and Biological Consequences with Applications*, ed. A. Mozumder and Y. Hatano, Marcel Dekker, New York, 2004, p. 403; J.A. LaVerne, *Radiat. Res.*, 2000, **153**, 487.

57 A. Appleby, *Radiat. Phys. Chem.*, 1989, **34**, 121.

58 C. Ferradini, *J. Chim. Phys.*, 1979, **76**, 636.

59 J.L. Magee and A. Chatterjee, in *Kinetics of Nonhomogeneous Processes*, ed. G.R. Freeman, Wiley, New York, 1987, p. 171; J.L. Magee and A. Chatterjee, *J. Phys. Chem.*, 1980, **84**, 3529; see also A.M. Miterev, *Physics-Uspekhi*, 2002, **45**, 1019.

60 D.R. Smith and W.H. Stevens, *Nature*, 1963, **200**, 66.

61 M. Anbar and J.K. Thomas, *J. Phys. Chem.*, 1964, **68**, 3829.

62 V. Kanike, J. Meesungnoen and J.-P. Jay-Gerin, *Austin J. Nucl. Med. Radiother.*, 2015, **2**, 1011.

63 V. Cobut, Y. Frongillo, J.P. Patau, T. Goulet, M.-J. Fraser and J.-P. Jay-Gerin, *Radiat. Phys. Chem.*, 1998, **51**, 229; V. Cobut, *Ph.D. thesis*, Université de Sherbrooke, Sherbrooke, Québec, Canada, 1993.

64 Y. Frongillo, T. Goulet, M.-J. Fraser, V. Cobut, J.P. Patau and J.-P. Jay-Gerin, *Radiat. Phys. Chem.*, 1998, **51**, 245.

65 Y. Muroya, J. Meesungnoen, J.-P. Jay-Gerin, A. Filali-Mouhim, T. Goulet, Y. Katsumura and S. Mankhetkorn, *Can. J. Chem.*, 2002, **80**, 1367.

66 S. Sanguanmith, Y. Muroya, J. Meesungnoen, M. Lin, Y. Katsumura, L. Mirsaleh Kohan, D.A. Guzonas, C.R. Stuart and J.-P. Jay-Gerin, *Chem. Phys. Lett.*, 2011, **508**, 224.

67 M. Tachiya, *Radiat. Phys. Chem.*, 1983, **21**, 167.

68 S.M. Pimblott, M.J. Pilling and N.J.B. Green, *Radiat. Phys. Chem.*, 1991, **37**, 377; S.M. Pimblott and N.J.B. Green, in *Research in Chemical Kinetics*, Vol. 3, ed. R.G. Compton and G. Hancock, Elsevier, Amsterdam, 1995, p. 117.

69 T. Goulet, M.-J. Fraser, Y. Frongillo and J.-P. Jay-Gerin, *Radiat. Phys. Chem.*, 1998, **51**, 85.

70 I. Plante, *Ph.D. thesis*, Université de Sherbrooke, Sherbrooke, Québec, Canada, 2009.

71 L. Mirsaleh Kohan, S. Sanguanmith, J. Meesungnoen, P. Causey, C.R. Stuart and J.-P. Jay-Gerin, *RSC Adv.*, 2013, **3**, 19282.

72 T. Tippayamontri, S. Sanguanmith, J. Meesungnoen, G.R. Sunaryo and J.-P. Jay-Gerin, *Recent Res. Devel. Physical Chem.*, 2009, **10**, 143.

73 S. Mustaree, J. Meesungnoen, S.L. Butarbutar, P. Causey, C.R. Stuart and J.-P. Jay-Gerin, *RSC Adv.*, 2014, **4**, 43572.

74 We should note that the use of high-energy protons as primary particles was more appropriate here than fast electrons since we wanted to study track segments over which the LET is essentially constant. In fact, a proton that has the same LET as an electron must also have an energy 2000 times larger and, consequently, its LET is much less affected by a given series of energy depositions.

75 D.E. Watt, *Quantities for Dosimetry of Ionizing Radiations in Liquid Water*, Taylor & Francis, London, 1996.

76 A.K. Pikaev, S.A. Kabakchi and A.A. Zansokhova, *Faraday Disc. Chem. Soc.*, 1977, **63**, 112.

77 B. Čerček and M. Kongshaug, *J. Phys. Chem.*, 1969, **73**, 2056.

78 R.F. Anderson, B. Vojnovic and B.D. Michael, *Radiat. Phys. Chem.*, 1985, **26**, 301.

79 G.C. Barker, P. Fowles, D.C. Sammon and B. Stringer, *Trans. Faraday Soc.*, 1970, **66**, 1498.

80 K.H. Schmidt and S.M. Ander, *J. Phys. Chem.*, 1969, **73**, 2846.

81 S. Sanguanmith, J. Meesungnoen and J.-P. Jay-Gerin, *Chem. Phys. Lett.*, 2013, **588**, 82.

82 As discussed in ref. 33, our calculated value of $r_o \sim 11.7$ nm is somewhat larger than the typical range of ~6.4-8.3 nm commonly used to describe the initial spatial distribution of hydrated electrons and their subsequent chemical evolution in current deterministic "average" spur models of liquid water radiolysis by low-LET radiation (see, for example, S.M. Pimblott and A. Mozumder, in *Charged Particle and Photon Interactions with Matter: Chemical, Physicochemical, and Biological Consequences with Applications*, ed. A. Mozumder and Y. Hatano, Marcel Dekker, New York, 2004, p. 75). This relatively large average electron thermalization distance value comes from the presence of a long tail in our simulated distribution of thermalization distances, which indicates that a number of electrons travel large distances (up to ~40 nm) from subexcitation to thermal energies (see: T. Goulet, J.-P. Jay-Gerin, Y. Frongillo, V. Cobut and M.-J. Fraser, *J. Chim. Phys.*, 1996, **93**, 111; see also ref. 63).

83 Equations (19) and (22) readily follow from the general relationship: $C = \rho \mathcal{D} G$, where $C$ is the concentration of species, $\rho$ is the density, $\mathcal{D}$ is the radiation dose, and $G$ is the chemical yield (see, for example, A. Hummel, *Radiation Chemistry: The Chemical Effects of Ionizing Radiation and their Applications*, IRI-TUD, Delft, 1995). Note that with $G$ in mol/J, $\mathcal{D}$ in J/kg (or Gy), $C$ in mol/dm$^3$, the density is to be expressed in kg/dm$^3$ in order to have a consistent set of units.

84 N. Autsavapromporn, *M.Sc. thesis*, Burapha University, Bangsaen, Chonburi, Thailand, 2006.

85 J.A. LaVerne and S.M. Pimblott, *Radiat. Res.*, 1995, **141**, 208.

86 R.E. Apfel, Y.Y. Sun and R. Nath, *Radiat. Res.*, 1992, **131**, 124.

87 J.A. LaVerne and G.G. Meisels, *Radiat. Phys. Chem.*, 1983, **21**, 329.

88 A. Norman, *Radiat. Res. Suppl.*, 1967, **7**, 33.

89 R. Meesat, H. Balmouaddine, J.-F. Allard, C. Tanguay-Renaud, R. Lemay, T. Brastaviceanu, L. Tremblay, B. Paquette, J.R. Wagner, J.-P. Jay-Gerin, M. Lepage, M.A. Huels and D. Houde, *Proc. Natl. Acad. Sci. USA*, 2012, **109**, E2508.

90 I.F. Tannock and D. Rotin, *Cancer Res.*, 1989, **49**, 4373.

91 M. Errera and A. Forssberg, *Mechanisms in Radiobiology: Multicellular Organisms*, Elsevier, Burlington, 2013.

92 B. Halliwell and J.M.C. Gutteridge, *Free Radicals in Biology and Medicine*, 4th ed., Oxford University Press, Oxford, 2007.

93 I.G. Draganić and Z.D. Draganić, *The Radiation Chemistry of Water*, Academic Press, New York, 1971.

94 H. Nagasawa and J.B. Little, *Cancer Res.*, 1992, **52**, 6394.

95 M. Buonanno, S.M. de Toledo, D. Pain and E.I. Azzam, *Radiat. Res.*, 2011, **175**, 405.

96 B. Ponnaiya, M. Suzuki, C. Tsuruoka, Y. Uchihori, Y. Wei and T.K. Hei, *Radiat. Res.*, 2011, **176**, 280.

97 C. Mothersill and C.B. Seymour, *Radiat. Res.*, 2001, **155**, 759.

98 E.I. Azzam and J.B. Little, *Hum. Exp. Toxicol.*, 2004, **23**, 61.

99 W.F. Morgan, *Radiat. Res.*, 2003, **159**, 581.

100 H.H. Kampinga, *Int. J. Hyperthermia*, 2006, **22**, 191.

101 W.C. Dewey, L.E. Hopwood, S.A. Sapareto and L.E. Gerweck, *Radiology*, 1977, **123**, 463.

102 M.R. Horsman and J. Overgaard, *Clin. Oncol.*, 2007, **19**, 418.

103 J.F. Hainfeld, L. Lin, D.N. Slatkin, F.A. Dilmanian, T.M. Vadas and H.M. Smilowitz, *Nanomedicine*, 2014, **10**, 1609.

# 5 - ARTICLE No. 3

## Generation of ultrafast transient acid spikes in high-temperature water irradiated with low linear energy transfer radiation

**Authors:** **V. Kanike,** J. Meesungnoen, S. Sanguanmith, D.A. Guzonas, C.R. Stuart and J.-P. Jay-Gerin

**Status**: Accepted for publication in ***CNL Nuclear Review*** on February 2nd, 2016.
Manuscript number: CNLNR-D-15-00052R1 (in press)

**Foreword**: In this third article, Monte Carlo track chemistry simulations are used in combination with a spherical spur model to examine the effect of temperature on the *in situ* formation of $H_3O^+$ ions and the corresponding abrupt transient "acid spike" response that is observed in the low-LET radiolysis of pure, deaerated water. At high temperatures, there is an increasingly acidic but shorter pH response. While at 25 °C the acid-spike effect is greatest for times shorter than ~1 ns with a pH equal to ~3.3, the pH is around 1.7 at 350 °C at times less than ~10 ps. At longer times, the pH gradually increases for all temperatures, ultimately reaching a constant value corresponding to the non-radiolytic, pre-irradiation concentration of $H_3O^+$ arising through water's autoprotolysis. As many in-core processes in a water-cooled nuclear reactor critically depend on pH, the present work raises the question of whether such acidic pH variations, even if highly localized and transitory, contribute to material corrosion and damage.

**Résumé** : Dans ce troisième article, nous examinons l'influence de la température sur la formation *in situ* d'ions $H_3O^+$ et l'effet de "pic acide" transitoire observé précédemment dans la radiolyse de l'eau pure, désaérée par un rayonnement à faible LET ou à TEL élevé, à 25 °C. On se limite ici au cas d'un rayonnement à faible TEL qui peut être décrit par un modèle de grappes isolées "sphériques". L'extension de nos simulations Monte Carlo de la chimie intervenant dans les trajectoires à des températures élevées jusqu'à 350 °C a révélé une réponse de pic acide beaucoup plus intense qu'à 25 °C mais de plus courte durée. Ainsi, le pH à 350 °C est ~1,7 (alors qu'il est de 3,3 à 25 °C) sur une échelle de temps de l'ordre de ~10 ps (au lieu de ~1 ns à 25 °C). Comme de nombreux processus intervenant dans le cœur d'un réacteur nucléaire refroidi à l'eau dépendent de façon critique de la valeur du pH, le présent travail soulève la question à savoir si de telles variations d'acidité, même si hautement localisées et transitoires, contribuent à la corrosion des matériaux et leur endommagement.

# Generation of ultrafast transient acid spikes in high-temperature water irradiated with low linear energy transfer radiation

**V. Kanike,[1] J. Meesungnoen,[1] S. Sanguanmith,[1] D.A. Guzonas,[2] C.R. Stuart[2] and J.-P. Jay-Gerin*,[1]**

[1]Département de Médecine Nucléaire et de Radiobiologie, Faculté de Médecine et des Sciences de la Santé, Université de Sherbrooke, 3001, 12e Avenue Nord, Sherbrooke, Québec, Canada, J1H 5N4

[2]Canadian Nuclear Laboratories, Reactor Chemistry and Corrosion, 20 Forest Avenue, Deep River, Ontario, Canada, K0J 1P0

***Corresponding author**: Prof. Jean-Paul Jay-Gerin, Department of Nuclear Medicine and Radiobiology, Faculty of Medicine and Health Sciences, Université de Sherbrooke, 3001, 12th Avenue North, Sherbrooke, QC J1H 5N4, Canada. Tel: (1) 819-821-8000, ext. 74682; Email: jean-paul.jay-gerin@USherbrooke.ca ca

*CNL Nucl Rev (2016)*

Received: September 18, 2015
Accepted: February 2, 2016
Published: In press

**ABSTRACT**

Monte Carlo track chemistry simulations of the low linear energy transfer radiolysis of pure, deaerated liquid water have been used in combination with a spherical spur model to examine the effect of temperature on the in situ formation of $H_3O^+$ ions and the corresponding abrupt transient "acid-spike" response that is observed after irradiation. The magnitude and duration of this acid-spike effect were found to be a very sensitive function of temperature. At 25 °C, it is most intense at times less than ~1 ns, with a pH of 3.3 remaining nearly constant. In contrast, at higher temperatures, there is an increasingly acidic but much shorter pH response. At 350 °C, the pH is around 1.7 on a time scale of ~10 ps. At longer times, the pH gradually increases for all temperatures, ultimately reaching a constant value corresponding to the non-radiolytic, pre-irradiation concentration of $H_3O^+$ arising through water's autoprotolysis at ~1-10 μs following irradiation. It does not appear that this transient acid-spike effect has been explored in water subject to ionizing radiation, either at ambient or at elevated temperatures. As many in-core processes in a water-cooled nuclear reactor critically depend on pH, the present work raises the question whether such abrupt highly acidic pH variations contribute to material corrosion and damage.

*Keywords*: nuclear reactor, high-temperature water, radiolysis, linear energy transfer (LET), hydronium and hydroxide ions, pH, radiation chemical yield (*G*-value), kinetics, spur model, Monte Carlo track chemistry simulations.

## 1. Introduction

One of the most significant challenges in controlling the water chemistry of current (Generation III or less) water reactor systems (which operate in the ~250-330 °C temperature range and ~7-15 MPa pressure) and proposed more efficient Generation IV nuclear reactor designs with water under supercritical conditions (typically, ~300-625 °C and 25 MPa) is understanding and mitigating water radiolysis effects [1-3]. The radiolytic decomposition of water is a particular concern as it leads to the formation of a variety of oxidizing (transient and stable) products such as $^{\bullet}OH$, $H_2O_2$ and its decomposition product $O_2$, and $O_2^{\bullet-}$ (or its protonated form $HO_2^{\bullet}$, depending on the pH). These products can increase corrosion and degradation rates of reactor components, as well as affect the transport and deposition of both corrosion products and radionuclides [4-8], thereby influencing the long-term integrity and performance of reactors. While the radiation-induced chemistry (radiolytic yields or *G* values and reaction rates) in water at elevated temperatures (say, up to 350 °C) is relatively well documented [9-11], there are only very limited experimental data available on supercritical water radiolysis [12-15]. Direct measurements at elevated temperatures and pressures are difficult, especially beyond the thermodynamic critical point of water ($t_c$ = 373.95 °C and $P_c$ = 22.06 MPa); thus theoretical modeling and computer simulations are an important route of investigation [3, 6, 16-20].

Recently, Monte Carlo track chemistry simulations were used to calculate, at 25 °C, the yields of hydronium ions ($H_3O^+$) formed in spurs/tracks of the low/high linear energy transfer (LET) radiolysis of pure, deaerated water during and shortly after irradiation [21]. Using simple spatio-temporal models of a spur or track, we found that the *in situ* radiolytic formation of $H_3O^+$ renders the spur/track regions temporarily more *acid* than the surrounding solution. This "acid spike" effect was observed to be greatest for times shorter than ~1 ns in isolated "spherical" spurs (*i.e.*, for low-LET radiation such as $^{60}$Co γ/fast electron irradiation, LET ~ 0.3 keV/μm). In this time range, the pH remained nearly constant at ~3.3. For an axially homogeneous "cylindrical" track (*i.e.*, for high-LET radiation), the acid spike response to ionizing radiation was far more intense than that for the spur (spherical) geometry. For example, for a 150-keV incident proton (LET ~ 70 keV/μm), the pH was found to be around 0.5 on a time scale of ~100 ps. At longer times,

the pH increased gradually for both cases (due to diffusion which moderates the high local ion concentrations), ultimately reaching a constant value of 7 (pH of the bulk solution at 25 °C) at ~1 μs for the spur model and ~0.1 ms for the track model [21].

In this study, we extended the calculations above to examine whether this transient acid pH effect observed in irradiated water at ambient temperature also exists at elevated temperatures, and then, we determined its magnitude and time dependence. This information may provide further insight into the initial events that lead to radiation damage in water-cooled reactors.

## 2. Low linear energy transfer (LET) radiolysis of liquid water

In this study, we limit ourselves to the action of low-LET radiation and treat the isolated spur (spherical in shape) as the track model. From the viewpoint of pure aqueous radiation chemistry, low-LET tracks are made up initially of strings of widely spaced Magee-type "spurs" (clusters of reactive species) [22, 23] that develop independently in time (without interference from the neighboring spurs). During the physical and physicochemical stages of radiation action in Platzman's classification [24] (*i.e.*, up to ~1 ps after the initial energy deposition), the radiolysis of water can be described by the following reactions [25-28]:

(1) $H_2O \sim\!\!\!\rightarrow H_2O^{\bullet+} + e^-$ (ionization)

(2) $H_2O \sim\!\!\!\rightarrow H_2O^*$ (excitation)

(3) $H_2O^{\bullet+} + H_2O \rightarrow H_3O^+ + {}^{\bullet}OH$ (proton transfer reaction, ~200 fs [29])

(4) $e^- \rightarrow e^-_{sub} \rightarrow e^-_{th} \rightarrow e^-_{tr} \rightarrow e^-_{aq}$ (slowing down to subexcitation energies (< 7.3 eV), thermalization, trapping, and hydration follow in quick succession [30], ~240 fs to 1 ps [31, 32])

(5) $e^- + H_2O^{\bullet+} \rightarrow H_2O^*$ (electron-cation geminate recombination [33-35])

(6) $e^- + H_2O \rightarrow H_2O^{\bullet-}{}^* \rightarrow H^- + {}^{\bullet}OH$ (resonant dissociative electron attachment, or DEA process [35-39])

followed by the formation of molecular hydrogen

(7) $H^- + H_2O \rightarrow H_2 + OH^-$

(8) $H_2O^* \rightarrow e^-_{aq} + H_2O^{\bullet+}$ (threshold at ~6.5 eV [40-42])

(9) $H_2O^* \rightarrow H^\bullet + {}^\bullet OH$

(10) $H_2O^* \rightarrow H_2 + O(^1D)$ (oxygen atom in its singlet $^1D$ first excited state) followed by

(11) $O(^1D) + H_2O \rightarrow H_2O_2$ (or possibly also $2\,{}^\bullet OH$ [43])

(12) $H_2O^* \rightarrow 2H^\bullet + {}^\bullet O^\bullet(^3P)$ (oxygen atom in its triplet $^3P$ ground state, rather inert to water but reacts with most additives [44]).

By ~1 ps, the various "initial" radiolysis products are the hydrated electron ($e^-_{aq}$), $H^\bullet$, ${}^\bullet OH$, $H_2$, $H_2O_2$, $H^+$ (or equivalently, $H_3O^+$ or $H^+_{aq}$), $OH^-$, $O_2^{\bullet-}$ (or $HO_2^\bullet$, depending on the pH; $pK_a(HO_2^\bullet/O_2^{\bullet-})$ = 4.8 at 25 °C), $O(^3P)$, *etc*. At this time, which may be regarded as the beginning of the (nonhomogeneous) chemical stage [24], these chemically reactive species begin to diffuse away from the site where they were originally produced. A fraction of them react together within the spurs as they develop in time while the remainder escape into the bulk solution. At 25 °C, the spur expansion is essentially complete by ~0.2 μs [45]. At this time, the species that have escaped from spur reactions become homogeneously distributed throughout the bulk solution and the radiation "track structure" no longer exists [46, 47].

The yields (quoted in units of molecules per 100 eV of absorbed energy) of the species that remain after spurs have dissipated are the so-called "primary" (or "escape") yields. They are denoted by $g(e^-_{aq})$, $g(H^\bullet)$, $g({}^\bullet OH)$, $g(H_2)$, $g(H_2O_2)$, *etc*. [a lower case *g* is commonly used for primary yields, while experimentally measured or final yields are always given in the form *G*(X)]. For $^{60}$Co γ-irradiated neutral water at 25 °C, in the absence of air or oxygen, the generally accepted values are: $g(e^-_{aq})$ = 2.65, $g(H^\bullet)$ = 0.6, $g({}^\bullet OH)$ = 2.8, $g(H_2)$ = 0.45, and $g(H_2O_2)$ = 0.68 molecules per 100 eV [for conversion into SI units (mol/J), 1 molecule per 100 eV ≈ 0.10364 μmol/J] [10, 26-28]. When the temperature is increased, measurements made in different laboratories with many different scavenger systems or directly by using pulse radiolysis (data up to 350 °C have recently been compiled and reviewed by Elliot and Bartels [10]) have shown that the *g*-values of the free radicals $e^-_{aq}$, $H^\bullet$, and ${}^\bullet OH$ continuously increase, while the molecular yield $g(H_2O_2)$ decreases. These results are explained by the fact that many spur reactions are not diffusion-controlled and therefore have rates that increase less with temperature than do the diffusion coefficients of the reactive species (under these conditions, these reactions occur

less as the temperature is increased) [9]. Although $H_2$ is a molecular product, $g(H_2)$ is observed to continue to increase with temperature, particularly above 200 °C. This anomalous increase in $g(H_2)$, which is an issue of much debate in the radiation chemistry of high-temperature water, has been discussed at length elsewhere [48-55]. From a theoretical perspective, we have recently performed Monte Carlo track chemistry simulations of the low-LET radiolysis of liquid water over the range 25-350 °C [51], incorporating newly measured or re-assessed experimental data. A very good overall and simultaneous agreement was obtained between calculated and experimental *g*-values for all the various radiolytic species up to 350 °C. These same Monte Carlo simulations [51] are used herein to specifically examine the effect of temperature on the yield of $H_3O^+$ ions that are formed in spurs of low-LET radiolysis of water.

## 3. Monte Carlo track chemistry simulations of high-temperature water radiolysis

A detailed description of our Monte Carlo code IONLYS-IRT that simulates, in a 3D geometrical environment, the complete sequence of events that are generated in the low-LET radiolysis of water in the range from ambient up to 350 °C, has been given previously [51, 56, 57]. Briefly, the IONLYS simulation program is used to model the early physical and physicochemical stages of radiation action up to ~1 ps in track development. It actually models, event by event, all the basic physical interactions (by which energy is transferred to the medium) and the subsequent conversion of the physical products created locally into the various initial radical and molecular products $e^-_{aq}$, $H_3O^+$, $H^\bullet$, $^\bullet OH$, $H_2$, $H_2O_2$, $OH^-$, $HO_2^\bullet/O_2^{\bullet-}$, $^\bullet O^\bullet$, $H^-$, $O^{\bullet-}$, *etc*., of the radiolysis, arranged in a highly nonhomogeneous track structure. The complete spatial distribution of reactants at the end of the physicochemical stage, which is provided as an output of the IONLYS program, is then used directly as the starting point for the subsequent nonhomogeneous chemical stage. This stage, during which the various radiolytic species diffuse randomly (at rates determined by their diffusion coefficients) and react with one another (or competitively with any dissolved solutes, if any) until all spur reactions are complete, is covered by our IRT program. This program employs the "independent reaction times" (IRT) method [58-60], a computer-efficient stochastic simulation technique that is used to model the kinetics of a spur by simulating

reaction times without having to follow the trajectories of the diffusing species (the IRT method relies on the approximation that the reaction time of each pair of reactants is independent of the presence of other reactants in the system). Its implementation has been described in detail [58] and its ability to give accurate time-dependent chemical yields under different irradiation conditions has been well validated by comparison with full random flights Monte Carlo simulations, which follow the reactant trajectories in detail [61, 62]. Finally, this IRT program can also be used to efficiently describe the reactions that occur in the bulk solution during the homogeneous chemical stage, *i.e.*, in the time domain beyond a few microseconds.

In this version of IONLYS-IRT, we used the self-consistent radiolysis data base assembled by Elliot and Bartels [10], which includes rate constants, reaction mechanisms, and *g*-values. This database provides recommendations for the best values to use in high-temperature modeling of light water radiolysis up to 350 °C. The reaction scheme for the radiolysis of pure liquid water is the same as used previously [51, 63, 64]. Values of the diffusion coefficients of the reactive species involved in the simulations and their temperature dependences are given in Table 1 of Hervé du Penhoat et al. [56].

To mimic the radiolysis with $^{60}$Co γ-radiation or fast electrons, we used short (typically, ~150 μm) segments of ~300-MeV proton tracks, over which the average LET value obtained in the simulations was nearly constant and equal to ~0.3 keV/μm at 25 °C (actually, the LET slightly decreases with increasing temperature, due to the fact that the density of pressurized water decreases with temperature). Such model calculations thus gave "track segment" yields at a well-defined LET. The number of proton histories (usually ~150) was chosen so as to ensure only small statistical fluctuations when calculating average yields, while keeping acceptable computer time limits.

All Monte Carlo simulations reported here are performed along the liquid-vapor coexistence curve, the density of the pressurized water decreasing from 1g/cm$^3$ (1 bar or 0.1 MPa) at 25 °C to ~0.575 g/cm$^3$ (~16.5 MPa) at 350 °C [65]. For this range of temperature, calculations show that *g*-values, to a large extent, depend relatively little on the applied pressure.

In the simulations reported here, the time evolution of $G(H_3O^+)$ has been followed over the interval of ~1 ps to 1 ms.

**4. Results and discussion**

Figures 1a and 1b show the time evolution of $G(H_3O^+)$ as obtained from our simulations of the radiolysis of pure, deaerated liquid water by 300-MeV incident protons at ambient temperature and at 350 °C, respectively. For comparison, available experimental data for $^{60}$Co γ/fast electron irradiation at 25 °C [66-70] are also shown in Figure 1a. Our simulated values (red solid line) are in very good agreement with the measured $H_3O^+$ yields. To our knowledge, there is no experimental information in the literature with which to compare our results on the time dependence of the yield of $H_3O^+$ at 350 °C (Figure 1b). As discussed previously [21], the observed decrease of $G(H_3O^+)$ is predominantly due to $H_3O^+$ reacting with $OH^-$ and with the hydrated electron [10, 56, 71, 72], according to:

(13) $H_3O^+ + OH^- \rightarrow 2\ H_2O$ $\quad k_{13} = 1.18 \times 10^{11}\ M^{-1}\ s^{-1}$ (25 °C)
$1.63 \times 10^{12}\ M^{-1}\ s^{-1}$ (350 °C)

(14) $H_3O^+ + e^-_{aq} \rightarrow H^\bullet + H_2O$ $\quad k_{14} = 2.13 \times 10^{10}\ M^{-1}\ s^{-1}$ (25 °C)
$2.07 \times 10^{12}\ M^{-1}\ s^{-1}$ (350 °C)

where $k_{13}$ and $k_{14}$ are the rate constants of the two individual reactions. There is also a very small contribution due to the following reaction [10]:

(15) $H_3O^+ + O^{\bullet-} \rightarrow {}^\bullet OH + H_2O$ $\quad k_{15} = 5 \times 10^{10}\ M^{-1}\ s^{-1}$ (25 °C)
$8.2 \times 10^{11}\ M^{-1}\ s^{-1}$ (350 °C)

This is clearly seen in Figures 2a and 2b where we show the time profiles of the extents – expressed as cumulative yield variations $\Delta G(H_3O^+)$ – of each of the reactions that contribute to the decay of $G(H_3O^+)$, which are calculated from our Monte Carlo simulations at 25 and 350 °C, respectively. Compared with the results at 25 °C, where $G(H_3O^+)$ decreases mainly by the recombination reaction of $H_3O^+$ with $OH^-$, the order of importance of reactions (13) and (14) is completely reversed at 350 °C: the contribution of the $H_3O^+$ reaction with $e^-_{aq}$ becomes predominant. This is understandable since the rate constant for this reaction increases much more steeply with temperature than that for reaction (13) [10]. We further see in Figure 2 that the contributions of reactions (13) and especially (14) to the

decay of $H_3O^+$ as spurs expand are greater at 350 °C than at 25 °C. This explains the faster decay kinetics of $G(H_3O^+)$ that is observed at 350 °C (Figure 1).

Another point that should be considered here is the magnitude of the yield of $OH^-$ ions, which are formed largely by the reaction [10]

(16) $^{\bullet}OH + e^-_{aq} \rightarrow OH^-$ $\quad k_{16} = 3.55 \times 10^{10}\ M^{-1}\ s^{-1}$ (25 °C)
$4.77 \times 10^{11}\ M^{-1}\ s^{-1}$ (350 °C)

during the track stage of the radiolysis. The reason for this is that hydroxide ions contribute to an *alkaline* spur and consequently counteract the acid-spike effect discussed in this work. Figure 1 shows that $G(OH^-)$ remains much smaller than $G(H_3O^+)$ over the time period of interest (especially at 350 °C). As a result, its effect only slightly modifies the quantitative features of the pH and can be ignored to a good approximation.

Figure 3 shows the time dependences of the yields of $H_3O^+$ calculated from our Monte Carlo simulations of the radiolysis of pure, deaerated liquid water at different temperatures between 25 and 350 °C in the interval from ~1 ps to 1 μs, for irradiating 300-MeV protons. As the temperature is increased, the decrease in $G(H_3O^+)$ becomes more pronounced as a function of time, and begins at shorter times. The sharp decrease of $G(H_3O^+)$ observed at long times largely results from reactions (13) and (14) in the homogeneous chemistry stage. The reasons underlying these results are, of course, the same as those discussed above (see Figures 1 and 2). Unfortunately, there are no experimental data available to test these temporal variations of $G(H_3O^+)$ at high temperatures.

Next, to calculate the pH values prevailing in the spur regions, we estimated the concentrations of $H_3O^+$ radiolytically generated *in situ* in these regions as a function of time. For this purpose, we assumed that the $H_3O^+$ ions are produced evenly in an isolated spherically symmetric spur. The spur's initial radius $r_o$ (prior to spur expansion) was chosen to be equal to the *average* electron thermalization distance ($r_{th}$) obtained from our simulations ($r_{th} \approx 11.7$ nm at 25 °C [35]) [33, 37, 56, 73]. The temperature dependence of $r_{th}$ used in this work is shown in Figure 4a. It was obtained from comparing our computed time-dependent $e^-_{aq}$ yield data to recent picosecond (~60 ps to 6 ns) and conventional nanosecond (using methyl viologen $MV^{2+}$ scavenging of electrons) pulse radiolysis measurements of the decay kinetics of $e^-_{aq}$ at several different temperatures between 25 and

350 °C [17, 51]. The spur concentrations of radiolytically produced $H_3O^+$ are derived from [21]

$$(17) \qquad \left[H_3O^+\right]_{\text{radiolytic}}(t) = G\left(H_3O^+\right)(t) \times \left( \frac{\text{Mean energy loss per event}}{\frac{4}{3}\pi\, r(t)^3} \right)$$

where the mean energy loss in a single energy deposition event (*i.e.*, the mean energy deposited in a spur) in liquid water is taken to be ~47 eV [63, 73-75] and

$$(18) \qquad r(t)^2 = r_o^2 + 6\, D\, t$$

represents the change with time of $r_o$ due to the (three-dimensional) diffusive expansion of the spur. Here, $t$ is time and $D$ is the diffusion coefficient of $H_3O^+$ in water. Equation (17) readily follows from the general relationship: $C = \rho \mathcal{D} G$, where $C$ is the concentration of species, $\rho$ is the density of the solution, $\mathcal{D}$ is the radiation dose, and $G$ is the chemical yield [76]. Note that with $C$ in mol/dm$^3$, $\mathcal{D}$ in J/kg (or Gy), and $G$ in mol/J, the density is expressed in kg/dm$^3$ in order to have a consistent set of units. The temperature dependence of $D(H_3O^+)$ used in the simulations was obtained from Elliot and Bartels [10] and is shown in Figure 4b.

Finally, at a given temperature, the total concentration of $H_3O^+$ is the sum of $[H_3O^+]_{\text{radiolytic}}$ given by Equations (17) and (18) and of the non-radiolytic, pre-irradiation concentration $[H_3O^+]_{\text{autoprotolysis}}$ that arises through water's autoprotolysis (see Figure 5):

$$(19) \qquad [H_3O^+]_{\text{total}}(t) = [H_3O^+]_{\text{radiolytic}}(t) + [H_3O^+]_{\text{autoprotolysis}}$$

The pH in the corresponding spur region is then simply given by the negative logarithm (to the base 10) of $[H_3O^+]_{\text{total}}$:

$$(20) \qquad \text{pH}(t) = -\log\{[H_3O^+]_{\tau\text{total}}(t)\}$$

The time evolution of the pH values calculated for 300-MeV irradiating protons in pure, deaerated liquid water using the spherical spur geometry described above is shown in Figure 6. As shown, for all temperatures considered in the range of 25-350 °C, there is an

abrupt temporary acid pH effect at early times immediately after the initial energy release. Its magnitude and duration clearly depend on the temperature. Up to ~100 °C, our calculations show that the curves of pH against time have shapes practically similar to that found at 25 °C in the spherical spur case for low-LET radiation [21]. The "acid spike" effect is most intense at times less than ~1 ns. In this time range, the pH remains nearly constant, equal to ~3.3. However, at higher temperatures, there is an increasingly more acidic but much shorter duration pH response. At 350 °C, the pH is around ~1.7 at times less than ~10 ps and then increases gradually with time. Ultimately, it reaches a constant value around ~1-10 μs (*i.e.*, slightly longer than the end of spur expansion; see Figure 3), equal to -log ($[H_3O^+]_{autoprotolysis}$), which depends on the temperature considered (Figure 5). These results are illustrated in Figure 7, which shows the pH value as a function of temperature over the range of 25-350 °C calculated from our simulations at three different times: 1 ps, 1 ns, and 1 μs following irradiation.

To the best of our knowledge, the early-time, acid-spike effect described above has never been explored in water subject to ionizing radiation, either at ambient or at elevated temperatures. As many in-core processes in nuclear reactors critically depend on pH, the present work raises the question of whether such abrupt highly acidic pH variations, which extend over spatial dimensions of the order of tens of nanometers, could contribute to material corrosion and damage [1, 77]. This can easily be envisioned, for example, when spurs or tracks are formed in the immediate neighboring of the metal-water interfaces. In this respect, this work should stimulate novel predictions that can then be tested through new measurements.

## 5. Conclusion

Monte Carlo track chemistry simulations have been used in an attempt to quantify the temperature dependence of the "acid spike" effect that is generated *in situ* in spurs in the radiolysis of pure, deaerated water during and shortly after irradiation. The results were obtained for an isolated spherical spur model, associated with low-LET radiation and under conditions of low dose-rates. The magnitude and duration of the observed transient acid pH response were found to be very sensitive functions of temperature. At 25 °C, the acid-spike

effect was greatest for times shorter than ~1 ns, the pH being nearly constant and equal to ~3.3. At higher temperatures, however, the acid spike response was far more intense but of a much shorter duration. At 350 °C, the pH was around 1.7 at times less than ~10 ps. At longer times, the pH increased gradually for all temperatures considered, ultimately reaching a constant value corresponding to the non-radiolytic, pre-irradiation concentration of $H_3O^+$ arising through water's autoprotolysis at ~1-10 μs following irradiation.

The transient acid pH effect that we have described is virtually unexplored in water subject to the action of ionizing radiation, either at ambient or at elevated temperatures. In this respect, this work raises questions about the potential implications of this effect for water-cooled reactors. For example, and most importantly, we may ask whether the generation of these *in situ* variations in acidity, even if transitory, contribute to material corrosion and damage.

**Acknowledgements**

The authors gratefully acknowledge funding from the Natural Sciences and Engineering Research Council of Canada/Natural Resources Canada/Atomic Energy of Canada Limited Generation IV Energy Technologies Program (Grant No. NNAPJ/424113-11).

**References**

[1] P. Cohen, 1980, "Water Coolant Technology of Power Reactors", American Nuclear Society, La Grange Park, Illinois.

[2] D. R. McCracken, K. T. Tsang, and P. J. Laughton, September 1998, "Aspects of the Physics and Chemistry of Water Radiolysis by Fast Neutrons and Fast Electrons in Nuclear Reactors", AECL-11895 Report, Atomic Energy of Canada Limited, Chalk River, Ontario, Canada.

[3] D. A. Guzonas, C. R. Stuart, J.-P. Jay-Gerin, and J. Meesungnoen, January 2010, "Testing Requirements for SCWR Radiolysis", AECL Report No. 153-127160-REPT-001, Atomic Energy of Canada Limited, Mississauga, Ontario, Canada.

[4] P. Kritzer, 2004, “Corrosion in high-temperature and supercritical water and aqueous solutions: A review”, J. Supercrit. Fluids, Vol. 29(1-2), pp. 1-29.

[5] G. S. Was, P. Ampornrat, G. Gupta, S. Teysseyre, E. A. West, T. R. Allen, K. Sridharan, L. Tan, Y. Chen, X. Ren, and C. Pister, 2007, “Corrosion and stress corrosion cracking in supercritical water”, J. Nucl. Mater., Vol. 371(1-3), pp. 176-201.

[6] D. Guzonas, F. Brosseau, P. Tremaine, J. Meesungnoen, and J.-P. Jay-Gerin, 2012, “Water chemistry in a supercritical water-cooled pressure tube reactor”, Nuclear Technology, Vol. 179(2), pp. 205-219.

[7] D. A. Guzonas and W. G. Cook, December 2012, “Cycle chemistry and its effect on materials in a supercritical water-cooled reactor: A synthesis of current understanding”, Corrosion Sci., Vol. 65, pp. 48-66.

[8] D. Guzonas and R. Novotny, November 2014, “Supercritical water-cooled reactor materials: Summary of research and open issues”, Prog. Nucl. Energy, Vol. 77, pp. 361-372.

[9] A. J. Elliot, M. P. Chenier, and D. C. Ouellette, 1993, “Temperature dependence of *g* values for $H_2O$ and $D_2O$ irradiated with low linear energy transfer radiation”, J. Chem. Soc. Faraday Trans., Vol. 89(8), pp. 1193-1197. See also A. J. Elliot, October 1994, “Rate Constants and *g*-Values for the Simulation of the Radiolysis of Light Water over the Range 0-300 °C”, AECL-11073 Report, Chalk River, Ontario, Canada.

[10] A. J. Elliot and D. M. Bartels, August 2009, “The Reaction Set, Rate Constants and *g*-Values for the Simulation of the Radiolysis of Light Water over the Range 20 to 350 °C Based on Information Available in 2008”, AECL Report No. 153-127160-450-001, Mississauga, Ontario, Canada.

[11] K. Kanjana, K. S. Haygarth, W. Wu, and D. M. Bartels, January 2013, “Laboratory studies in search of the critical hydrogen concentration”, Radiat. Phys. Chem., Vol. 82, pp. 25-34.

[12] D. M. Bartels, M. Anderson, P. Wilson, T. Allen, and K. Sridharan, 2006, "Supercritical Water Radiolysis Chemistry. Supercritical Water Corrosion", Idaho National Laboratory, Idaho Falls, Idaho. Available from http://nuclear.inl.gov/ deliverables/docs/ uwnd_scw_level_ii_sep_2006_v3.pdf

[13] M. Lin, Y. Muroya, G. Baldacchino, and Y. Katsumura, 2010, "Radiolysis of supercritical water", in "Recent Trends in Radiation Chemistry", edited by J. F. Wishart and B. S. M. Rao, World Scientific, Singapore, pp. 255-277.

[14] P. Causey and C. R. Stuart, October 2011, "Test Plan for Pulse Radiolysis Studies of Water at High Temperature and Pressure", AECL Report No. 217-127160-TP-001, Chalk River, Ontario, Canada.

[15] M. Lin and Y. Katsumura, 2011, "Radiation chemistry of high temperature and supercritical water and alcohols", in "Charged Particle and Photon Interactions with Matter: Recent Advances, Applications, and Interfaces", edited by Y. Hatano, Y. Katsumura, and A. Mozumder, Taylor and Francis Group, Boca Raton, Florida, pp. 401-424.

[16] J. Meesungnoen, D. Guzonas, and J.-P. Jay-Gerin, 2010, "Radiolysis of supercritical water at 400 °C and liquid-like densities near 0.5 g/cm$^3$. A Monte Carlo calculation", Can. J. Chem., Vol. 88(7), pp. 646-653.

[17] Y. Muroya, S. Sanguanmith, J. Meesungnoen, M. Lin, Y. Yan, Y. Katsumura, and J.-P. Jay-Gerin, 2012, "Time-dependent yield of the hydrated electron in subcritical and supercritical water studied by ultrafast pulse radiolysis and Monte Carlo simulation", Phys. Chem. Chem. Phys., Vol. 14(41), pp. 14325-14333.

[18] M.-Y. Wang, T.-K. Yeh, H.-M. Liu, and M. Lee, 2013, "Predicted water chemistry in the primary coolant circuit of a supercritical water reactor", Nucl. Sci. Eng., Vol. 174(2), pp. 179-187.

[19] N. Yousefi, September 2014, "Gamma-Radiolysis Kinetics of Liquid, Vapour and Supercritical Water", Master thesis, University of Western Ontario, London, Ontario, Canada.

[20] S. L. Butarbutar, J. Meesungnoen, D. A. Guzonas, C. R. Stuart, and J.-P. Jay-Gerin, 2014, “Modeling the radiolysis of supercritical water by fast neutrons: Density dependence of the yields of primary species at 400 °C”, Radiat. Res., Vol. 182(6), pp. 695-704.

[21] V. Kanike, J. Meesungnoen, and J.-P. Jay-Gerin, 2015, “Acid spike effect in spurs/tracks of the low/high linear energy transfer radiolysis of water: Potential implications for radiobiology”, RSC Adv., Vol. 5(54), pp. 43361-43370.

[22] J. L. Magee, 1953, “Radiation chemistry”, Annu. Rev. Nucl. Sci., Vol. 3, pp. 171-192.

[23] G. R. Freeman, 1982, “Basics of radiation chemistry”, in “The Study of Fast Processes and Transient Species by Electron Pulse Radiolysis”, edited by J. H. Baxendale and F. Busi, D. Reidel, Dordrecht, pp. 19-34.

[24] R. L. Platzman, 1958, “The physical and chemical basis of mechanisms in radiation biology”, in “Radiation Biology and Medicine. Selected Reviews in the Life Sciences”, edited by W. D. Claus, Addison-Wesley, Reading, pp. 15-72.

[25] J. Meesungnoen and J.-P. Jay-Gerin, 2011, “Radiation chemistry of liquid water with heavy ions: Monte Carlo simulation studies”, in “Charged Particle and Photon Interactions with Matter: Recent Advances, Applications, and Interfaces”, edited by Y. Hatano, Y. Katsumura, and A. Mozumder, Taylor and Francis Group, Boca Raton, Florida, pp. 355-400.

[26] G. V. Buxton, 1987, “Radiation chemistry of the liquid state: (1) Water and homogeneous aqueous solutions”, in “Radiation Chemistry: Principles and Applications”, edited by Farhataziz and M. A. J. Rodgers, VCH Publishers, New York, pp. 321-349.

[27] J. W. T. Spinks and R. J. Woods, 1990, “An Introduction to Radiation Chemistry”, Third Edition, Wiley, New York.

[28] C. Ferradini and J.-P. Jay-Gerin, 1999, “La radiolyse de l’eau et des solutions aqueuses: historique et actualité”, Can. J. Chem., Vol. 77(9), pp. 1542-1575.

[29] J. Li, Z. Nie, Y. Y. Zheng, S. Dong, and Z.-H. Loh, 2013, "Elementary electron and ion dynamics in ionized liquid water", J. Phys. Chem. Lett., Vol. 4, pp. 3698-3703.

[30] A. Mozumder and J. L. Magee, 1975, "The early events of radiation chemistry", Int. J. Radiat. Phys. Chem., Vol. 7(2-3), pp. 83-93.

[31] C.-R. Wang, T. Luo, and Q.-B. Lu, 2008, "On the lifetimes and physical nature of incompletely relaxed electrons in liquid water", Phys. Chem. Chem. Phys., Vol. 10(30), pp. 4463-4470.

[32] C. Pépin, T. Goulet, D. Houde, and J.-P. Jay-Gerin, 1997, "Observation of a continuous spectral shift in the solvation kinetics of electrons in neat liquid deuterated water", J. Phys. Chem. A, Vol. 101(24), pp. 4351-4360.

[33] T. Goulet, J. P. Patau, and J.-P. Jay-Gerin, 1990, "Influence of the parent cation on the thermalization of subexcitation electrons in solid water", J. Phys. Chem., Vol. 94(18), pp. 7312-7316.

[34] D. M. Bartels, D. Gosztola, and C. D. Jonah, 2001, "Spur decay kinetics of the solvated electron in heavy water radiolysis", J. Phys. Chem. A, Vol. 105(34), pp. 8069-8072.

[35] J. Meesungnoen and J.-P. Jay-Gerin, 2005, "High-LET radiolysis of liquid water with $^{1}H^{+}$, $^{4}He^{2+}$, $^{12}C^{6+}$, and $^{20}Ne^{9+}$ ions: Effects of multiple ionization", J. Phys. Chem. A, Vol. 109(29), pp. 6406-6419.

[36] R. L. Platzman, 1962, "Dissociative attachment of subexcitation electrons in liquid water, and the origin of radiolytic 'molecular' hydrogen", in "Abstracts of Papers", Second International Congress of Radiation Research, Harrogate, England, p. 128.

[37] T. Goulet and J.-P. Jay-Gerin, 1989, "Thermalization of subexcitation electrons in solid water", Radiat. Res., Vol. 118(1), pp. 46-62.

[38] P. Rowntree, L. Parenteau, and L. Sanche, 1991, "Electron stimulated desorption via dissociative attachment in amorphous $H_2O$", J. Chem. Phys., Vol. 94(12), pp. 8570-8576.

[39] V. Cobut, J.-P. Jay-Gerin, Y. Frongillo, and J. P. Patau, 1996, "On the dissociative electron attachment as a potential source of molecular hydrogen in irradiated liquid water", Radiat. Phys. Chem., Vol. 47(2), pp. 247-250.

[40] D. N. Nikogosyan, A. A. Oraevsky, and V. I. Rupasov, 1983, "Two-photon ionization and dissociation of liquid water by powerful laser UV radiation", Chem. Phys., Vol. 77(1), pp. 131-143.

[41] A. Migus, Y. Gauduel, J.-L. Martin, and A. Antonetti, 1987, "Excess electrons in liquid water: First evidence of a prehydrated state with femtosecond lifetime", Phys. Rev. Lett., Vol. 58(15), pp. 1559-1562.

[42] A. Bernas, C. Ferradini, and J.-P. Jay-Gerin, 1997, "On the electronic structure of liquid water: Facts and reflections", Chem. Phys., Vol. 222(2-3), pp. 151-160.

[43] D. Biedenkapp, L. G. Hartshorn, and E. J. Bair, 1997, "The $O(^1D) + H_2O$ reaction", Chem. Phys. Lett., Vol. 5(6), pp. 379-381.

[44] O. Amichai and A. Treinin, 1969, "Chemical reactivity of $O(^3P)$ atoms in aqueous solution", Chem. Phys. Lett., Vol. 3(8), pp. 611-613.

[45] S. Sanguanmith, J. Meesungnoen, Y. Muroya, M. Lin, Y. Katsumura, and J.-P. Jay-Gerin, 2012, "On the spur lifetime and its temperature dependence in the low linear energy transfer radiolysis of water", Phys. Chem. Chem. Phys., Vol. 14(48), pp. 16731-16736.

[46] I. Plante, A. Filali-Mouhim, and J.-P. Jay-Gerin, 2005, "SimulRad: A Java interface for a Monte Carlo simulation code to visualize in 3D the early stages of water radiolysis", Radiat. Phys. Chem., Vol. 72(2-3), pp. 173-180.

[47] Y. Muroya, I. Plante, E. I. Azzam, J. Meesungnoen, Y. Katsumura, and J.-P. Jay-Gerin, 2006, "High-LET ion radiolysis of water: Visualization of the formation and evolution of ion tracks and relevance to the radiation-induced bystander effect", Radiat. Res., Vol. 165(4), pp. 485-491.

[48] D. Swiatla-Wojcik and G. V. Buxton, 2005, "On the possible role of the reaction $H^{\bullet} + H_2O \rightarrow H_2 + {}^{\bullet}OH$ in the radiolysis of water at high temperatures", Radiat. Phys. Chem., Vol. 74(3-4), pp. 210-219.

[49] D. M. Bartels, 2009, "Comment on the possible role of the reaction $H^{\bullet} + H_2O \rightarrow H_2 + {}^{\bullet}OH$ in the radiolysis of water at high temperatures", Radiat. Phys. Chem., Vol. 78(3), pp. 191-194.

[50] D. Swiatla-Wojcik and G. V. Buxton, 2010, "Reply to comment on the possible role of the reaction $H + H_2O \rightarrow H_2 + OH$ in the radiolysis of water at high temperatures", Radiat. Phys. Chem., Vol. 79(1), pp. 52-56.

[51] S. Sanguanmith, Y. Muroya, J. Meesungnoen, M. Lin, Y. Katsumura, L. Mirsaleh Kohan, D. A. Guzonas, C. R. Stuart, and J.-P. Jay-Gerin, 2011, "Low-linear energy transfer radiolysis of liquid water at elevated temperatures up to 350 °C: Monte Carlo simulations", Chem. Phys. Lett., Vol. 508(4-6), pp. 224-230.

[52] S. L. Butarbutar, Y. Muroya, L. Mirsaleh Kohan, S. Sanguanmith, J. Meesungnoen, and J.-P. Jay-Gerin, 2013, "On the temperature dependence of the rate constant of the bimolecular reaction of two hydrated electrons", Atom Indonesia J., Vol. 39(2), pp. 51-56.

[53] J. Meesungnoen, S. Sanguanmith, and J.-P. Jay-Gerin, 2015, "Yields of $H_2$ and hydrated electrons in low-LET radiolysis of water determined by Monte Carlo track chemistry simulations using phenol/$N_2O$ aqueous solutions up to 350 °C", RSC Adv., Vol. 5(94), pp. 76813-76824.

[54] M. Sterniczuk, P. A. Yakabuskie, J. C. Wren, J. A. Jacob, and D. A. Bartels, 2016, "Low LET radiolysis escape yields for reducing radicals and $H_2$ in pressurized high temperature water", Radiat. Phys. Chem., Vol. 121, pp. 35-42.

[55] M. Sterniczuk and D. M. Bartels, 2016, "Source of molecular hydrogen in high temperature water radiolysis", J. Phys. Chem. A, Vol. 120(2), pp. 200-209.

[56] M.-A. Hervé du Penhoat, T. Goulet, Y. Frongillo, M.-J. Fraser, Ph. Bernat, and J.-P. Jay-Gerin, 2000, "Radiolysis of liquid water at temperatures up to 300 °C: A Monte Carlo simulation study", J. Phys. Chem. A, Vol. 104(50), pp. 11757-11770.

[57] T. Tippayamontri, S. Sanguanmith, J. Meesungnoen, G. R. Sunaryo, and J.-P. Jay-Gerin, 2009, "Fast neutron radiolysis of the ferrous sulfate (Fricke) dosimeter: Monte Carlo simulations", Recent Res. Devel. Physical Chem., Vol. 10, pp. 143-211.

[58] Y. Frongillo, T. Goulet, M.-J. Fraser, V. Cobut, J. P. Patau, and J.-P. Jay-Gerin, 1998, "Monte Carlo simulation of fast electron and proton tracks in liquid water. II. Nonhomogeneous chemistry", Radiat. Phys. Chem., Vol. 51(3), pp. 245-254.

[59] M. Tachiya, 1983, "Theory of diffusion-controlled reactions: Formulation of the bulk reaction rate in terms of the pair probability", Radiat. Phys. Chem., Vol. 21(1-2), pp. 167-175.

[60] S. M. Pimblott, M. J. Pilling, and N. J. B. Green, 1991, "Stochastic models of spur kinetics in water", Radiat. Phys. Chem., Vol. 37(3), pp. 377-388.

[61] T. Goulet, M.-J. Fraser, Y. Frongillo, and J.-P. Jay-Gerin, 1998, "On the validity of the independent reaction times approximation for the description of the nonhomogeneous kinetics of liquid water radiolysis", Radiat. Phys. Chem., Vol. 51(1), pp. 85-91.

[62] I. Plante, July 2009, "Développement de codes de simulation Monte Carlo de la radiolyse de l'eau par des électrons, ions lourds, photons et neutrons. Applications à divers sujets d'intérêt expérimental", Ph.D. thesis, Université de Sherbrooke, Sherbrooke, Quebec, Canada.

[63] L. Mirsaleh Kohan, S. Sanguanmith, J. Meesungnoen, P. Causey, C. R. Stuart, and J.-P. Jay-Gerin, 2013, "Self-radiolysis of tritiated water. 1. A comparison of the effects of $^{60}$Co γ-rays and tritium β-particles on water and aqueous solutions at room temperature", RSC Adv., Vol. 3(42), pp. 19282-19299.

[64] S. Sanguanmith, J. Meesungnoen, and J.-P. Jay-Gerin, November 2013, "Time-dependent yield of OH radicals in the low linear energy transfer radiolysis of water between 25 and 350 °C", Chem. Phys. Lett., Vol. 588, pp. 82-86.

[65] P. J. Linstrom and W. G. Mallard (Eds.), 2005, "NIST Chemistry WebBook", NIST Standard Reference Database No. 69, National Institute of Standards and Technology, Gaithersburg, MD. Available from http://webbook.nist.gov

[66] A. K. Pikaev, S. A. Kabakchi, and A. A. Zansokhova, 1977, "Yields and reactions of hydrogen ions on radiolysis of water and aqueous solutions", Faraday Discuss. Chem. Soc., Vol. 63, pp. 112-123.

[67] B. Čerček and M. Kongshaug, 1969, "Hydrogen ion yields in the radiolysis of neutral aqueous solutions", J. Phys. Chem., Vol. 73(6), pp. 2056-2058.

[68] R. F. Anderson, B. Vojnovic, and B. D. Michael, 1985, "The radiation-chemical yields of $H_3O^+$ and $OH^-$ as determined by nanosecond conductimetric measurements, Radiat. Phys. Chem., Vol. 26(3), pp. 301-303.

[69] G. C. Barker, P. Fowles, D. C. Sammon, and B. Stringer, 1970, "Pulse radiolysis induced transient electrical conductance in liquid solutions. Part 1. Technique and the radiolysis of water", Trans. Faraday Soc., Vol. 66, pp. 1498-1508.

[70] K. H. Schmidt and S. M. Ander, 1969, "Formation and recombination of $H_3O^+$ and hydroxide in irradiated water", J. Phys. Chem., Vol. 73(9), pp. 2846-2852.

[71] D. Swiatla-Wojcik and G. V. Buxton, 1995, "Modeling of radiation spur processes in water at temperatures up to 300 °C", J. Phys. Chem., Vol. 99(29), pp. 11464-11471.

[72] C. M. Stanisky, D. M. Bartels, and K. Takahashi, 2010, "Rate constants for the reaction of hydronium ions with hydrated electrons up to 350 °C", Radiat. Phys. Chem., Vol. 79(1), pp. 64-65.

[73] V. Cobut, Y. Frongillo, J. P. Patau, T. Goulet, M.-J. Fraser, and J.-P. Jay-Gerin, 1998, "Monte Carlo simulation of fast electron and proton tracks in liquid water. I. Physical and physicochemical aspects", Radiat. Phys. Chem., Vol. 51(3), pp. 229-243.

[74] N. Autsavapromporn, March 2006, "The effects of pH and radiation quality (LET) on the radiolysis of liquid water and aqueous solutions: A study by using Monte Carlo simulations", Master thesis, Burapha University, Bangsaen, Chonburi, Thailand.

[75] J. A. LaVerne and S. M. Pimblott, 1995, "Electron energy-loss distributions in solid, dry DNA", Radiat. Res., Vol. 141(2), pp. 208-215.

[76] A. Hummel, 1995, "Radiation Chemistry: The Chemical Effects of Ionizing Radiation and their Applications", IRI-TUD, Delft, The Netherlands.

[77] D. Féron and J.-M. Olive (Eds.), 2007, "Corrosion Issues in Light Water Reactors. Stress Corrosion Cracking", Woodhead Publishing Ltd., Cambridge, England.

**List of Figures**

Figure 6: Time evolution of pH in a spur calculated for pure, deaerated liquid water at different temperatures between 25 and 350 °C and in the interval of ~1 ps to 10 μs, for irradiating 300-MeV protons using the isolated spherical spur model, characteristic of low-LET radiation.

Figure 7: Variation of pH with temperature over the range of 25-350 °C calculated for pure, deaerated liquid water for irradiating 300-MeV protons using the isolated spherical spur model, at three different times during spur expansion: 1 ps, 1 ns, and 1 μs.

Figure 1

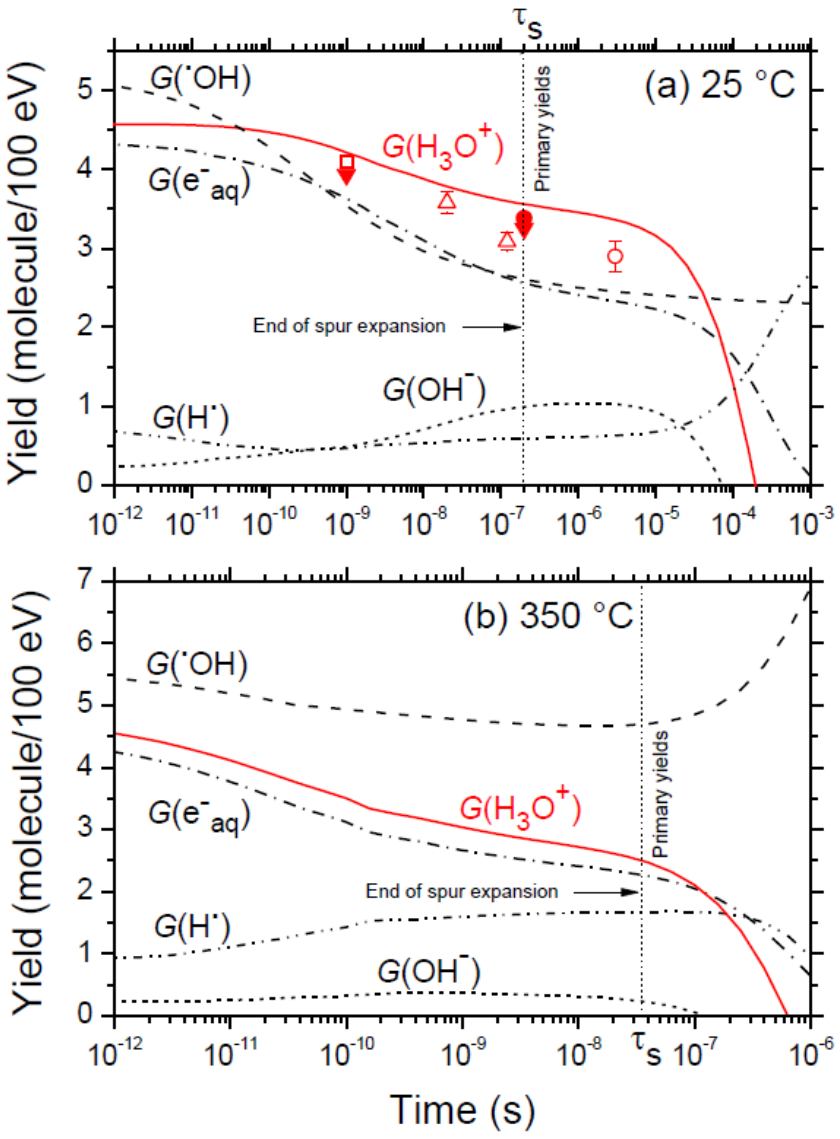
τs
(a) 25 °C
G(˙OH)
G(e⁻aq)
G(H3O+)
Primary yields
End of spur expansion
G(OH⁻)
G(H˙)
Yield (molecule/100 eV)
(b) 350 °C
G(˙OH)
G(e⁻aq)
G(H3O+)
Primary yields
End of spur expansion
G(H˙)
G(OH⁻)
τs
Yield (molecule/100 eV)
Time (s)

Figure 2

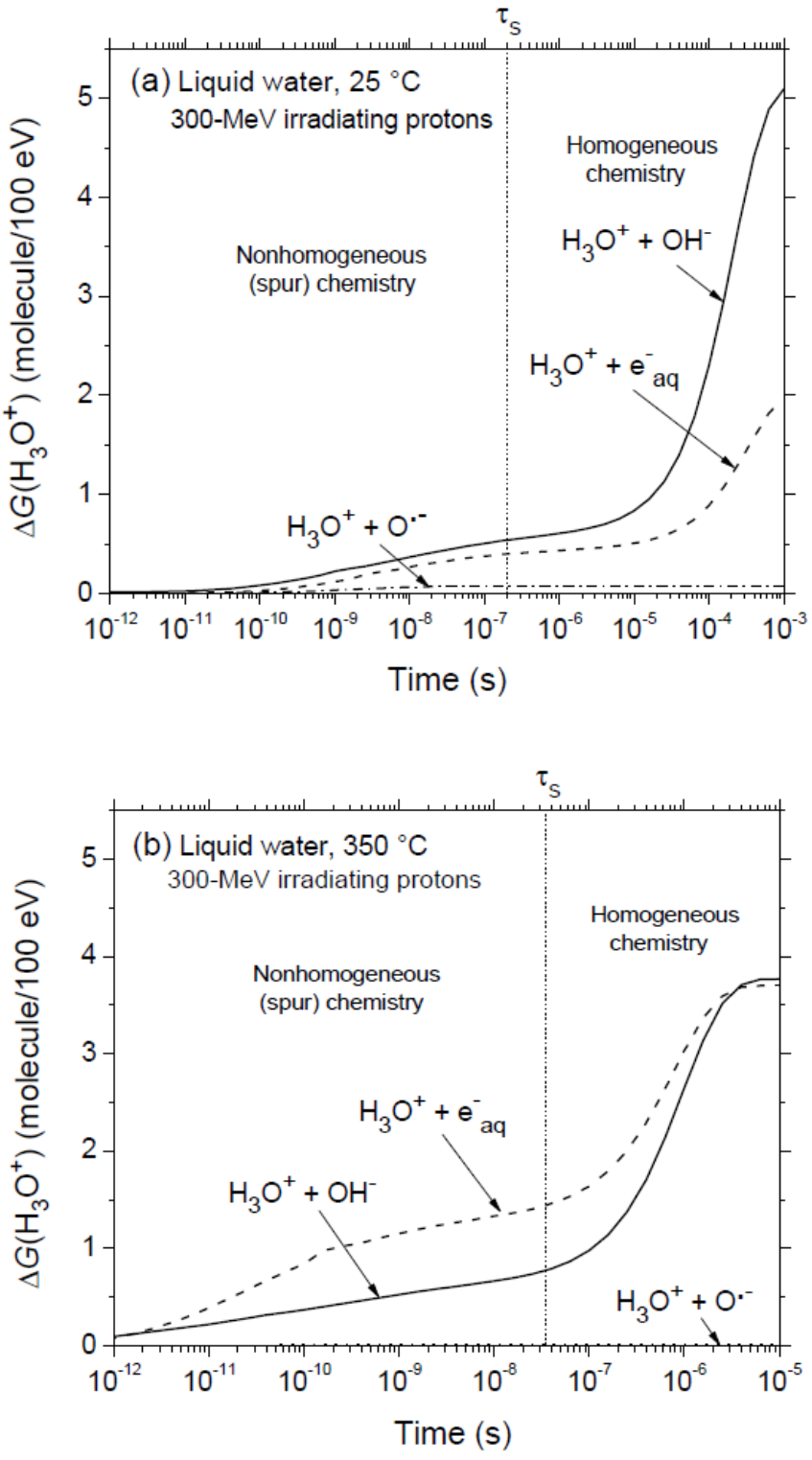
τs
(a) Liquid water, 25 °C
300-MeV irradiating protons
Homogeneous chemistry
Nonhomogeneous (spur) chemistry
H3O+ + OH-
H3O+ + e-aq
H3O+ + O·-
ΔG(H3O+) (molecule/100 eV)
Time (s)
τs
(b) Liquid water, 350 °C
300-MeV irradiating protons
Homogeneous chemistry
Nonhomogeneous (spur) chemistry
H3O+ + e-aq
H3O+ + OH-
H3O+ + O·-
ΔG(H3O+) (molecule/100 eV)
Time (s)

Figure 3

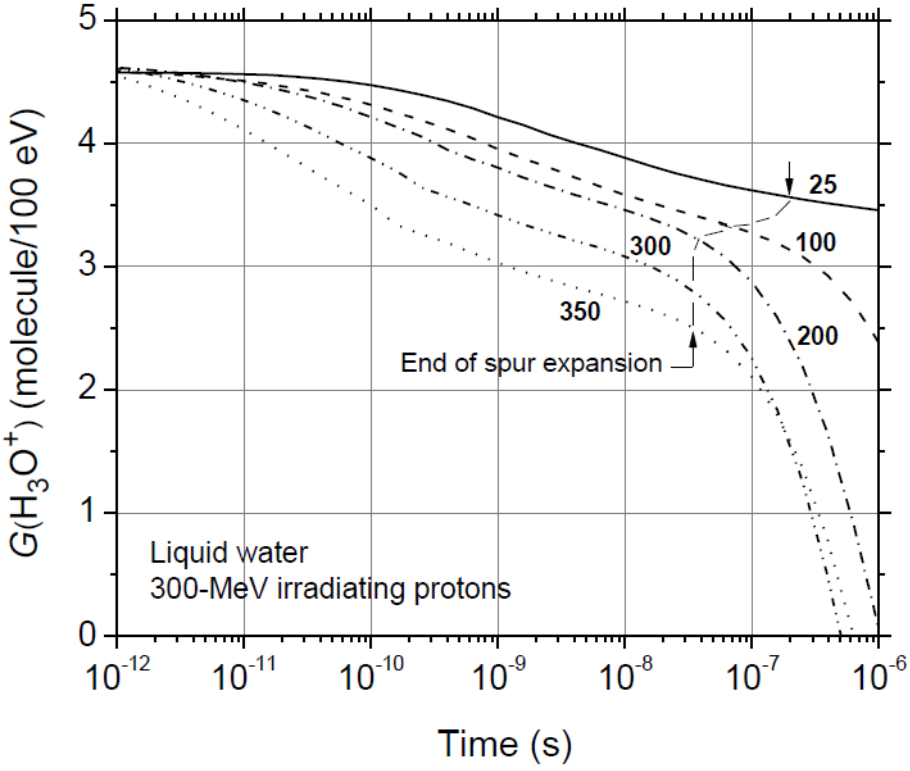
5
4
3
2
1
0
$G(H_3O^+)$ (molecule/100 eV)
25
100
200
300
350
End of spur expansion
Liquid water
300-MeV irradiating protons
$10^{-12}$
$10^{-11}$
$10^{-10}$
$10^{-9}$
$10^{-8}$
$10^{-7}$
$10^{-6}$
Time (s)

Figure 4

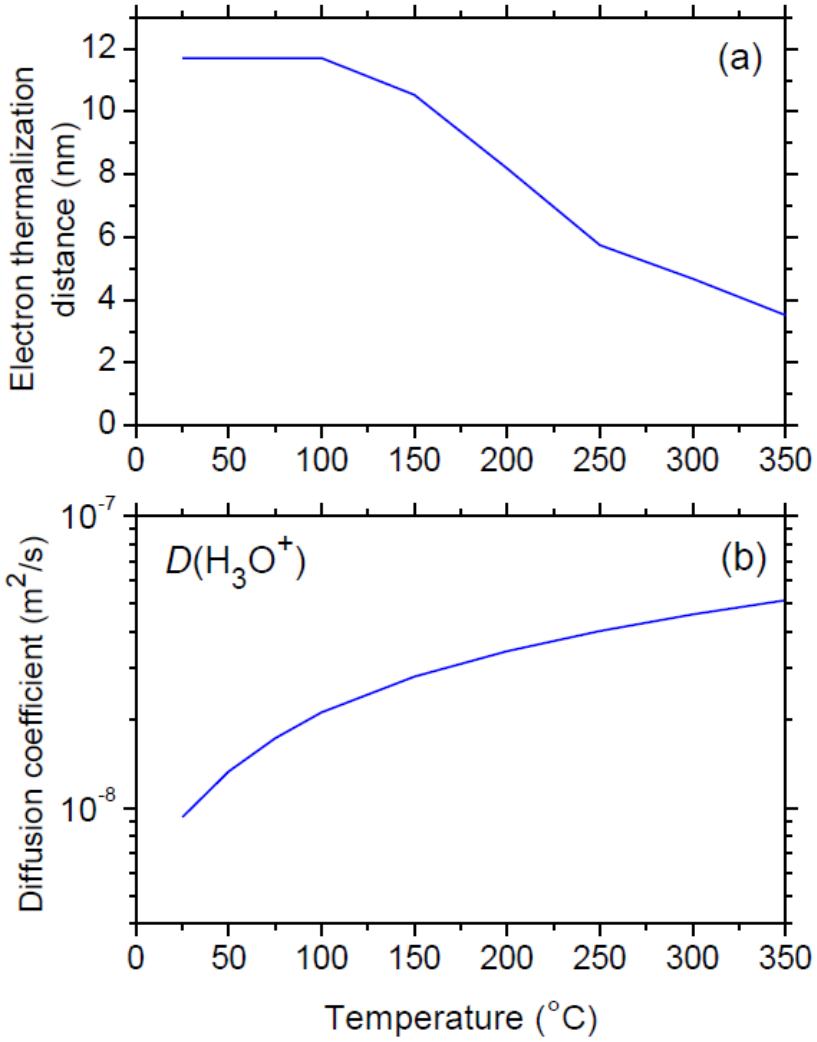
Electron thermalization distance (nm)
(a)
0
2
4
6
8
10
12
0
50
100
150
200
250
300
350
Diffusion coefficient (m2/s)
D(H3O+)
(b)
10-7
10-8
0
50
100
150
200
250
300
350
Temperature (°C)

Figure 5

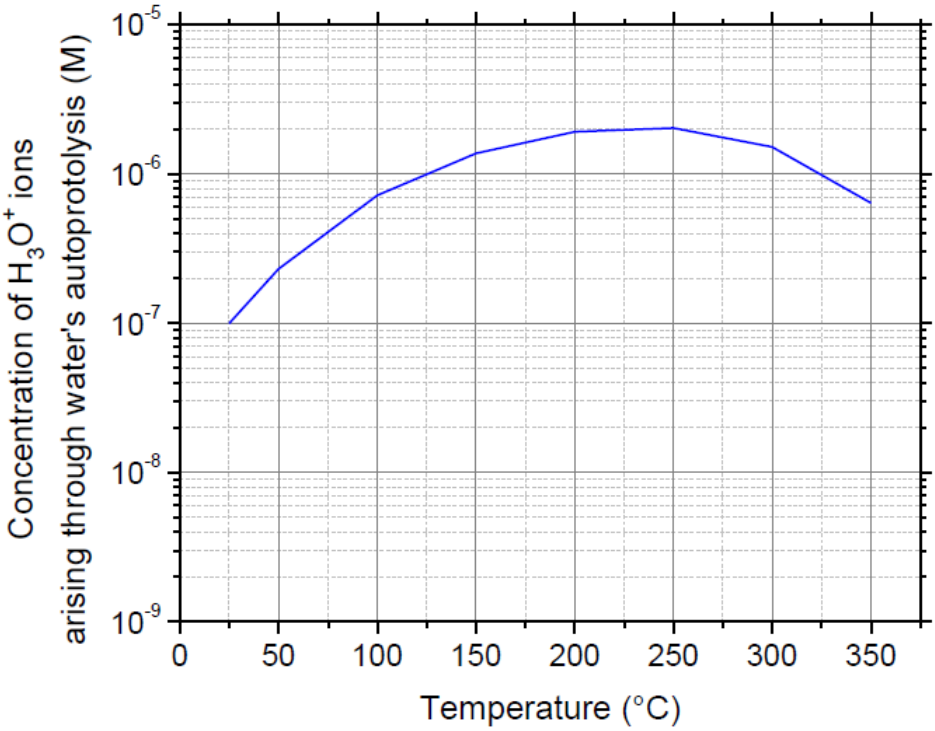
Concentration of $H_3O^+$ ions arising through water's autoprotolysis (M)
$10^{-5}$
$10^{-6}$
$10^{-7}$
$10^{-8}$
$10^{-9}$
0
50
100
150
200
250
300
350
Temperature (°C)

Figure 6

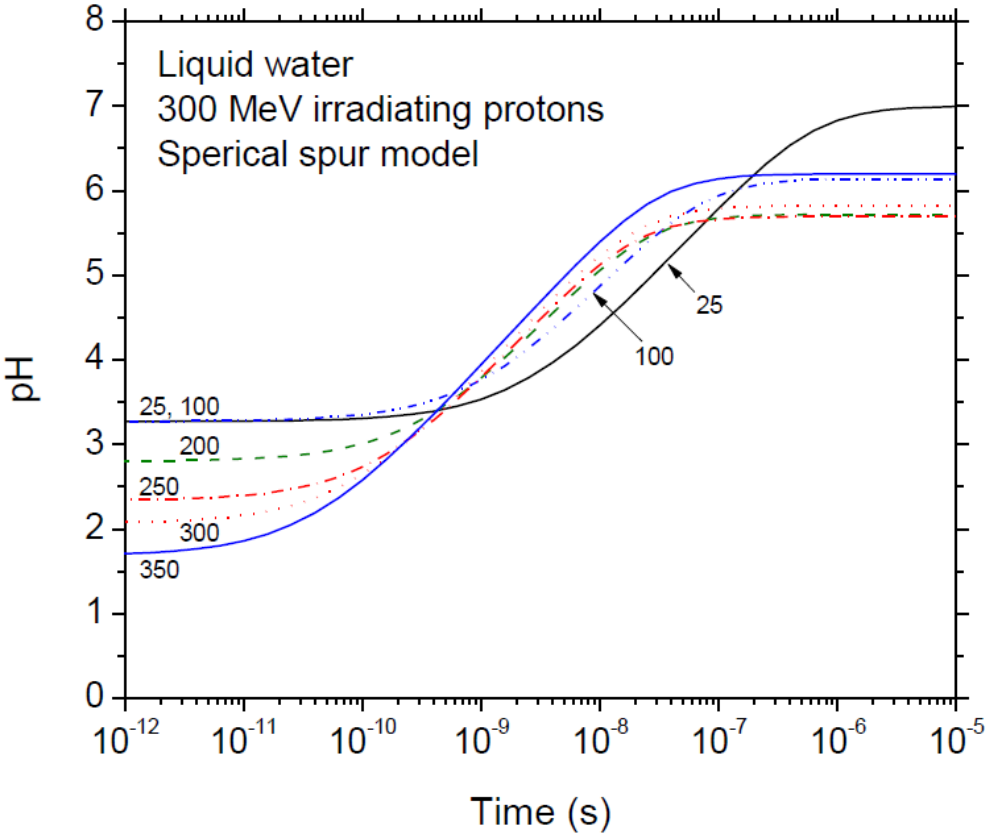
Liquid water
300 MeV irradiating protons
Sperical spur model
pH
Time (s)
25, 100
200
250
300
350
25
100
0
1
2
3
4
5
6
7
8
10-12
10-11
10-10
10-9
10-8
10-7
10-6
10-5

Figure 7

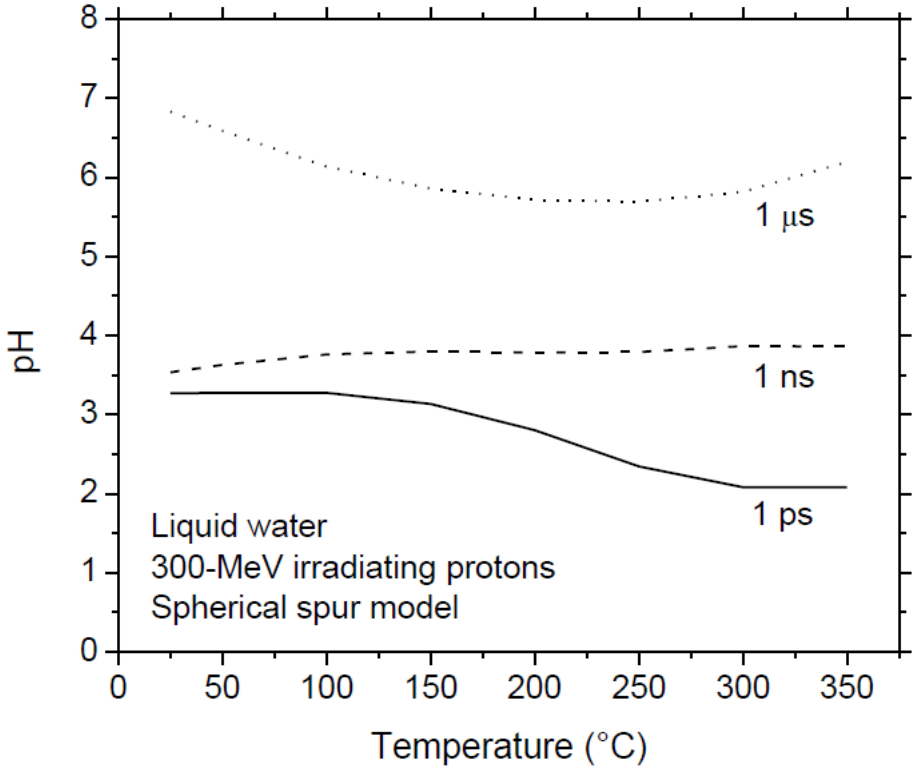
pH
Temperature (°C)
1 μs
1 ns
1 ps
Liquid water
300-MeV irradiating protons
Spherical spur model
0
1
2
3
4
5
6
7
8
0
50
100
150
200
250
300
350

# 6 - DISCUSSION

Although damage can be randomly induced in all biomolecules (*e.g.*, DNA, membrane lipids, and proteins), *DNA and its associated water molecules* are considered to be the critical target in defining the radiobiological response. Exposure to ionizing radiation is known to cause a *plethora of DNA damage*, including single- and double-strand breaks, base damage, abasic sites, destruction of sugars, tandem lesions, cross-links, defects in mitochondrial functions, and "clustered" damage (for reviews, see: CADET et al., 1997, 2012; BERNHARD and CLOSE, 2004; von SONNTAG, 2006; HALL and GIACCIA, 2006; LEHNERT, 2008; AZZAM et al., 2012). Clustered damage is the most biologically-relevant DNA damage induced by radiation because it is less readily repaired by the cell. These various types of damage are produced primarily within one or two turns of the DNA helix (~ 3 - 12 base pairs). Damage is caused either directly or indirectly through chemical attack by radiolytic products as the radiation track passes through and deposits energy near to (mostly bulk water) or in the DNA.

The damage caused in irradiated cells may spread to neighboring, *non-targeted bystander cells* through *intercellular communication mechanisms*, especially following low doses of ionizing radiation [11] (for example, see: NAGASAWA and LITTLE, 1992; MOTHERSILL and SEYMOUR, 2001; AZZAM et al., 2003; HEI et al., 2011; AUTSAVAPROMPORN et al., 2011; SUZUKI and YAMASHITA, 2014). Observations of these effects have challenged the DNA-centric dogma of classical radiobiology (*i.e.*, no effect was expected in cells whose nucleus was not directly traversed by a radiation track). Indeed, extra-nuclear and extracellular events may also contribute to the final biological consequences of radiation exposure.

Many cellular processes depend on pH. These include synthesis of macromolecules and cell proliferation, transport of metabolites and drugs, and the activity of enzymes (TANNOCK and ROTIN, 1989). In the present chapter, we first give some specific

[11] Ionizing radiation-induced bystander effects, commonly observed in cell populations exposed to low- and high-LET radiations, are initiated by damage to a cellular molecule which then gives rise to a toxic signal exported to neighboring cells not directly hit by radiation. Cellular phenotype, radiation quality (or LET), and dose are likely modulators of molecular and biochemical signalling events involved.

examples of molecular processes that could intervene in irradiated cells in response to the highly localized and transitory acid-spike effect described in this work. Our results are then compared with recent simulations of water radiolysis under high dose-rate conditions prevailing in electron microscope imaging experiments (SCHNEIDER et al., 2014; GROGAN et al., 2014). Finally, based on this comparison, we examine, somewhat provocatively, the possible relevance of our work on three radiotherapy methodologies in which the dose is given under different dose-rate irradiation conditions, namely, continuous, conventional (clinical) radiotherapy (≤ 0.03 Gy/s), pulsed FLASH irradiation (4.5-MeV electron pulses with a dose rate per pulse of ~$10^6$ Gy/s) (FAVAUDON et al., 2014, 2015), and femtosecond laser-induced filamentation (effective dose rate up to ~5 × $10^{11}$ Gy/s) (MEESAT et al., 2012).

### 6.1 Examples of molecular processes intervening in cells in an acidic environment

An acid may be defined as a donor of protons ($H^+$). The strength of an acid refers to its ability or tendency to lose a proton. Strong acids (*e.g.*, HCl, $HNO_3$, $H_2SO_4$)[12] are completely dissociated when they go into solution in water. However, most acids in living systems (*e.g.*, $HNO_2$, HOCl, $HO_2^{\bullet}$) are weak acids and are only partly dissociated in water or an aqueous solution, according to the equilibrium:

$$HA \underset{}{\overset{K_a}{\rightleftharpoons}} H^+ + A^-, \qquad [35]$$

where $A^-$ is the conjugate base of the weak acid HA. The equilibrium constant (also called the "acid dissociation constant"), $K_a$, is given by

$$K_a = [H^+][A^-] / [HA] \qquad [36]$$

at equilibrium. Values of $K_a$ are affected by temperature. By analogy to the definition of pH, we often use p$K_a$ as the negative logarithm (base 10) of $K_a$:

$$pK_a = -\log(K_a), \qquad [37]$$

[12] For sulfuric acid $H_2SO_4$, only the first proton ionization is complete. Dissociation of the second proton has an equilibrium constant of $10^{-2}$.

which means that the stronger an acid, the smaller the value of its p$K_a$. The $K_a$ (or p$K_a$) values of many weak acids in aqueous solution at various temperatures are listed in table form in handbooks (for example, see: DEAN, 1987; HAYNES and LIDE, 2010).

Rearranging the $K_a$ equilibrium expression [36], we can derive the Henderson-Hasselbalch equation (HARRIS, 2013):

$$pH = pK_a + \log_{10} \{[A^-] / [HA]\} , \qquad [38]$$

which tells us that, if equal amounts of a weak acid and its conjugate base are mixed (then the log term in equation [38] is 0), the pH of the resulting solution equals the p$K_a$ of the acid. Equation [38] also indicates that a factor-of-10 change in the ratio $[A^-]/[HA]$ changes the pH by only one unit.

The Henderson-Hasselbalch equation is the central equation for *buffers*. [13] Biochemists are most interested in buffers because the functioning of biological systems depends critically on pH. For example, this is especially important for enzymes, which are proteins that act as catalysts for important biological reactions. Most enzymes only work within a certain pH range (see Sect. 6.1.3).

### *6.1.1 Superoxide radical anion ($O_2^{\bullet -}$)*

If $O_2$ is present, the hydrated electrons formed by ionizing radiation can reduce it to $O_2^{\bullet -}$ (see Sect. 1.1.2, reaction [12]). The superoxide radical anion thus formed is far less reactive than $^{\bullet}OH$. It does not react with most biological molecules in aqueous solution. However, it does react quickly with several other radicals, such as nitric oxide ($^{\bullet}NO$), iron-sulphur clusters in certain enzymes, and some phenoxyl radicals (HALLIWELL and GUTTERIDGE, 2015). The $O_2^{\bullet -}$ radical is always in a pH-dependent equilibrium with its protonated form, the hydroperoxyl radical $HO_2^{\bullet}$:

$$HO_2^{\bullet} \rightleftharpoons H^+ + O_2^{\bullet -} , \qquad [39]$$

[13] A buffer consists of a solution containing a weak acid and its conjugate base, which minimizes pH change on the addition of small amounts of acid or base. The p$K_a$ value is used to choose a buffer when needed. Choosing an acid where p$K_a$ is close to the pH needed gives the best results.

the p$K_a$ of the protonation/deprotonation equilibrium being around 4.8 in water at 25 °C (BIELSKI et al., 1985).

Although at the pH of most body tissues the ratio of $[O_2^{\bullet-}]/[HO_2^{\bullet}]$ is large (100/1 at pH 6.8, 1000/1 at pH 7.8, according to equation [38]), the high reactivity of $HO_2^{\bullet}$ with biomolecules [*e.g.*, $HO_2^{\bullet}$, but not $O_2^{\bullet-}$, is responsible in part of initiation of lipid peroxidation reactions in the inner membrane of mitochondria (KOWALD, 1999)] and its uncharged nature (which might allow it to traverse membranes more readily than the charged $O_2^{\bullet-}$) suggest that it has the potential to cause damage (DE GREY, 2002; HALLIWELL and GUTTERIDGE, 2015) and that it can contribute to the propagation of signalling events among cells (*e.g.*, leading to bystander effects) (AZZAM et al., 2012).

As the pH is lowered, the proportion of $O_2^{\bullet-}$ that is protonated increases ($[O_2^{\bullet-}]/[HO_2^{\bullet}]$ = 1/100 in an aqueous solution at pH 2.8). The conversion of the harmless $O_2^{\bullet-}$ into the harmful $HO_2^{\bullet}$ may consequently result in an increased growth of potentially toxic effects *in vivo*.

### *6.1.2 Nitric oxide ($^{\bullet}$NO)*

Nitric oxide is a small, uncharged, relatively stable, enzymatically generated, free-radical gas[14] that readily diffuses into cells and permeates cell membranes where it reacts with molecular targets. The precise reactions and the eventual cellular response depend on the concentration of $^{\bullet}$NO achieved (GROSS and WOLIN, 1995). As mentioned in Sect. 1.1.2, ionizing radiation can induce high levels of $^{\bullet}$NO attributable to the expression of the iNOS enzyme activity, combined with a simultaneous increased production of $O_2^{\bullet-}$ from the damaged mitochondrial electron transport chain complexes.[15] A large part of the toxicity of $^{\bullet}$NO *in vivo* is due to its diffusion-limited reaction with $O_2^{\bullet-}$ to give a powerful (non-radical) oxidant, peroxynitrite ($ONOO^-$) (for example, see: PRYOR and SQUADRITO, 1995; KOPPENOL, 1998; JAY-GERIN and FERRADINI, 2000):

$$^{\bullet}NO + O_2^{\bullet-} \rightarrow ONOO^- \qquad k_{40} = 1.9 \times 10^{10}\ M^{-1}\ s^{-1} \qquad [40]$$

[14] It is moderately soluble in water (1.93 mM at 25 °C and 1.63 mM at 37 °C, 1 atm) (KOPPENOL, 1998) and is 6-9 times more soluble in organic solvents.

[15] Radiation can damage mitochondria, causing more electron leakage to $O_2$.

with a rate constant that is approximately 5 times higher than that for the Cu,Zn-SOD-catalyzed dismutation of $O_2^{\bullet-}$:

$$O_2^{\bullet-} + O_2^{\bullet-} + 2H^+ \xrightarrow{\text{SOD}} H_2O_2 + O_2 \qquad k_{41} = 4 \times 10^9\ M^{-1}\ s^{-1} \qquad [41]$$

It has been shown (RADI et al., 2000) that $^{\bullet}NO$ is the only biomolecule known to react fast enough and to be produced in sufficient concentrations (which is indeed the case upon cellular exposure to radiation) to outcompete SOD for its reaction with $O_2^{\bullet-}$.

The p$K_a$ of peroxynitrite is 6.8 at 37 °C; it is protonated in acidic solution to form the neutral peroxynitrous acid ONOOH:

$$ONOO^- + H^+ \rightleftharpoons ONOOH\ . \qquad [42]$$

For instance, at pH 6.2, ~75% of peroxynitrite will be in the protonated form. The stability and reactivity of $ONOO^-$ and ONOOH are quite different (HALLIWELL and GUTTERIDGE, 2015), and therefore, the biochemistry of peroxynitrite in biological systems is highly pH-dependent. Peroxynitrite in its protonated (acid) form is much more reactive than $ONOO^-$. Although some controversy still exists as to the mode of action of peroxynitrous acid (KOPPENOL et al., 2012; RADI, 2013), it has been proposed that peroxynitrite in its protonated (acid) form spontaneously decomposes to two potent one-electron oxidants, nitrogen dioxide ($^{\bullet}NO_2$) and an extremely reactive species with hydroxyl-radical-like properties, each capable of oxidizing a large variety of biological macromolecules (for example, see: CROW and BECKMAN, 1996). In contrast, peroxynitrite in its anionic form is stable enough to diffuse several cell diameters to reach critical cellular targets before becoming protonated and decomposing.

### *6.1.3 Activity of enzymes*

Enzymes are protein-based substances which serve as *catalysts* in living organisms, meaning they significantly speed up the rates at which reactants interact to form products in chemical reactions, while not being consumed in the reactions (STRAYER, 1995). As all catalysts, they bring reactants (that biochemists also call “substrates”) together in an optimal orientation so as to decrease the “activation energy (or barrier)” of the reaction

(*i.e.*, the energy that reacting molecules need to have when they collide to break/make the first chemical bonds and get the reaction going).[16] In other words, the combination of substrate and enzyme creates a new reaction pathway whose activation barrier is lower than that of the uncatalyzed reaction.

Enzymes are usually highly selective, catalyzing specific reactions only. This specificity is due mainly to the shapes of the enzyme molecules. The recognition of substrates by enzymes, and consequently the formation of an enzyme-substrate complex, is a dynamic process during which molecules that do not have a sufficiently complementary shape are rejected.

Each enzyme shows its optimal activity under certain experimental conditions. For instance, the intra- and intermolecular bonds that hold proteins in their structures are disrupted by changes in pH. This affects shapes and so the catalytic activity of an enzyme is pH sensitive. Most enzymes are active only within a narrow pH range, usually between 5 and 9. Figure 6.1 illustrates the dependence of the catalytic rate on pH, which is represented by a bell-shaped curve. As can be seen, the enzymatic activity drops sharply on either side of the optimal pH.

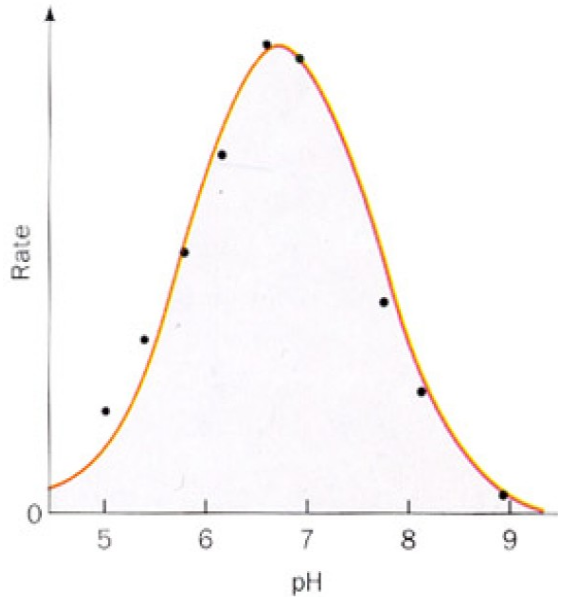


Figure 6.1 Effect of pH on the activity of enzymes (PARK and ZIPP, 2000).

[16] If this required activation energy is high, the reaction can be slow or may not occur at all.

### *6.1.4 Loss of bases (DNA abasic sites by hydrolytic, acid-catalyzed N-C bond cleavage)*

The loss of purines or pyrimidines[17] by hydrolytic cleavage of the base-sugar (N-C glycosidic) bond in DNA is acid catalyzed and thus increases at low pH. In the reaction mechanism, the depurination is promoted by the protonation of the purine base, thus, weakening the N-C glycosidic bond and increasing the leaving ability of the base (Figure 6.2). Acid-catalyzed depyrimidination also proceeds in a similar mechanism as depurination (SHEPPARD et al., 2000; von SONNTAG, 2006; GATES, 2009).

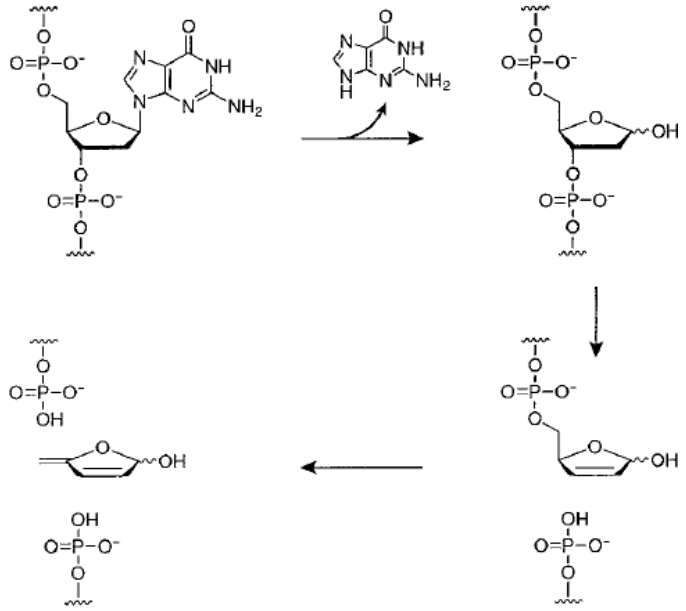

Figure 6.2 N-C bond cleavage leads to base release in acidic pH (guanine is taken here as an example). Acid-catalyzed hydrolysis at the C1' position of the N-glycosidic bond of deoxyguanosine results in release of guanine and formation of an AP site (**1**). This abasic site can lead to DNA single strand scission by β-elimination of the adjacent 3' phosphate residue (**2**). The subsequent elimination of the phosphate on the 5'-side of the abasic site is slow under physiological conditions, but occurs readily under alkaline conditions. From SHEPPARD et al. (2000), with permission.

[17] In DNA, there are four different nucleobases, the pyrimidines thymine (Thy) and cytosine (Cyt), and the purines guanine (Gua) and adenine (Ade). As the word suggests, an *abasic site* lacks the nucleobase. Abasic sites are also known as AP (for apurinic and apyrimidinic) sites.

Abasic sites are common DNA lesions. Under physiological conditions, it has been estimated that about $10^4$ purines (this number could even be an order of magnitude higher) and 500 pyrimidines are lost from DNA in a typical mammalian cell each day (NAKAMURA and SWENBERG, 1999). These observations are consistent with studies showing that the purine N-glycosidic bond is more stable than the pyrimidine N-glycosidic bond.

If unrepaired efficiently, abasic sites arising from depurination/depyridimination can inhibit DNA replication and transcription and contribute to cytotoxicity or mutagenesis (DEMPLE and HARRISON, 1994). Indeed, a DNA strand with one or more abasic sites makes a poor template because it lacks the information required to direct accurate replication and transcription. Moreover, abasic sites can generate DNA single strand-cleavage reactions via β-elimination of the phosphate residue on the 3'-side of the abasic site position (Figure 6.2) (MINKO et al., 2016). The biological consequences induced by DNA single-strand breaks have received a lot of attention and are well documented in the literature (for example, see: CHADWICK and LEENHOUTS, 1981; von SONNTAG, 2006).

### 6.2 Comparison of our results with liquid electron microscopy simulations

Liquid cell electron microscopy enables direct *in situ* imaging of processes in liquids and objects suspended in liquids with nanoscale resolution. However, the irradiating electrons affect the chemistry of the suspending medium, typically an aqueous solution, producing molecular and radical products such as hydrogen, oxygen, and hydrated (solvated) electrons. Ionizing radiation (photons, γ-rays, neutrons, electrons, etc.) readily transfers energy to the irradiated medium with effects that are relatively independent of the type of radiation. This energy excites and dislodges orbital electrons, which results in the generation of heat and radical and molecular species. In liquid cell electron microscopy experiments, beam-induced temperature changes are usually insignificant. Under typical operating conditions, energy transfer from the electron beam to water increases the water temperature by, at most, a few °C (GROGAN et al., 2014). In contrast, the radiation-induced chemical reactions lead to significant changes in the solution composition. Although radiolysis has been investigated extensively due to its importance in diverse

disciplines such as medicine and nuclear industry (for example, see: DRAGANIĆ and DRAGANIĆ, 1971; SPINKS and WOODS, 1990; BENSASSON et al., 1993; LAVERNE, 2004; ELLIOT and BARTELS, 2009; LIN and KATSUMURA, 2011), the conditions encountered during electron microscopy are vastly different. For example, the dose rate associated with a 300 keV electron beam of 1 μm radius and 1 nA current is $7.5 \times 10^7$ Gy/s, which is 7 orders of magnitude greater than the typical dose rate (~1 Gy/s) generated by common radiation sources (SCHNEIDER et al., 2014). Hence, much of the data available in the literature is not directly applicable to the conditions prevailing in the electron microscope.

Recently, SCHNEIDER et al. (2014) have utilized a kinetic model for water radiolysis and applied it to the high dose rate regime encountered during liquid cell electron microscopy. These authors calculated the concentrations of radiolysis products as functions of electron beam irradiation parameters, time, space, and solution composition, under conditions typical for electron microscopy. Their work explained qualitatively several phenomena observed during liquid cell imaging such as bubble nucleation and growth, precipitation of cations from solution, the dissolution of metals and the aggregation of colloids.

Since the radiolysis products include $H_3O^+$ ions, electron beam irradiation alters the solution's pH. Figure 6.3 shows the steady state pH of the irradiated volume as a function of dose rate for pure, deaerated water with pre-irradiation pH = 7 (SCHNEIDER et al., 2014). When the dose rate is low ($<10^3$ Gy/s), the pH of the solution is nearly unaffected by irradiation and is independent of the dose rate. For higher dose rates, the pH of the irradiated solution decreases from 7 to ~3.25.

In the Monte Carlo track chemistry simulations presented above, we studied the low-LET radiolysis of liquid water at room temperature with the aim of calculating the pH that prevails in independent (spherical) spurs as they develop in time (say, before a microsecond) (KANIKE et al., 2015*a*,*b*). We found, for times shorter than ~1 ns, a nearly constant, very acidic intra-spur pH, equal to about 3.3. As it turns out, these results compare very well with the model predictions of SCHNEIDER et al. (2014) that reveal the steady state pH value of ~3.25 for a solution irradiated with very high dose rates of radiation (see Figure 6.3). A plausible hypothesis that could explain this quantitative

agreement is that, at these high intensities, there is significant early overlap of the spurs of the irradiating electron tracks[18] so that the irradiated solution, as a whole, can roughly be viewed as a single, very large spur where homogeneity of all species is approached. Under these conditions, our pH = 3.3 value obtained at early time for an isolated spur should indeed correspond to a limiting value for the steady state pH of the solution calculated by SCHNEIDER et al. (2014) at very high dose rates.

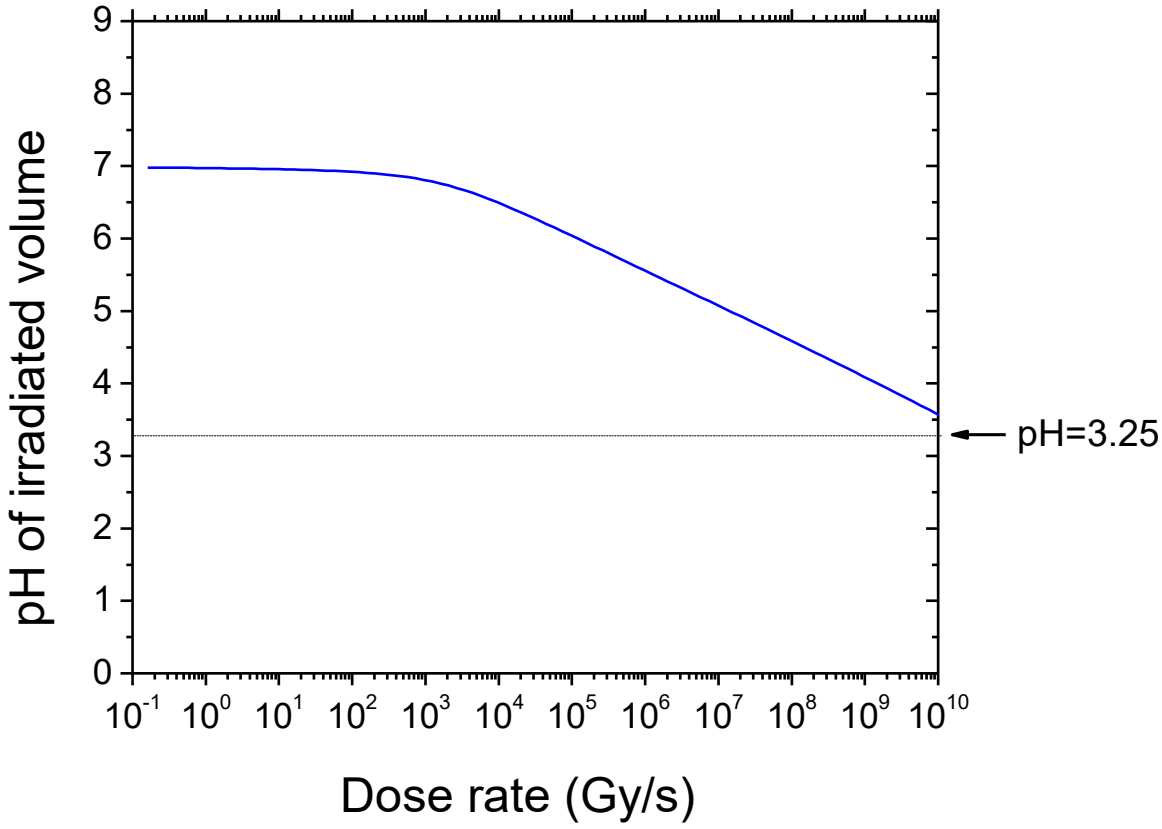


Figure 6.3 Steady state pH of pure, deaerated water irradiated by a 300-keV electron beam as a function of dose rate (in Gy/s). The pH of the irradiated solution decreases from the initial pre-irradiation value of 7 to a value approaching pH = 3.25 at the highest dose rates used in liquid cell electron microscopy experiments. From SCHNEIDER et al. (2014), with permission, and private communication.

[18] In other words, the distribution function for nearest-neighbor interspur distances at the time of spur formation contains a large fraction of near-zero distances.

### 6.3 Application to radiotherapy: Conventional, FLASH and filamentation irradiations

Radiation therapy, or radiotherapy, uses controlled high-energy radiation to shrink tumors and kill cancer cells. Briefly, radiation works by damaging the DNA inside cells making them stop dividing or die. Abnormal cancer cells are more sensitive to radiation because they divide more quickly than normal cells. Normal healthy cells can also be damaged by radiation, but they can have more efficient repair, depends on type of damage. The goal of radiotherapy is to eradicate tumors while sparing normal tissues (for example, see: HALL and GIACCIA, 2006; TUBIANA, 2008; LAWRENCE et al., 2008).

The effects of radiation are not immediate. Typically, more aggressive tumors, whose cells divide rapidly, respond more quickly to radiation. Benign tumors, whose cells divide slowly, may take several months to a year to show an effect. Radiation may be used alone or in combination with other treatments such as surgery, chemotherapy or immunotherapy. Conventional, or fractionated, radiotherapy is a form of external beam radiation that delivers a fraction of the complete radiation dose over many sessions to shrink or destroy tumors. Dividing a dose into a number of fractions allows, in most cases, better tumor control for a given level of normal tissue toxicity than a single large dose. However, whatever the type of cancer being treated, radiation-induced damage to the surrounding healthy tissues is a major problem, which can cause long-term complications (fibrosis, radiation-induced cancers, etc.) and limits the amount of radiation that can be safely delivered to the tumor.

Recently, FAVAUDON et al. (2014, 2015) have proposed a new radiation methodology, called FLASH, in which the dose is delivered in short ($\leq$ 500 ms) pulses of 4.5-MeV electrons at ultrahigh dose rate ($\sim 10^6$ Gy/s per pulse with a mean dose rate $\geq$ 40 Gy/s) and which causes less damage to the healthy tissues than continuous, conventional dose-rate ($\leq$ 0.03 Gy/s, CONV) radiotherapy at the same total dose. These authors investigated the model of lung fibrogenesis in C57BL/6J mice exposed either to FLASH or to CONV irradiation. They demonstrated that FLASH irradiation was as efficient as CONV in the regression of tumor growth, but the results showed a complete lack of acute pneumonitis and late lung fibrosis at doses known to trigger the development of pulmonary fibrosis in 100% of animals after CONV irradiation. Moreover, FLASH irradiation was

shown to spare vascular and bronchial normal smooth muscle and epithelial cells from radiation-induced acute apoptosis. Cutaneous lesions were also reduced in severity. Based on these observations, the authors suggested that FLASH radiotherapy might be a viable option for treating lung tumors, although this will need to be confirmed in human patients.

The cellular and molecular mechanisms underlying the differential response between normal and tumor tissues to FLASH versus CONV irradiation have not yet been determined. FAVAUDON et al. (2014, 2015) suggested, however, that one possible working hypothesis to explain this differential effect is that the pattern of DNA damage to target cells by FLASH is different from the one resulting from CONV irradiation (PONETTE et al., 2000; FERNET et al., 2000).

Conventional radiation sources (γ or X rays, electrons) used for decades in cancer radiotherapy inevitably deposit the majority of their dose in front or behind the tumor, thus damaging healthy tissue and causing secondary cancers years after treatment or promoting invasion and migration of cancer cells. MEESAT et al. (2012) have developed a novel irradiation method based on a nonlinear photonic process, called "filamentation" (CHIN et al., 2005; COUAIRON and MYSYROWICZ, 2007), which can, not only solve the problem of the undesirable dose distribution upon tissue entry, but also deposit a very large dose at unprecedented microscopic dose rates (up to $5 \times 10^{11}$ Gy/s) deep inside an adjustable, well-controlled macroscopic volume. Briefly, this method is related to the self-focusing of an intense infrared (IR) laser pulse, induced by the Kerr effect, yielding a self-regulated generation of spatially homogeneous low-density plasma spots along the laser-beam propagation axis. This plasma makes it possible to produce a high rate of ionizations ($\sim 10^{18}$ electrons/cm$^3$) in the heart of such filaments. These ionizing properties of laser-induced filamentation thus give rise to changes in the medium that are equivalent to conventional therapeutic ionizing radiation.

To test the therapeutic curative potential of this high-power fs IR laser pulse irradiation technique, MEESAT et al. (2012) studied its effects on a well-known and validated subcutaneous animal tumor model. Tumors were grown in female Balb/c mice by subcutaneous injection of mouse mammary carcinoma cells (MC7-L1) in both legs, irradiating only one. Three weeks after laser irradiation, in one out of three cases the tumor (6-8 mm diameter) was completely eradicated while in the other cases tumor involution

was clearly observed in the treated leg. The authors explained their results by hypothesizing a massive necrosis triggered by the laser-induced local plasma, followed by the release of a cascade of cytokines and other inflammatory mediators.

Acidic pH is toxic to many cells, including tumors. Indeed, cells whether cancerous or normal can only live and reproduce (undergo mitosis) in a (median) pH range of between 6.5 and 7.5 (for example, see: WIKE-HOOLEY et al., 1984; TANNOCK and ROTIN, 1989; LAN et al., 2007). In light of the present study, we may wonder, rather provocatively, whether the radiation-induced, early-time generation of strongly acidic regions, which extend over spatial dimensions of the order of tens of nanometers,[19] has any noticeable contribution to the initial events that lead to cell damage, enhanced lethality, bystander responses, or genomic instability in progeny of irradiated cells and their neighbouring bystanders (KANIKE et al., 2015*a*,*b*).

Moreover, when combined with the steady-state pH predictions of SCHNEIDER et al. (2014) at very high dose rates (see Figure 6.3), our study prompts important questions as to the possible influence of a strong acidic environment in the clinical outcome of tumor therapy in reference to the three radiotherapy methodologies described above in which the dose is given under different dose-rate irradiation conditions (CONV, FLASH, and laser-induced filamentation). According to Figure 6.3, for a CONV irradiation ($\leq$ 0.03 Gy/s) the steady state pH of the solution is about 7 and is independent of the dose rate. In sharp contrast, for FLASH (~$10^6$ Gy/s) and filamentation ($5 \times 10^{11}$ Gy/s) irradiations, the pH values are about 5.5 and 3, respectively, assuming an initial pre-irradiation pH value of 7. In the two latter cases, the steady state of the irradiated volume is clearly strongly acidic, and it may be hypothezised that those conditions potentially have major toxic effects against tumors.

Based on the above results, it is suggested that radiotherapy would greatly benefit of using pulsed radiation machines capable of delivering short pulses of radiation with a very high dose per pulse. Under these conditions, tumor cells would be submitted not only to the effect of the radiation itself but also to a highly acidic environment, which would both act

[19] For the sake of comparison, recall here that the diameter of the DNA (B conformation) is 2 nm, *i.e.*, much small than a "native" spur radius (~11.7 nm) (MEESUNGNOEN and JAY-GERIN, 2005*a*).

in synergy and perhaps also with less long-term complications of conventional, low-dose rate radiotherapy.

# 7 - CONCLUSION

In our work, Monte Carlo track chemistry simulations have been used in an attempt to quantify the "acid-spike" effect that is generated in spur/tracks of the radiolysis of pure, deaerated water during and shortly after irradiation. Two different track models were considered, depending on the quality (LET) of the radiation: an isolated "spherical" spur model and a "cylindrical" track model. The magnitude and duration of the observed transient acid pH response were found to be very sensitive functions of the LET. For instance, at 25 °C, in isolated spurs, the acid-spike effect was greatest for times shorter than ~1 ns, the pH being nearly constant and equal to ~3.3. For cylindrical tracks, however, the acid-spike response to the ionizing radiation was far more intense than that for the spherical spur geometry. Indeed, on a time scale of ~100 ps, the pH was found to be ~0.5 for the three high-LET radiation tracks considered. At longer times, the pH increased gradually in all cases, ultimately reaching a value of 7 (neutral pH) at ~1 μs for the spherical geometry and ~0.1 ms for the cylindrical geometry.

Our work was next extended to examine the effect of temperature, ranging from 25 to 350 °C, on the *in situ* formation of $H_3O^+$ ions and the corresponding abrupt transient acid-spike response that is observed after irradiation. The results were obtained for an isolated spherical spur model, associated with low-LET radiation and under conditions of low dose-rates. At elevated temperatures, the acid-spike response was far more intense but of a shorter duration. For instance, at 350 °C, the pH was ~1.7 at times less than ~10 ps. At longer times, the pH increased gradually for all temperatures considered, ultimately reaching a constant value corresponding to the non-radiolytic, pre-irradiation concentration of $H_3O^+$ arising through water's autoprotolysis at ~1-10 μs following irradiation.

The transient acid pH effect that we have described does not appear to have been explored in water or in a cellular environment subject to the action of ionizing radiation, especially high-LET radiation, either at ambient or at elevated temperatures. In this regard, our work raises a number of questions about the potential implications of this effect for radiobiology or for water-cooled nuclear reactors, some of which have been briefly evoked.

Finally, our work suggests that radiotherapy would greatly benefit of using machines that deliver short pulses of radiation at very high dose rate (say, $>10^3$ Gy/s).

Under these conditions, tumor cells would be submitted not only to the effect of the radiation itself but also to a strong acidic environment, which would both act in synergy and perhaps also with less long-term complications of conventional, low-dose rate radiotherapy.

# ACKNOWLEDGMENTS

I would like to thank the Department of Nuclear Medicine and Radiobiology, Faculty of Medicine and Health Sciences, Université de Sherbrooke.

I would like to thank Prof. Jean-Paul Jay-Gerin, my supervisor, for the opportunity he gave me to join his group, his advices, numerous discussions, encouragement, and offering me a scholarship from his research funding (NSERC).

I also thank the members of my jury, Prof. Richard Wagner and Prof. Klaus Klarskov, for their insight and suggestions.

I would like to thank Prof. Benoit Paquette, Dr. Tithitip Tippayamontri and Dr. Guru S Madugundu, for their proposals and providing linked references on my research work.

I appreciated the help and support of my lab members Dr. Jintana Meesungnoen, Sunuchakan Sanguanmith, Shayla Mustaree and, more recently, Muhammad Mainul Islam.

I am grateful to Prof. Edouard I. Azzam (New Jersey Medical School Cancer Center) and Prof. Yusa Muroya (Osaka University, Japan) for valuable comments at various stages of this work. Special thanks go also to Dr. Nicholas M. Schneider (University of Pennsylvania) and Dr. Frances M. Ross (IBM T.J. Watson Research Center) for providing us with their Monte Carlo simulation data of the steady state pH of irradiated water as a function of dose rate, shown in Fig. 6.3.

Finally, I would like to extend my deepest gratitude to my husband, Dr. Guru S Madugundu and our two cheerful children, Sanjay Kumar and Mahidhar, I would like to offer my appreciation of the love and support they have given me through my master's career.

# REFERENCES

ALLEN, A.O., 1948. Radiation chemistry of aqueous solutions. J. Phys. Colloid Chem. **52**, 479-490.

ALLEN, A.O., 1961. The Radiation Chemistry of Water and Aqueous Solutions. D. Van Nostrand Co., Princeton, NJ.

AMICHAI, O. and TREININ, A. 1969. Chemical reactivity of O($^3P$) atoms in aqueous solution. Chem. Phys. Lett. **3**, 611-613.

ANBAR, M. and THOMAS, J.K., 1964. Pulse radiolysis studies of aqueous sodium chloride solutions. J. Phys. Chem. **68**, 3829-3835.

AUTSAVAPROMPORN, N., 2006. The effects of pH and radiation quality (LET) on the radiolysis of liquid water and aqueous solutions: A study by using Monte Carlo simulations. M.Sc. Thesis, Burapha University, Bangsaen (Thailand).

AUTSAVAPROMPORN, N., MEESUNGNOEN, J., PLANTE, I., and JAY-GERIN, J.-P., 2007. Monte Carlo simulation study of the effects of acidity and LET on the primary free-radical and molecular yields of water radiolysis. Application to the Fricke dosimeter. Can. J. Chem. **85**, 214-229.

AUTSAVAPROMPORN, N., de TOLEDO, S.M., LITTLE, J.B., JAY-GERIN, J.-P., HARRIS, A.L., and AZZAM, E.I., 2011. The role of gap junction communication and oxidative stress in the propagation of toxic effects among high-dose α-particle-irradiated human cells. Radiat. Res. **175**, 347-357.

AZZAM, E.I., de TOLEDO, S.M., and LITTLE, J.B., 2003. Oxidative metabolism, gap junctions and the ionizing radiation-induced bystander effect. Oncogene **22**, 7050-7057.

AZZAM, E.I., JAY-GERIN, J.-P., and PAIN, D., 2012. Ionizing radiation-induced metabolic oxidative stress and prolonged cell injury. Cancer Lett. **327**, 48-60.

BALDACCHINO, G., DE WAELE, V., MONARD, H., SORGUES, S., GOBERT, F., LARBRE, J.P., VIGNERON, G., MARIGNIER, J.-L., POMMERET, S., and

MOSTAFAVI, M., 2006. Hydrated electron decay measurements with picosecond pulse radiolysis at elevated temperatures up to 350 °C. Chem. Phys. Lett. **424**, 77-81.

BALLARINI, F., BIAGGI, M., MERZAGORA, M., OTTOLENGHI, A., DINGFELDER, M., FRIEDLAND, W., JACOB, P., and PARETZKE, H.G., 2000. Stochastic aspects and uncertainties in the prechemical and chemical stages of electron tracks in liquid water: A quantitative analysis based on Monte Carlo simulations. Radiat. Environ. Biophys. **39**, 179-188.

BANDURA, A.V. and LVOV, S.N., 2006. The ionization constant of water over wide ranges of temperature and density. J. Phys. Chem. Ref. Data **35**, 15-30.

BARTELS, D.M., 2009. Comment on the possible role of the reaction $H + H_2O \rightarrow H_2 + OH$ in the radiolysis of water at high temperatures. Radiat. Phys. Chem. **78**, 191-194.

BARTELS, D.M., HENSHAW, J. and SIMS, H.E., 2013. Modeling the critical hydrogen concentration in the AECL test reactor. Radiat. Phys. Chem. **82**, 16-24.

BECKER, D. and SEVILLA, M.D., 1993. The chemical consequences of radiation damage to DNA. Adv. Radiat. Biol. **17**, 121-180.

BECKER, D., ADHIKARY, A., and SEVILLA, M.D., 2011. Physicochemical mechanisms of radiation-induced DNA damage. In: Charged Particle and Photon Interactions with Matter. Recent Advances, Applications, and Interfaces (Hatano, Y., Katsumura, Y., and Mozumder, A., Eds.), pp. 503-541. Taylor and Francis Group, Boca Raton, FL.

BĚGUSOVÁ, M. and PIMBLOTT, S.M., 2002. Stochastic simulation of γ radiolysis of acidic ferrous sulfate solution at elevated temperatures. Radiat. Prot. Dosim. **99**, 73-76.

BENSASSON, R.V., LAND, E.J., and TRUSCOTT, T.G., 1993. Excited States and Free Radicals in Biology and Medicine. Contributions from Flash Photolysis and Pulse Radiolysis. Oxford University Press, Oxford.

BERNHARD, W.A. and CLOSE, D.M., 2004. DNA damage dictates the biological consequences of ionizing irradiation: The chemical pathways. In: Charged Particle and Photon Interactions with Matter: Chemical, Physicochemical, and Biological

Consequences with Applications (Mozumder, A. and Hatano, Y., Eds.), pp. 431-470. Marcel Dekker, New York.

BERNAS, A., FERRADINI, C., and JAY-GERIN, J.-P., 1997. On the electronic structure of liquid water: Facts and reflections. Chem. Phys. **222**, 151-160.

BETHE, H., 1930. Zur Theorie des Durchgangs schneller Korpuskularstrahlen durch Materie. Ann. Physik **397**, 325-400.

BETHE, H.A. and ASHKIN, J., 1953. Passage of radiations through matter. In: Experimental Nuclear Physics (Segrè, E., Ed.), Vol. 1, pp. 166-357. Wiley, New York.

BIEDENKAPP, D., HARTSHORN, L.G., and BAIR, E.J., 1970. The $O(^1D)$ + $H_2O$ reaction. Chem. Phys. Lett. **5**, 379-380.

BIELSKI, B.H.J., CABELLI, D.E., ARUDI, R.L., and ROSS, A.B., 1985. Reactivity of $HO_2/O_2^-$ radicals in aqueous solution. J. Phys. Chem. Ref. Data **14**, 1041-1100.

BURNS, W.G. and MARSH, W.R., 1981. Radiation chemistry of high-temperature (300-410 °C) water. Part 1. Reducing products from gamma radiolysis. J. Chem. Soc., Faraday Trans. 1 77, 197-215.

BURTON, M., 1969. Radiation chemistry: A godfatherly look at its history and its relation to liquids. Chem. Eng. News **47**, 86-96.

BUTARBUTAR, S.L., SANGUANMITH, S., MEESUNGNOEN, J., SUNARYO, G.R., and JAY-GERIN, J.-P., 2014. Calculation of the yields for the primary species formed from the radiolysis of liquid water by fast neutrons at temperatures between 25-350 °C. Radiat. Res. **181**, 659-665.

BUTARBUTAR, S.L., SUNARYO, G.R., MEESUNGNOEN, J., and JAY-GERIN, J.-P., 2016. Temperature dependence of the primary species yields of liquid water radiolysis by 0.8-MeV fast neutrons. Atom Indonesia **42**, 13-18.

BUXTON, G.V., 1987. Radiation chemistry of the liquid state: (1) Water and homogeneous aqueous solutions. In: Radiation Chemistry. Principles and Applications (Farhataziz and Rodgers, M.A.J., Eds.), pp. 321-349. VCH Publishers, New York.

CADET, J., BERGER, M., DOUKI, T., and RAVANAT, J.L., 1997. Oxidative damage to DNA: formation, measurement, and biological significance. Rev. Physiol. Biochem. Pharmacol. **131**, 1-87.

CADET, J., DOUKI, T., GASPARUTTO, D., RAVANAT, J.-L., and WAGNER, J.R., 2012. Oxidatively generated nucleobase modifications in isolated and cellular DNA. In: Encyclopedia of Radicals in Chemistry, Biology, and Materials (Chatgilialoglu, C. and Studer, A., Eds.), p. 1319-1344. Wiley, Chichester, UK.

CHADWICK, K.H. and LEENHOUTS, H.P., 1981. The Molecular Theory of Radiation Biology. Springer-Verlag, Berlin.

CHATTERJEE, A. and HOLLEY, W.R., 1993. Computer simulation of initial events in the biochemical mechanisms of DNA damage. Adv. Radiat. Biol. **17**, 181-226.

CHATTERJEE, A. and SCHAEFER, H.J., 1976. Microdosimetric structure of heavy ion tracks in tissue. Radiat. Environ. Biophys. **13**, 215-227.

CHIN, S.L., HOSSEINI, S.A., LIU, W., LUO, Q., THÉBERGE, F., AKÖZBEK, N., BECKER, A., KANDIDOV, V.P., KOSAREVA, O.G., and SCHROEDER, H., 2005. The propagation of powerful femtosecond laser pulses in optical media: Physics, applications, and new challenges. Can. J. Phys. **83**, 863-905.

CHRISTENSEN, H., 2006. Fundamental aspects of water coolant radiolysis. SKI Report 2006:16. Swedish Nuclear Power Inspectorate, Stockholm, Sweden.

CLIFFORD, P., GREEN, N.J.B., OLDFIELD, M.J., PILLING, M.J., and PIMBLOTT, S.M., 1986. Stochastic models of multi-species kinetics in radiation-induced spurs. J. Chem. Soc. Faraday Trans. 1, **82**, 2673-2689.

COBUT, V., 1993. Simulation Monte Carlo du transport d'électrons non relativistes dans l'eau liquide pure et de l'évolution du milieu irradié: rendements des espèces créées de $10^{-15}$ à $10^{-7}$ s. Ph.D. Thesis, Université de Sherbrooke, Sherbrooke, Québec, Canada.

COBUT, V., FRONGILLO, Y., JAY-GERIN, J.-P., and PATAU, J.P., 1994. Calcul des rendements des produits de la radiolyse de l'eau en fonction du temps par une méthode Monte Carlo. J. Chim. Phys. **91**, 1018-1024.

COBUT, V., JAY-GERIN, J.-P., FRONGILLO, Y., and PATAU, J.P., 1996. On the dissociative electron attachment as a potential source of molecular hydrogen in irradiated liquid water. Radiat. Phys. Chem. **47**, 247-250.

COBUT, V., FRONGILLO, Y., PATAU, J.P., GOULET, T., FRASER, M.-J., and JAY-GERIN, J.-P., 1998. Monte Carlo simulation of fast electron and proton tracks in liquid water. I. Physical and physicochemical aspects. Radiat. Phys. Chem. **51**, 229-243.

COHEN, P., 1980. Water Coolant Technology of Power Reactors. American Nuclear Society, La Grange Park, Illinois.

COLLINSON, E., DAINTON, F.S., SMITH, D.R., and TAZUKÉ, S., 1962. Evidence for the unit negative charge on the "hydrogen atom" formed by the action of ionising radiation on aqueous systems. Proc. Chem. Soc. 140-141.

COOK, W.G. and LISTER, D.H., 2014. Chemistry in CANDU process systems. In: The Essential CANDU (Garland, W.J., Ed.), Chapter 15. University Network of Excellence in Nuclear Engineering (UNENE), Hamilton, Ontario, Canada. ISBN 0-9730040.

COUAIRON, A. and MYSYROWICZ, A., 2007. Femtosecond filamentation in transparent media. Phys. Rep. **441**, 47-189.

CROW, J.P. and BECKMAN, J.S., 1996. The importance of superoxide in nitric oxide-dependent toxicity. Evidence for peroxynitrite-mediated injury. In: Biological Reactive Intermediates V. Basic Mechanistic Research in Toxicology and Human Risk Assessment (Snyder, R., Kocsir, J.J., Sipes, I.G., Kalf, G.F., Jollow, D.J., Greim, H., Monks, T.J., and Witmer, C.M., Eds.), pp. 147-161. Springer Science, New York.

CZAPSKI, G. and SCHWARZ, H.A., 1962. The nature of the reducing radical in water radiolysis. J. Phys. Chem. **66**, 471-474.

DEAN, J.A., 1987. Handbook of Organic Chemistry. McGraw-Hill, New York.

DE GREY, A.D.N.J., 2002. $HO_2^{\bullet}$: The forgotten radical. DNA Cell Biol. **21**, 251-257.

DEMPLE, B. and HARRISON, L., 1994. Repair of oxidative damage to DNA: Enzymology and biology. Annu. Rev. Biochem. **63**, 915-948.

DINGFELDER, M., INOKUTI, M., and PARETZKE, H.G., 2000. Inelastic-collision cross sections of liquid water for interactions of energetic protons. Radiat. Phys. Chem. **59**, 255-275.

DINGFELDER, M. and FRIEDLAND, W., 2001. Basic data for track structure simulations: Electron interaction cross-sections in liquid water. In: Advanced Monte Carlo for Radiation Physics, Particle Transport Simulation and Applications (Kling, A., Barão, F.J.C., Nakagawa, M., Távora, L., and Vaz, P., Eds.), pp. 267-272. Springer-Verlag, Berlin.

DINGFELDER, M., RITCHIE, R.H., TURNER, J.E., FRIEDLAND, W., PARETZKE, H.G., and HAMM, R.N., 2008. Comparisons of calculations with PARTRAC and NOREC: Transport of electrons in liquid water. Radiat. Res. **169**, 584-594.

DRAGANIĆ, I.G. and DRAGANIĆ, Z.D., 1971. The Radiation Chemistry of Water. Academic Press, New York.

ELLIOT, A.J. and McCRACKEN, D.R., 1990. Computer modelling of the radiolysis in an aqueous lithium salt blanket: Suppression of radiolysis by addition of hydrogen. Fusion Eng. Design **13**, 21-27.

ELLIOT, A.J., McCRACKEN, D.R., BUXTON, G.V., and WOOD, N.D., 1990. Estimation of rate constants for near-diffusion-controlled reactions in water at high temperatures. J. Chem. Soc. Faraday Trans. **86**, 1539-1547.

ELLIOT, A.J., CHENIER, M.P., and OUELLETTE, D.C., 1993. Temperature dependence of $g$ values for $H_2O$ and $D_2O$ irradiated with low linear energy transfer radiation. J. Chem. Soc. Faraday Trans. **89**, 1193-1197.

ELLIOT, A.J., 1994. Rate constants and $g$-values for the simulation of the radiolysis of light water over the range 0-300 °C. Report AECL-11073. Atomic Energy of Canada Limited, Chalk River, Ontario, Canada.

ELLIOT, A.J., OUELLETTE, D.C., and STUART, C.R., 1996. The temperature dependence of the rate constants and yields for the simulation of the radiolysis of

heavy water. Report AECL-11658. Atomic Energy of Canada Limited, Chalk River, Ontario, Canada.

ELLIOT, A.J. and BARTELS, D.M., 2009. The reaction set, rate constants and *g*-values for the simulation of the radiolysis of light water over the range 20° to 350 °C based on information available in 2008. Report AECL No. 153-127160-450-001. Atomic Energy of Canada Limited, Chalk River, Ontario, Canada.

FARAGGI, M. and DÉSALOS, J., 1969. Effect of positively charged ions on the "molecular" hydrogen yield in the radiolysis of aqueous solutions. Int. J. Radiat. Phys. Chem. **1**, 335-344.

FAVAUDON, V., CAPLIER, L., MONCEAU, V., POUZOULET, F., SAYARATH, M., FOUILLADE, C., POUPON, M.-F., BRITO, I., HUPÉ, Ph., BOURHIS, J., HALL, J., FONTAINE, J.-J., and VOZENIN, M.-C., 2014. Ultrahigh dose-rate FLASH irradiation increases the differential response between normal and tumor tissue in mice. Sci. Transl. Med. **6**, 245ra93.

FAVAUDON, V., FOUILLADE, C., and VOZENIN, M.-C., 2015. La radiothérapie FLASH pour épargner les tissus sains. Médecine/Sciences **31**, 121-123.

FERNET, M., PONETTE, V., DENIAUD-ALEXANDRE, E., MÉNISSIER-DE MURCIA, J., DE MURCIA, G., GIOCANTI, N., MEGNIN-CHANET, F., and FAVAUDON, V., 2000. Poly(ADP-ribose) polymerase, a major determinant of early cell response to ionizing radiation. Int. J. Radiat. Biol. **76**, 1621-1629.

FÉRON, D. and OLIVE, J.-M. (Eds.), 2007. Corrosion Issues in Light Water Reactors. Stress Corrosion Cracking. Woodhead Publishing Ltd., Cambridge, UK.

FERRADINI, C., 1979. Actions chimiques des radiations ionisantes. J. Chim. Phys. **76**, 636-644.

FERRADINI, C., 1990. Aspect hétérogène des phénomènes radiolytiques. In: Actions Biologique et Chimique des Radiations, Vol. 1, pp. 52-63. Éditions Ciaco, Bruxelles.

FERRADINI and PUCHEAULT, 1983. Biologie de l'action des rayonnements ionisants. Masson, Paris.

FERRADINI, C. and JAY-GERIN, J.-P., 1999. La radiolyse de l'eau et des solutions aqueuses: historique et actualité. Can. J. Chem. **77**, 1542-1575.

FERRADINI, C. and JAY-GERIN, J.-P., 2000. The effect of pH on water radiolysis: A still open question. A minireview. Res. Chem. Intermed. **26**, 549-565.

FRONGILLO, Y., FRASER, M.-J., COBUT, V., GOULET, T., JAY-GERIN, J.-P., and PATAU, J.P., 1996. Évolution des espèces produites par le ralentissement de protons rapides dans l'eau liquide : simulation fondée sur l'approximation des temps de réaction indépendants. J. Chim. Phys. **93**, 93-102.

FRONGILLO, Y., GOULET, T., FRASER, M.-J., COBUT, V., PATAU, J.P., and JAY-GERIN, J.-P., 1998. Monte Carlo simulation of fast electron and proton tracks in liquid water. II. Nonhomogeneous chemistry. Radiat. Phys. Chem. **51**, 245-254.

GATES, K.S., 2009. An overview of chemical processes that damage cellular DNA: Spontaneous hydrolysis, alkylation, and reactions with radicals. Chem. Res. Toxicol. **22**, 1747-1760.

GOULET, T. and JAY-GERIN, J.-P., 1989. Thermalization of subexcitation electrons in solid water. Radiat. Res. **118**, 46-62.

GOULET, T. and JAY-GERIN, J.-P., 1992. On the reactions of hydrated electrons with $^{\bullet}OH$ and $H_3O^+$. Analysis of photoionization experiments. J. Chem. Phys. **96**, 5076-5087.

GOULET, T., PATAU, J.P., and JAY-GERIN, J.-P., 1990. Influence of the parent cation on the thermalization of subexcitation electrons in solid water. J. Phys. Chem. **94**, 7312-7316.

GOULET, T., JAY-GERIN, J.-P., FRONGILLO, Y., COBUT, V., and FRASER, M.-J., 1996. Rôle des distances de thermalisation des électrons dans la radiolyse de l'eau liquide. J. Chim. Phys. **93**, 111-116.

GOULET, T., FRASER, M.-J., FRONGILLO, Y., and JAY-GERIN, J.-P., 1998. On the validity of the independent reaction times approximation for the description of the nonhomogeneous kinetics of liquid water radiolysis. Radiat. Phys. Chem. **51**, 85-91.

GREEN, N.J.B., PILLING, M.J., PIMBLOTT, S.M., and CLIFFORD, P., 1990. Stochastic modeling of fast kinetics in a radiation track. J. Phys. Chem. **94**, 251-258.

GROGAN, J.M., SCHNEIDER, N.M., ROSS, F.M., and BAU, H.H., 2014. Bubble and pattern formation in liquid induced by an electron beam. Nano Lett. **14**, 359-364.

GROSS, S.S. and WOLIN, M.S., 1995. Nitric oxide: Pathophysiological mechanisms. Annu. Rev. Physiol. **57**, 737-769.

GUZONAS, D.A., STUART, C.R., JAY-GERIN, J.-P., and MEESUNGNOEN, J., 2010. Testing requirements for SCWR radiolysis, AECL Report No. 153-127160-REPT-001, Atomic Energy of Canada Limited, Mississauga, Ontario, Canada.

GUZONAS, D., BROSSEAU, F., TREMAINE, P., MEESUGNOEN, J., and JAY-GERIN, J.-P., 2012. Water chemistry in a supercritical water-cooled pressure tube reactor. Nucl. Technol. **179**, 205-219.

HALL, E.J. and GIACCIA, A.J., 2006. Radiobiology for the Radiologist, 6th edn. Lippincott, Williams &Wilkins, Philadelphia.

HALLIWELL, B. and GUTTERIDGE, J.M.C., 2015. Free Radicals in Biology and Medicine, 5th edn. Oxford University Press, Oxford, UK.

HARRIS, D.C., 2013. Exploring Chemical Analysis, 5th edn. W.H. Freeman, New York.

HARRIS, R.E. and PIMBLOTT, S.M., 2002. On $^{3}$H β-particle and $^{60}$Co γ irradiation of aqueous systems. Radiat. Res. **158**, 493-504.

HART, E.J. and ANBAR, M., 1970. The Hydrated Electron. Wiley-Interscience, New York.

HAYNES, W.M. and LIDE, D.R. (Eds.), 2010. CRC Handbook of Chemistry and Physics, 91st edn. Taylor and Francis Group, Boca Raton, FL.

HEI, T.K., ZHOU, H., CHAI, Y., PONNAIYA, B., and IVANOV, V.N., 2011. Radiation induced non-targeted response: Mechanism and potential clinical implications. Curr. Mol. Pharmacol. **4**, 96-105.

HELLER, J.M., Jr., HAMM, R.N., BIRKHOFF, R.D., and PAINTER, L.R., 1974. Collective oscillation in liquid water. J. Chem. Phys. **60**, 3483-3486.

HERVÉ DU PENHOAT, M.-A., GOULET, T., FRONGILLO, Y., FRASER, M.-J., BERNAT, Ph., and JAY-GERIN, J.-P., 2000. Radiolysis of liquid water at temperatures up to 300 °C: A Monte Carlo simulation study. J. Phys. Chem. A **104**, 11757-11770.

HERVÉ DU PENHOAT, M.-A., MEESUNGNOEN, J., GOULET, T., FILALI- MOUHIM, A., MANKHETKORN, S., and JAY-GERIN, J.-P., 2001. Linear-energy-transfer effects on the radiolysis of liquid water at temperatures up to 300 °C. A Monte Carlo study. Chem. Phys. Lett. **341**, 135-143.

HOCHANADEL, C.J. and GHORMLEY, J.A., 1962. Effect of temperature on the decomposition of water by gamma rays. Radiat. Res. **16**, 653-660.

HUMMEL, A., 1995. Radiation Chemistry: The Chemical Effects of Ionizing Radiation and their Applications. IRI-TUD, Delft, The Netherlands.

ICRU REPORT 55, 1996. Secondary electron spectra from charged particle interactions. International Commission on Radiation Units and Mesurements, Bethesa, MD.

INOKUTI, M., 1971. Inelastic collisions of fast charged particles with atoms and molecules: The Bethe theory revisited. Rev. Mod. Phys. **43**, 297-347.

ISHIGURE, K., KATSUMURA, Y., SUNARYO, G.R., and HIROISHI, D., 1995. Radiolysis of high temperature water. Radiat. Phys. Chem. **46**, 557-560.

JANIK, D., JANIK, I., and BARTELS, D.M., 2007. Neutron and β/γ radiolysis of water up to supercritical conditions. 1. β/γ yields for $H_2$, $H^{\bullet}$ atom, and hydrated electron. J. Phys. Chem. A **111**, 7777-7786.

JAY-GERIN, J.-P. and FERRADINI, C., 2000. Are there protective enzymatic pathways to regulate high local nitric oxide ($^{\bullet}$NO) concentrations in cells under stress conditions? Biochimie **82**, 161-166.

JAY-GERIN, J.-P., LIN, M., KATSUMURA, Y., HE, H., MUROYA, Y., and MEESUNGNOEN, J., 2008. Effect of water density on the absorption maximum of hydrated electrons in sub- and supercritical water up to 400 °C. J. Chem. Phys. **129**, 114511.

JONAH, C.D., 1995. A short history of the radiation chemistry of water. Radiat. Res. **144**, 141-147.

KABAKCHI, S.A. and BUGAENKO, V.L., 1992. Mathematical modeling of radiolysis of liquid water at high temperatures. High Energy Chem. **26**, 319-323.

KANIKE, V., MEESUNGNOEN, J., and JAY-GERIN, J.-P., 2015*a*. Transient acid pH effect in tracks in the radiolysis of water: Does this effect contribute to biological damage caused by ionizing radiation? Austin J. Nucl. Med. Radiother. **2**, 1011-1016.

KANIKE, V., MEESUNGNOEN, J., and JAY-GERIN, J.-P., 2015*b*. Acid spike effect in spurs/tracks of the low/high linear energy transfer radiolysis of water: Potential implications for radiobiology. RSC Adv. **5**, 43361-43370.

KANIKE, V., MEESUNGNOEN, J., SANGUANMITH, S., GUZONAS, D.A., STUART, C.R., and JAY-GERIN, J.-P., 2016. Generation of ultrafast transient acid spikes in high-temperature water irradiated with low linear energy transfer radiation. CNL Nucl. Rev., in press.

KANJANA, K., HAYGARTH, K.S., WU, W., and BARTELS, D.M., 2013. Laboratory studies in search of the critical hydrogen concentration. Radiat. Phys. Chem. **82**, 25-34.

KAPLAN, I.G. and MITEREV, A.M., 1987. Interaction of charged particles with molecular medium and track effects in radiation chemistry. Adv. Chem. Phys. **68**, 255-386.

KARAMITROS, M., MANTERO, A., INCERTI, S., et al. (23 authors), 2011. Modeling radiation chemistry in the Geant4 toolkit. Prog. Nucl. Sci. Technol. **2**, 503-508.

KATSUMURA, Y., SUNARYO, G., HIROISHI, D., and ISHIGURE, K., 1998. Fast neutron radiolysis of water at elevated temperatures relevant to water chemistry. Prog. Nucl. Energy **32**, 113-121.

KATZ, R., 1970. RBE, LET and $z/\beta^{\alpha}$. Health Phys. **18**, 175.

KENT, M.C. and SIMS, H.E., 1992*a*. The yield of γ-radiolysis products from water at temperatures up to 300 °C. In: Proceedings of the 6$^{th}$ International Conference on

Water Chemistry of Nuclear Reactor Systems, Bournemouth, 12-15 October 1992. Vol. 2, pp. 153-160. British Nuclear Energy Society, London.

KENT, M.C. and SIMS, H.E., 1992*b*. The yield of γ-radiolysis products from water at temperatures up to 270 °C. Report AEA-RS-2302. Atomic Energy Authority, Harwell, UK.

KIMMEL, G.A., ORLANDO, T.M., VÉZINA, C., and SANCHE, L., 1994. Low-energy electron-stimulated production of molecular hydrogen from amorphous water ice. J. Chem. Phys. **101**, 3282-3286.

KOPPENOL, W.H., 1998. The basic chemistry of nitrogen monoxide and peroxynitrite. Free Radic. Biol. Med. **25**, 385-391.

KOPPENOL, W.H., BOUNDS, P.L., NAUSER, T., KISSNER, R., and RÜEGGER, H., 2012. Peroxynitrous acid: Controversy and consensus surrounding an enigmatic oxidant. Dalton Trans. **41**, 13779-13787.

KOWALD, A., 1999. The mitochondrial theory of aging: Do damaged mitochondria accumulate by delayed degradation? Exp. Gerontol. **34**, 605-612.

KREIPL, M.S., FRIEDLAND, W., and PARETZKE, H.G., 2009. Time- and space-resolved Monte Carlo study of water radiolysis for photon, electron and ion irradiation. Radiat. Environ. Biophys. **48**, 11-20.

KROH, J. (Ed.), 1989. Early Developments in Radiation Chemistry. The Royal Society of Chemistry, Cambridge, UK.

KUPPERMANN, A., 1959. Theoretical foundations of radiation chemistry. J. Chem. Educ. **36**, 279-285.

LAN, A., LAGADIC-GOSSMANN, D., LEMAIRE, C., BRENNER, C., and JAN, G., 2007. Acidic extracellular pH shifts colorectal cancer cell death from apoptosis to necrosis upon exposure to propionate and acetate, major end-products of the human probiotic propionibacteria. Apoptosis **12**, 573-591.

LAVERNE, J.A., 2000. Track effects of heavy ions in liquid water. Radiat. Res. **153**, 487-496.

LAVERNE, J.A., 2004. Radiation chemical effects of heavy ions. In: Charged Particle and Photon Interactions with Matter: Chemical, Physicochemical, and Biological Consequences with Applications (Mozumder, A. and Hatano, Y., Eds.), pp. 403-429. Marcel Dekker, New York.

LAVERNE, J.A. and MOZUMDER, A., 1993. Concerning plasmon excitation in liquid water. Radiat. Res. **133**, 282-288.

LAVERNE, J.A. and PIMBLOTT, S.M., 1993. Diffusion-kinetic modeling of the electron radiolysis of water at elevated temperatures. J. Phys. Chem. **97**, 3291-3297.

LAVERNE, J.A. and PIMBLOTT, S.M., 1995. Electron energy-loss distributions in solid, dry DNA. Radiat. Res. **141**, 208-215.

LAVERNE, J.A. and SCHULER, R.H., 1987. Track effects in radiation chemistry: Production of $HO_2^{\bullet}$ in the radiolysis of water by high-LET $^{58}Ni$ ions. J. Phys. Chem. **91**, 6560-6563.

LAWRENCE, T.S., TEN HAKEN, R.K., and GIACCIA, A., 2008. Principles of radiation oncology. In: Cancer: Principles and Practice of Oncology, 8th edn (DeVita, V.T., Jr., Lawrence, T.S., and Rosenberg, S.A., Eds.), pp. 307-336. Lippincott Williams and Wilkins, Philadelphia.

LEHNERT, S., 2008. Biomolecular Action of Ionizing Radiation. Taylor & Francis, Boca Raton, FL.

LI, J., NIE, Z., ZHENG, Y.Y., DONG, S., and LOH, Z.-H., 2013. Elementary electron and ion dynamics in ionized liquid water. J. Phys. Chem. Lett. **4**, 3698-3703.

LIN, M. and KATSUMURA, Y., 2011. Radiation chemistry of high temperature and supercritical water and alcohols. In: Charged Particle and Photon Interactions with Matter. Recent Advances, Applications, and Interfaces (Hatano, Y., Katsumura, Y., and Mozumder, A., Eds.), pp. 401-424. Taylor and Francis Group, Boca Raton, FL.

LINSTROM, P.J. and MALLARD, W.G. (Eds.), 2005. NIST Chemistry WebBook, NIST Standard Reference Database No. 69. National Institute of Standards and Technology, Gaithersburg, MD. Available from http://webbook.nist.gov

MAGEE, J.L., 1953. Radiation chemistry. Annu. Rev. Nucl. Sci. **3**, 171-192.

MAGEE, J.L. and CHATTERJEE, A., 1980. Radiation chemistry of heavy-particle tracks. 1. General considerations. J. Phys. Chem. **84**, 3529-3536.

MAGEE, J.L and CHATTERJEE, A. 1987. Track reactions of radiation chemistry. In: Kinetics of Nonhomogeneous Processes (Freeman, G.R., Ed.), pp. 171-214. Wiley, New York.

MATSUYAMA, A. and NAMIKI, M., 1965. The evidence for the formation of chlorine atoms in neutral aqueous solution containing chloride ions by ionizing radiations. Agr. Biol. Chem. **29**, 593-594.

McCRACKEN, D.R., TSANG, K.T., and LAUGHTON, P.J., 1998. Aspects of the physics and chemistry of water radiolysis by fast neutrons and fast electrons in nuclear reactors. AECL-11895 Report. Atomic Energy of Canada Limited, Chalk River, Ontario, Canada.

McDANIEL, E.W., MITCHELL, J.B.A., and RUDD, M.E., 1993. Atomic Collisions: Heavy Particle Projectiles. Wiley, New York.

MEESAT, R., SANGUANMITH, S., MEESUNGNOEN, J., LEPAGE, M., KHALIL, A., and JAY-GERIN, J.-P., 2012*a*. Utilization of the ferrous sulfate (Fricke) dosimeter for evaluating the radioprotective potential of cystamine: Experiment and Monte Carlo simulation. Radiat. Res. **177**, 813-826.

MEESAT, R., BELMOUADDINE, H., ALLARD, J.-F., TANGUAY-RENAUD, C., LEMAY, R., BRASTAVICEANU, T., TREMBLAY, L., PAQUETTE, B., WAGNER, J.R., JAY-GERIN, J.-P., LEPAGE, M., HUELS, M.A., and HOUDE, D., 2012*b*. Cancer radiotherapy based on femtosecond IR laser-beam filamentation yielding ultra-high dose rates and zero entrance dose. Proc. Natl. Acad. Sci. USA **109**, E2508-E2513.

MEESUNGNOEN, J., BENRAHMOUNE, M., FILALI-MOUHIM, A., MANKHETKORN, S., and JAY-GERIN, J.-P., 2001. Monte Carlo calculation of the primary radical and molecular yields of liquid water radiolysis in the linear energy transfer range 0.3-6.5 keV/μm: Application to $^{137}$Cs gamma rays. Radiat. Res. **155**, 269-278.

MEESUNGNOEN, J., JAY-GERIN, J.-P., FILALI-MOUHIM, A., and MANKHETKORN, S., 2002*a*. On the temperature dependence of the primary yield and the product $G\varepsilon_{max}$ of hydrated electrons in the low-LET radiolysis of liquid water. Can. J. Chem. **80**, 767-773.

MEESUNGNOEN, J., JAY-GERIN, J.-P., FILALI-MOUHIM, A., and MANKHETKORN, S., 2002*b*. Low-energy electron penetration range in liquid water. Radiat. Res. **158**, 657-660.

MEESUNGNOEN, J., FILALI-MOUHIM, A., SNITWONGSE NA AYUDHYA, N., MANKHETKORN, S., and JAY-GERIN, J.-P., 2003. Multiple ionization effects on the yields of $HO_2^{\bullet}/O_2^{\bullet-}$ and $H_2O_2$ produced in the radiolysis of liquid water with high-LET $^{12}C^{6+}$ ions: A Monte Carlo simulation study. Chem. Phys. Lett. **377**, 419-425.

MEESUNGNOEN, J. and JAY-GERIN, J.-P., 2005*a*. High-LET radiolysis of liquid water with $^{1}H^{+}$, $^{4}He^{2+}$, $^{12}C^{6+}$, and $^{20}Ne^{9+}$ ions: Effects of multiple ionization. J. Phys. Chem. A **109**, 6406-6419.

MEESUNGNOEN, J. and JAY-GERIN, J.-P., 2005*b*. Effect of multiple ionization on the yield of $H_2O_2$ produced in the radiolysis of aqueous 0.4 M $H_2SO_4$ solutions by high-LET $^{12}C^{6+}$ and $^{20}Ne^{9+}$ ions. Radiat. Res. **164**, 688-694.

MEESUNGNOEN, J. and JAY-GERIN, J.-P., 2011. Radiation chemistry of liquid water with heavy ions: Monte Carlo simulation studies. In: Charged Particle and Photon Interactions with Matter. Recent Advances, Applications, and Interfaces (Hatano, Y., Katsumura, Y., and Mozumder, A., Eds.), pp. 355-400. Taylor and Francis Group, Boca Raton, FL.

MEESUNGNOEN, J., GUZONAS, D., and JAY-GERIN, J.-P., 2010. Radiolysis of supercritical water at 400 °C and liquid-like densities near 0.5 g/cm$^3$. A Monte Carlo calculation. Can. J. Chem. **88**, 646-653.

MEESUNGNOEN, J., SANGUANMITH, S., and JAY-GERIN, J.-P., 2015. Yields of $H_2$ and hydrated electrons in low-LET radiolysis of water determined by Monte Carlo track chemistry simulations using phenol/$N_2O$ aqueous solutions up to 350 °C. RSC Adv. **5**, 76813-76824.

MICHAUD, M., CLOUTIER, P., and SANCHE, L., 1991. Low-energy electron-energy-loss spectroscopy of amorphous ice: Electronic excitations. Phys. Rev. A. **44**, 5624-5627.

MICHAUD, M., WEN, A., and SANCHE, L., 2003. Cross sections for low-energy (1-100 eV) electron elastic and inelastic scattering in amorphous ice. Radiat. Res. **159**, 3-22.

MIGUS, A., GAUDUEL, Y., MARTIN, J.-L., and ANTONETTI, A., 1987. Excess electrons in liquid water: First evidence of a prehydrated state with femtosecond lifetime. Phys. Rev. Lett. **58**, 1559-1562.

MIKKELSEN, R.B. and WARDMAN, P., 2003. Biological chemistry of reactive oxygen and nitrogen and radiation-induced signal transduction mechanisms. Oncogene **22**, 5734-5754.

MINKO, I.G., JACOBS, A.C., de LEON, A.R., GRUPPI, F., DONLEY, N., HARRIS, T.M., RIZZO, C.J., McCULLOUGH, A.K., and LLOYD, R.S., 2016. Catalysts of DNA strand cleavage at apurinic/apyrimidinic sites. Sci. Rep. **6**, 28894.

MIRSALEH KOHAN, L., SANGUANMITH, S., MEESUNGNOEN, J., CAUSEY, P., STUART, C.R., and JAY-GERIN, J.-P., 2013. Self-radiolysis of tritiated water. 1. A comparison of the effects of $^{60}$Co γ-rays and tritium β-particles on water and aqueous solutions at room temperature. RSC Adv. **3**, 19282-19299.

MONK, P.M.S., 2004. Physical Chemistry: Understanding our Chemical World. Wiley, Chichester, UK.

MOTHERSILL, C. and SEYMOUR, C.B., 2001. Radiation-induced bystander effects: Past history and future directions. Radiat. Res. **155**, 759-767.

MOZUMDER, A. and MAGEE, J.L., 1966*a*. Model of tracks of ionizing radiations for radical reaction mechanisms. Radiat. Res. **28**, 203-214.

MOZUMDER, A. and MAGEE, J.L., 1966*b*. Theory of radiation chemistry. VII. Structure and reactions in low LET tracks. J. Chem. Phys. **45**, 3332-3341.

MOZUMDER, A., CHATTERJEE, A., and MAGEE, J.L., 1968. Theory of radiation chemistry. IX. Model and structure of heavy particle tracks in water. Adv. Chem. Series **81**, 27-48.

MOZUMDER, A. and MAGEE, J.L., 1975. The early events of radiation chemistry. Int. J. Radiat. Phys. Chem. **7**, 83-93.

MOZUMDER, A., 1999. Fundamentals of Radiation Chemistry. Academic Press, San Diego, CA.

MUROYA, Y., MEESUNGNOEN, J., JAY-GERIN, J.-P., FILALI-MOUHIM, A., GOULET, T., KATSUMURA, Y., and MANKHETKORN, S., 2002. Radiolysis of liquid water: An attempt to reconcile Monte Carlo calculations with new experimental hydrated electron yield data at early times. Can. J. Chem. **80**, 1367-1374.

MUROYA, Y., PLANTE, I., AZZAM, E.I., MEESUNGNOEN, J., KATSUMURA, Y., and JAY-GERIN, J.-P., 2006. High-LET ion radiolysis of water: Visualization of the formation and evolution of ion tracks and relevance to the radiation-induced bystander effect. Radiat. Res. **165**, 485-491.

MUROYA, Y., LIN, M., DE WAELE, V., HATANO, Y., KATSUMURA, Y., and MOSTAFAVI, M., 2010. First observation of picosecond kinetics of hydrated electrons in supercritical water. J. Phys. Chem. Lett. **1**, 331-335.

MUROYA, Y., SANGUANMITH, S., MEESUNGNOEN, J., LIN, M., YAN, Y., KATSUMURA, Y., and JAY-GERIN, J.-P., 2012. Time-dependent yield of the hydrated electron in subcritical and supercritical water studied by ultrafast pulse radiolysis and Monte Carlo simulation. Phys. Chem. Chem. Phys. **14**, 14325-14333.

MUSTAREE, S., MEESUNGNOEN, J., BUTARBUTAR, S.L., CAUSEY, P., STUART, C.R., and JAY-GERIN, J.-P., 2014. Self-radiolysis of tritiated water. 3. The $^{\bullet}OH$ scavenging effect of bromide ions on the yield of $H_2O_2$ in the radiolysis of water by $^{60}Co$ $\gamma$-rays and tritium $\beta$-particles at room temperature. RSC Adv. **4**, 43572-43581.

NAGASAWA, H. and LITTLE, J.B., 1992. Induction of sister chromatid exchanges by extremely low doses of $\alpha$-particles. Cancer Res. **52**, 6394-6396.

NAKAMURA, J. and SWENBERG, J.A., 1999. Endogenous apurinic/apyrimidinic sites in genomic DNA of mammalian tissues. Cancer Res. **59**, 2522-2526.

NIKOGOSYAN, D.N., ORAEVSKY, A.A., and RUPASOV, V.I., 1983. Two-photon ionization and dissociation of liquid water by powerful laser UV radiation. Chem. Phys. **77**, 131-143.

OGURA, H. and HAMILL, W.H., 1973. Positive hole migration in pulse-irradiated water and heavy water. J. Phys. Chem. **77**, 2952-2954.

OKA, Y. and KOSHIZUKA, S., 1998. Conceptual design study of advanced power reactors. Prog. Nucl. Energy **32**, 163-177.

O'NEILL, P., 2001. Radiation-induced damage in DNA. In: Radiation Chemistry: Present Status and Future Trends (Jonah, C.D. and Rao, B.S.M., Eds.), pp. 585-622. Elsevier, Amsterdam.

O'NEILL, P. and WARDMAN, P., 2009. Radiation chemistry comes before radiation biology. Int. J. Radiat. Biol. **85**, 9-25.

PARETZKE, H.G., 1987. Radiation track structure theory. In: Kinetics of Nonhomogeneous Processes (Freeman, G.R., Ed.), pp. 89-170. Wiley, New York.

PARK, C.-W. and ZIPP, E., 2000. The effects of temperature and pH on enzyme kinetics. A webpage for introduction to biochemical engineering. Available from http://www.rpi.edu/dept/chem-eng/Biotech-Environ/Projects00/temph/enzyme.html

PASTINA, B., ISABEY, J., and HICKEL, B., 1999. The influence of water chemistry on the radiolysis of the primary coolant water in pressurized water reactors. J. Nucl. Mater. **264**, 309-318.

PASTINA, B., LAVERNE, J.A., and PIMBLOTT, S.M., 1999. Dependence of molecular hydrogen formation in water on scavengers of the precursor to the hydrated electron. J. Phys. Chem. A. **103**, 5841-5846.

PIMBLOTT, S.M., LAVERNE, J.A., MOZUMDER, A., and GREEN, N.J.B., 1990. Structure of electron tracks in water. 1. Distribution of energy deposition events. J. Phys. Chem. **94**, 488-495.

PIMBLOTT, S.M. and MOZUMDER, A., 1991. Structure of electron tracks in water. 2. Distribution of primary ionizations and excitations in water radiolysis. J. Phys. Chem. **95**, 7291-7300.

PIMBLOTT, S.M. and MOZUMDER, A., 2004. Modeling of physicochemical and chemical processes in the interactions of fast charged particles with matter. In: Charged Particle and Photon Interactions with Matter: Chemical, Physicochemical, and Biological Consequences with Applications (Mozumder, A. and Hatano, Y., Eds.), pp. 75-103. Marcel Dekker, New York.

PIMBLOTT, S.M., PILLING, M.J., and GREEN, N.J.B., 1991. Stochastic models of spur kinetics in water. Radiat. Phys. Chem. **37**, 377-388.

PIMBLOTT, S.M. and GREEN, N.J.B., 1995. Recent advances in the kinetics of radiolytic processes. Res. Chem. Kinet. **3**, 117-174.

PLANTE, I., FILALI-MOUHIM, A., and JAY-GERIN, J.-P., 2005. SimulRad: A Java interface for a Monte Carlo simulation code to visualize in 3D the early stages of water radiolysis. Radiat. Phys. Chem. **72**, 173-180.

PLANTE, I., 2009. Développement de codes de simulation Monte-Carlo de la radiolyse de l'eau et de solutions aqueuses par des électrons, ions lourds, photons et neutrons. Applications à divers sujets d'intérêt expérimental. Ph.D. Thesis, Université de Sherbrooke, Sherbrooke, Québec, Canada.

PLATZMAN, R.L., 1955. Subexcitation electrons. Radiat. Res. **2**, 1-7.

PLATZMAN, R.L., 1958. The physical and chemical basis of mechanisms in radiation biology. In: Radiation Biology and Medicine. Selected Reviews in the Life Sciences (Claus, W.D., Ed.), pp. 15-72. Addison-Wesley, Reading, MA.

PLATZMAN, R.L., 1962*a*. Superexcited states of molecules. Radiat. Res. **17**, 419-425.

PLATZMAN, R.L., 1962*b*. Dissociative attachment of subexcitation electrons in liquid water, and the origin of radiolytic "molecular" hydrogen. In: Abstracts of Papers, Second International Congress of Radiation Research, Harrogate, England, August 5-11, 1962, p. 128.

PONETTE, V., LE PÉCHOUX, C., DENIAUD-ALEXANDRE, E., FERNET, M., GIOCANTI, N., TOURBEZ, H., and FAVAUDON, V., 2000. Hyperfast, early cell response to ionizing radiation. Int. J. Radiat. Biol. **76**, 1233-1243.

PRYOR, W.A. and SQUADRITO, G.L., 1995. The chemistry of peroxynitrite: A product from the reaction of nitric oxide with superoxide. Am. J. Physiol. **268** (Lung Cell. Mol. Physiol. 12), L699-L722.

PUCHEAULT, J., 1961. Actions des rayons alpha sur les solutions aqueuses. In: Actions Chimiques et Biologiques des Radiations (Haïssinsky, M., Ed.), Vol. 5, pp. 31-84. Masson, Paris.

RADI, R., DENICOLA, A., ALVAREZ, B., FERRER-SUETA, G., and RUBBO, H., 2000. The biological chemistry of peroxynitrite. In: Nitric Oxide: Biology and Pathobiology (Ignarro, L.J., Ed.), pp. 57-82. Academic Press, San Diego.

RADI, R., 2013. Peroxynitrite, a stealthy biological oxidant. J. Biol. Chem. **288**, 26464-26472.

ROWNTREE, P., PARENTEAU, L., and SANCHE, L., 1991. Electron stimulated desorption via dissociative attachment in amorphous $H_2O$. J. Chem. Phys. **94**, 8570-8576.

SANGUANMITH, S., MUROYA, Y., MEESUNGNOEN, J., LIN, M., KATSUMURA, Y., MIRSALEH KOHAN, L., GUZONAS, D.A., STUART, C.R., and JAY-GERIN, J.-P., 2011*a*. Low-linear energy transfer radiolysis of liquid water at elevated temperatures up to 350 °C: Monte Carlo simulations. Chem. Phys. Lett. **508**, 224-230.

SANGUANMITH, S., MUROYA, Y., TIPPAYAMONTRI, T., MEESUNGNOEN, J., LIN, M., KATSUMURA, Y., and JAY-GERIN, J.-P., 2011*b*. Temperature dependence of the Fricke dosimeter and spur expansion time in the low-LET high-temperature radiolysis of water up to 350 °C: A Monte Carlo simulation study. Phys. Chem. Chem. Phys. **13**, 10690-10698.

SANGUANMITH, S., MEESUNGNOEN, J., MUROYA, Y., LIN, M., KATSUMURA, Y., and JAY-GERIN, J.-P., 2012. On the spur lifetime and its temperature dependence in

the low linear energy transfer radiolysis of water. Phys. Chem. Chem. Phys. **14**, 16731-16736.

SAUER, M.C., Jr., SCHMIDT, K.H., HART, E.J., NALEWAY, C.A., and JONAH, C.D., 1977. LET dependence of transient yields in the pulse radiolysis of aqueous systems with deuterons and α particles. Radiat. Res. **70**, 91-106.

SCHNEIDER, N.M., NORTON, M.M., MENDEL, B.J., GROGAN, J.M., ROSS, F.M., and BAU, H.H., 2014. Electron-water interactions and implications for liquid cell electron microscopy. J. Phys. Chem. C **118**, 22373-22382.

SCHULER, R.H. and ALLEN, A.O., 1957. Radiation chemistry studies with cyclotron beams of variable energy: Yields in aerated ferrous sulfate solution. J. Am. Chem. Soc. **79**, 1565-1572.

SHEPPARD, T.L., ORDOUKHANIAN, P., and JOYCE, G.F., 2000. A DNA enzyme with N-glycosylase activity. Proc. Natl. Acad. Sci. USA **97**, 7802-7807.

SMITH, D.R. and STEVENS, W.H., 1963. Radiation-induced hydrolysis of acetal: Evidence for the reaction of $H_3O^+$ ions in spurs in the radiolysis of water. Nature **200**, 66-67.

SPINKS, J.W.T. and WOODS, R.J., 1990. An Introduction to Radiation Chemistry, 3rd edn. Wiley, New York.

ŠTEFANIĆ, I. and LAVERNE, J.A., 2002. Temperature dependence of the hydrogen peroxide production in the γ-radiolysis of water. J. Phys. Chem. A **106**, 447-452.

STERNICZUK, M. and BARTELS, D.M., 2016. Source of molecular hydrogen in high-temperature water radiolysis. J. Phys. Chem. A **120**, 200-209.

STRYER, L., 1995. Biochemistry, 4th edn. W.H. Freeman and Co., New York.

SUNARYO, G.R., KATSUMURA, Y., HIROISHI, D., and ISHIGURE, K., 1995. Radiolysis of water at elevated temperatures – II. Irradiation with γ-rays and fast neutrons up to 250 °C. Radiat. Phys. Chem. **45**, 131-139.

SUZUKI, K. and YAMASHITA, S., 2014. Radiation-induced bystander response: Mechanism and clinical implications. Adv. Wound Care (New Rochelle) **3**, 16-24.

SWIATLA-WOJCIK, D., 2008. Computation of the effect of pH on spur chemistry in water radiolysis at elevated temperatures. Nukleonika **53** (Supplement 1), S31-S37.

SWIATLA-WOJCIK, D. and BUXTON, G.V., 1995. Modeling of radiation spur processes in water at temperatures up to 300 °C. J. Phys. Chem. **99**, 11464-11471.

SWIATLA-WOJCIK, D. and BUXTON, G.V., 1998. Modelling of linear energy transfer effects on track core processes in the radiolysis of water up to 300 °C. J. Chem. Soc., Faraday Trans. **94**, 2135-2141.

SWIATLA-WOJCIK, D. and BUXTON, G.V., 2000. Diffusion-kinetic modelling of the effect of temperature on the radiation chemistry of heavy water. Phys. Chem. Chem. Phys. **2**, 5113-5119.

SWIATLA-WOJCIK, D. and BUXTON, G.V., 2001. Isotopic effect in the radiolysis of water. Diffusion-kinetic modelling up to 300 °C. Res. Chem. Intermed. **27**, 875-889.

SWIATLA-WOJCIK, D. and BUXTON, G.V., 2005. On the possible role of the reaction $H^{\bullet} + H_2O \rightarrow H_2 + {}^{\bullet}OH$ in the radiolysis of water at high temperatures. Radiat. Phys. Chem. **74**, 210-219.

SWIATLA-WOJCIK, D. and BUXTON, G.V., 2010. Reply to comment on the possible role of the reaction $H + H_2O \rightarrow H_2 + OH$ in the radiolysis of water at high temperatures. Radiat. Phys. Chem. **79**, 52-56.

TACHIYA, M., 1983. Theory of diffusion-controlled reactions: Formulation of the bulk reaction rate in terms of the pair probability. Radiat. Phys. Chem. **21**, 167-175.

TANNOCK, I.F. and ROTIN, D., 1989. Acid pH in tumors and its potential for therapeutic exploitation. Cancer Res. **49**, 4373-4384.

TAUBE, H., 1957. Photochemical reactions of ozone in solution. Trans. Faraday Soc. **53**, 656-665.

TIPPAYAMONTRI, T., SANGUANMITH, S., MEESUNGNOEN, J., SUNARYO, G.R., and JAY-GERIN, J.-P., 2009. Fast neutron radiolysis of the ferrous sulfate (Fricke) dosimeter: Monte Carlo simulations. Recent Res. Devel. Physical Chem. **10**, 143-211.

TOBUREN, L.H., 2004. Ionization and secondary electron production by fast charged particles. In: Charged Particle and Photon Interactions with Matter: Chemical, Physicochemical, and Biological Consequences with Applications (Mozumder, A. and Hatano, Y., Eds.), pp. 31-74. Marcel Dekker, New York.

TUBIANA, M. (Ed.), 2008. Radiobiologie. Hermann/Médecine, Paris.

TURNER, J.E., MAGEE, J.L., HAMM, R.N., CHATTERJEE, A., WRIGHT, H.A., and RITCHIE, R.H., 1981. Early events in irradiated water. In: Seventh Symposium on Microdosimetry, Oxford, UK, Sept. 8-12, 1980 (Booz, J., Ebert, H.G., and Hartfiel, H.D., Eds.), pp. 507-520. Harwood Academic Publ., London.

TURNER, J.E., MAGEE, J.L., WRIGHT, H.A., CHATTERJEE, A., HAMM, R.N., and RITCHIE, R.H., 1983. Physical and chemical development of electron tracks in liquid water. Radiat. Res. **96**, 437-449.

TURNER, J.E., HAMM, R.N., WRIGHT, H.A., RITCHIE, R.H., MAGEE, J.L., CHATTERJEE, A., and BOLCH, W.E., 1988*a*. Studies to link the basic radiation physics and chemistry of liquid water. Radiat. Phys. Chem. **32**, 503-510.

TURNER, J.E., HAMM, R.N., SOULEYRETTE, M.L., MARTZ, D.E., RHEA, T.A., and SCHMIDT, D.W., 1988*b*. Calculations for β dosimetry using Monte Carlo code (OREC) for electron transport in water. Health Phys. **55**, 741-750.

UEHARA, S. and NIKJOO, H., 2006. Monte Carlo simulation of water radiolysis for low-energy charged particles. J. Radiat. Res. **47**, 69-81.

von SONNTAG, C., 2006. Free-Radical-Induced DNA Damage and its Repair. A Chemical Perspective. Springer-Verlag, Berlin.

WARDMAN, P., 2009. The importance of radiation chemistry to radiation and free radical biology (The 2008 Silvanus Thompson Memorial Lecture). Br. J. Radiol. **82**, 89-104.

WATT, D.E. 1996. Quantities for Dosimetry of Ionizing Radiations in Liquid Water. Taylor & Francis, London.

WALIGÓRSKI, M.P.R., HAMM, R.N., and KATZ, R., 1986. The radial distribution of dose around the path of a heavy ion in liquid water. Nucl. Tracks Radiat. Measur. **11**, 309-319.

WIKE-HOOLEY, J.L., HAVEMAN, J., and REINHOLD, H.S., 1984. The relevance of tumour pH to the treatment of malignant disease. Radiother. Oncol. **2**, 343-366.

WILSON, C.D., DUKES, C.A., and BARAGIOLA, R.A., 2001. Search for the plasmon in condensed water. Phys. Rev. B **63**, 121101.

YAMASHITA, S., KATSUMURA, Y., LIN, M., MUROYA, Y., MAEYAMA, T., and MURAKAMI, T., 2008. Water radiolysis with heavy ions of energies up to 28 GeV. 2. Extension of primary yield measurements to very high LET values. Radiat. Phys. Chem. **77**, 1224-1229.

ZAIDER, M. and BRENNER, D.J., 1984. On the stochastic treatment of fast chemical reactions. Radiat. Res. **100**, 245-256.

ZIEGLER, J.F., BIERSACK, J.P., and ZIEGLER, M.D., 2015. SRIM - The Stopping and Range of Ions in Matter, 15th edn. Lulu Press, Morrisville, NC.

ZIMBRICK, J.D., 2002. Radiation chemistry and the Radiation Research Society: A history from the beginning. Radiat. Res. **158**, 127-140.